

STIMULI-RESPONSIVE CHITOSAN-BASED HYDROGELS FOR ANTIBIOTIC DELIVERY



Miss Tu Tran Vo Minh

A Dissertation Submitted in Partial Fulfillment of the Requirements
for the Degree of Doctor of Philosophy in Materials Science
Department of Materials Science
FACULTY OF SCIENCE
Chulalongkorn University
Academic Year 2022
Copyright of Chulalongkorn University

ไฮโดรเจลจากไคโตซานที่ตอบสนองต่อสิ่งเร้าสำหรับการนำส่งยาปฏิชีวนะ



วิทยานิพนธ์นี้เป็นส่วนหนึ่งของการศึกษาตามหลักสูตรปริญญาวิทยาศาสตรดุษฎีบัณฑิต

สาขาวิชาวัสดุศาสตร์ ภาควิชาวัสดุศาสตร์

คณะวิทยาศาสตร์ จุฬาลงกรณ์มหาวิทยาลัย

ปีการศึกษา 2565

ลิขสิทธิ์ของจุฬาลงกรณ์มหาวิทยาลัย

Thesis Title	STIMULI-RESPONSIVE CHITOSAN-BASED HYDROGELS FOR ANTIBIOTIC DELIVERY
By	Miss Tu Tran Vo Minh
Field of Study	Materials Science
Thesis Advisor	Professor PRANUT POTIYARAJ, Ph.D.
Thesis Co Advisor	Professor TAKAOMI KOBAYASHI, Ph.D. Thananchai Piroonpan, Ph.D.

Accepted by the FACULTY OF SCIENCE, Chulalongkorn University in
Partial Fulfillment of the Requirement for the Doctor of Philosophy

..... Dean of the FACULTY OF
SCIENCE
(Professor POLKIT SANGVANICH, Ph.D.)

DISSERTATION COMMITTEE

..... Chairman
(Associate Professor SIREERAT CHARUCHINDA,
Ph.D.)

..... Thesis Advisor
(Professor PRANUT POTIYARAJ, Ph.D.)

..... Thesis Co-Advisor
(Professor TAKAOMI KOBAYASHI, Ph.D.)

..... Thesis Co-Advisor
(Thananchai Piroonpan, Ph.D.)

..... Examiner
(Professor DUANGDAO AHT-ONG, Ph.D.)

..... Examiner
(Associate Professor KAWEE SRIKULKIT, Ph.D.)

..... External Examiner
(Associate Professor Wanvimol Pasanphan, Ph.D.)

บท ทราน โว มินห์ : ไฮโดรเจลจากไคโตซานที่ตอบสนองต่อสิ่งเร้าสำหรับการนำส่งยาปฏิชีวนะ. (STIMULI-RESPONSIVE CHITOSAN-BASED HYDROGELS FOR ANTIBIOTIC DELIVERY) อ.ที่ปรึกษาหลัก : ศ. ดร.ประณัฐ

โพธิยธราช, อ.ที่ปรึกษาร่วม : ศ. ดร.ทศานโอมิ โภบายาชิ, ดร. ธัญชัช พิรุณพันธ์

งานวิจัยนี้มีวัตถุประสงค์เพื่อศึกษาไฮโดรเจลที่เตรียมโดยใช้แนวทางที่เป็นมิตรกับสิ่งแวดล้อมเพื่อนำไปใช้งานด้านการนำส่งยา การใช้พอลิเมอร์ที่สามารถเข้ากันได้ทางชีวภาพ เป็นเมทริกซ์ในระบบการนำส่งยาได้รับความนิยมนในช่วงที่ผ่านมา เนื่องจากสามารถปรับปรุงประสิทธิภาพและความปลอดภัยของการนำส่งยาโดยการปลดปล่อยยาได้ตรงเป้าหมายและสามารถออกฤทธิ์ยาได้แต่เนิ่น จึงมีปริมาณการใช้ปริมาณยานี้น้อยลง รวมทั้งทำให้ผู้ป่วยได้รับความสะดวกยิ่งขึ้น ไคโตซานเป็นพอลิเมอร์ชนิดหนึ่งที่มีนิยมนำมาใช้เพื่อวัตถุประสงค์ดังกล่าว เนื่องจากสามารถอุ้มน้ำได้ดี และมีความพรุนตัวทำให้มีช่องว่างสำหรับกักเก็บยาไว้ในเมทริกซ์ อย่างไรก็ตาม การควบคุมการปลดปล่อยยาด้วยสิ่งเร้าทั้งภายในและภายนอกยังคงมีการศึกษาวิจัยอย่างต่อเนื่อง งานวิจัยเป็นการพัฒนาไฮโดรเจลฐานไคโตซานที่สามารถควบคุมการปลดปล่อยอะม็อกซิซิลลินได้อย่างตรงเป้าหมาย การศึกษานี้แบ่งออกเป็นสองส่วน ส่วนแรกเป็นการขึ้นรูปไฮโดรเจลจากไคโตซาน (CS) และ โพลีไวนิลแอลกอฮอล์ (PVA) ด้วยรังสีแกมมาและตรวจสอบสมบัติของไฮโดรเจลที่ได้ โดยเริ่มจากการหาอัตราส่วนที่เหมาะสมระหว่าง CS และ PVA ภายใต้ปริมาณการฉายรังสีแกมมาที่แตกต่างกันตั้งแต่ 10 kGy ถึง 30 kGy ผลการทดลองพบว่าอัตราส่วนของ CS/PVA เท่ากับ 50/50 ปริมาณเจล เสถียรภาพทางความร้อน ความแข็งแรงเชิงกล และระดับขึ้นการบวมตัวเพิ่มขึ้นอย่างมีนัยสำคัญ เมื่อเทียบกับไฮโดรเจลจาก PVA หรือ CS ที่ถูกฉายรังสีปริมาณ 25 kGy การทำหน้าที่ยานี้เป็นตัวนำส่งยาที่ตอบสนองตามความเป็นกรดเป็นด่างของไฮโดรเจลที่เตรียมขึ้นนี้ เกิดจากกลไกการรับและให้โปรตอนของหมู่อะมิโนบนสายโซ่หลักของไคโตซาน โดยมีการปลดปล่อยอะม็อกซิซิลลินประมาณร้อยละ 85 และ 50 ในน้ำเกลือบัฟเฟอร์ฟอสเฟตที่ pH 2.1 และ 7.4 ตามลำดับ โดยปริมาณของอะม็อกซิซิลลินอยู่ที่ประมาณร้อยละ 34 ในน้ำดีไอออนซ์ ที่ pH 5.5 สำหรับงานวิจัยส่วนที่สอง CS/EDGE ถูกเตรียมเป็นไฮโดรเจลโดยการกระตุ้นด้วยคลื่นเสียงความถี่สูง ที่กำลัง 0 10 20 และ 35 วัตต์ ความถี่ 43 กิโลเฮิร์ตซ์ จากนั้นนำมาทดสอบการปลดปล่อยอะม็อกซิซิลลิน พบว่ามีอัตราสูงที่สุดเมื่อความเข้มข้นของ CS เท่ากับร้อยละ 2 เมื่อเปรียบเทียบกับไฮโดรเจลที่มีความเข้มข้นของ CS ร้อยละ 1.5 2.5 และ 3 อันเป็นผลมาจากประสิทธิภาพในการห่อหุ้มยาและความหนาแน่นของการเชื่อมขวาง จากนั้นวิเคราะห์ผลของคลื่นเสียงความถี่สูงต่อการอ่อนตัวของพอลิเมอร์เมทริกซ์ด้วยพฤติกรรมวิสโคอีลาสติกของไฮโดรเจล พบว่ามีความเข้มข้นของไคโตซานน้อยกว่าร้อยละ 2 ไฮโดรเจลมีความอ่อนนุ่ม แต่เมื่อความเข้มข้นของไคโตซานสูงขึ้นเป็นร้อยละ 2.5 และร้อยละ 3.0 ไฮโดรเจลมีความแข็งแรงมากขึ้นหลังจากได้รับคลื่นเสียงความถี่สูงเกินกว่า 120 นาที และจากการศึกษากลไกการปลดปล่อยอะม็อกซิซิลลินโดยใช้โมเดลต่าง ๆ ได้แก่ zero-order, first-order, Higuchi, Hixson-Crowell และ Korsmeyer-Peppas ซึ่งให้เห็นว่าการปลดปล่อยอะม็อกซิซิลลินเป็นกลไกการถ่ายโอนแบบนอนฟิฟิเคียนกล่าวคือ การปลดปล่อยขึ้นกับการแพร่และความสามารถในการบวมตัวของเมทริกซ์

สาขาวิชา วัสดุศาสตร์
ปีการศึกษา 2565

ลายมือชื่อนิติศ
ลายมือชื่อ อ.ที่ปรึกษาหลัก
ลายมือชื่อ อ.ที่ปรึกษาร่วม
ลายมือชื่อ อ.ที่ปรึกษาร่วม

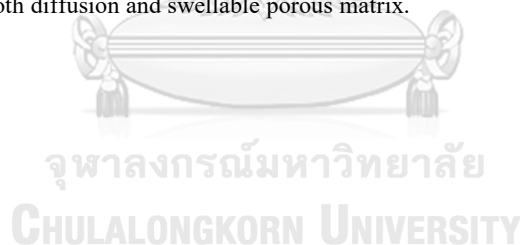
จุฬาลงกรณ์มหาวิทยาลัย
CHULALONGKORN UNIVERSITY

6273014823 : MAJOR MATERIALS SCIENCE

KEYWORD: Chitosan; polyvinyl alcohol; ethylene glycol diglycidyl ether; gamma irradiation; drug delivery system

Tu Tran Vo Minh : STIMULI-RESPONSIVE CHITOSAN-BASED HYDROGELS FOR ANTIBIOTIC DELIVERY. Advisor: Prof. PRANUT POTIYARAJ, Ph.D. Co-advisor: Prof. TAKAOMI KOBAYASHI, Ph.D., Thananchai Piroonpan, Ph.D.

This study aims to investigate hydrogels fabricated via green approaches for drug delivery application. Biocompatible polymer-based drug delivery systems (DDS) have gained popularity in recent years because of their ability to improve the efficacy and safety of drug delivery by providing targeted and sustained release of drugs to reduce the frequency of dosing, making it more convenient for patients. Chitosan is one of the polymers commonly used for this purpose due to their higher water retention and porosity, which create space for loading medicine into the matrix. However, the potential utilization of endogenous and exogenous stimuli controlling drug release still remains challenging. Therefore, this research is focusing develop chitosan hydrogels used for targeted and controlled amoxicillin release. This study is divided into two main parts. Firstly, the fabrication and characterization of γ -irradiated chitosan (CS)/ polyvinyl alcohol (PVA) hydrogels were conducted to figure out the optimal ratio of CS and PVA under different gamma irradiation doses from 10 kGy to 30 kGy. At the ratio of CS/PVA of 50/50, the gel contents, thermal stabilities, mechanical strengths, and swelling degrees significantly increased as compared to those of the neat PVA and CS hydrogels at 25 kGy. Based on the protonate and de-protonate of amino groups on CS backbones in an acidic or basic environment, those γ -irradiated CS/PVA hydrogels were explored as pH-responsive drug carriers. The percentage release of amoxicillin (Amox) was estimated at 85 % and 50 % at pH 2.1 and 7.4 in PBS media. Meanwhile, the amount of Amox was around 34 % at pH 5.5 in DI water. Secondly, ultrasound (US) triggered DDS based on CS/EGDE hydrogel was investigated. The release of Amox from the hydrogel matrix was triggered by US under different US powers (0, 10, 20, and 35 W) at 43 kHz using CS solutions of concentrations ranging from 1.5 wt% to 3 wt%. The greater Amox release was observed in 2% CS compared to 1.5, 2.5, and 3 wt% because of drug-encapsulated effectiveness, crosslink density, and the effect of US on the polymer matrix. Viscoelasticity of CS/EGDE/Amox hydrogel with or without US was carried out to evaluate the softening effect of US on CS/EGDE/Amox hydrogel for lower CS content at 1.5 and 2 wt%, meanwhile at 2.5 or 3 wt% of CS remained unchanged G' value at 0.01 % strain. Moreover, the hydrogels at higher CS concentrations like 2.5 and 3 wt% became somewhat rigid after US irradiation for 120 mins. To study the Amox release mechanism, several models consisting of zero-order, first-order, Higuchi, Hixson-Crowell, and Korsmeyer-Peppas were applied. It indicated that Amox release is mediated by a non-Fickian transport mechanism which means the release depended on both diffusion and swellable porous matrix.



Field of Study: Materials Science
Academic Year: 2022

Student's Signature
Advisor's Signature
Co-advisor's Signature
Co-advisor's Signature

ACKNOWLEDGEMENTS

The funding for this dissertation was made possible by the GAICCE DDP Scholarship received from ASEAN University Network/Southeast Asia Engineering Education Development Network (AUN/SEED-Net), as well as the 60/40 Study Scholarship/Overseas Research Experience Scholarship for Graduate Students. This Ph.D. journey has been an incredible experience for me, as it allowed me to conduct research in both Thailand and Japan. I would like to take this opportunity to express my heartfelt appreciation to my supervisor, Prof. Pranut Potiyaraj, for his unwavering support, patience, and extensive knowledge. His guidance and expertise were instrumental in executing this research and writing this thesis.

I am also deeply indebted to Prof. Takaomi Kobayashi, my co-supervisor, for giving me the chance to work on a part of my research in Japan and for his enthusiastic guidance. My sincere thanks also go to Dr. Thananchai Piroonpan, who provided me with raw materials and access to radiation facilities for conducting my experiments and valuable discussions. Without their support, I would not have been able to present this dissertation as a real researcher.

Apart from my advisor and co-advisor, I am also grateful to the chairman and all members of the doctoral degree program committee, including the external examiner, for their valuable time, attention, and guidance on my dissertation. Being a student of the Department of Materials Science, Faculty of Science, Chulalongkorn University has been an impressive experience, and I am thankful to my department for providing me with knowledge, skills, laboratory facilities, instrument support, and financial subsidies. I would also like to thank the Metallurgy and Materials Science Research Institute (MMRI) for supporting my research with the best instruments and advice. Moreover, I would like to express my gratitude to all the laboratory, department, and faculty staff for their technical and document support during my doctoral double degree program.

Finally, I would like to dedicate this thesis to my parents, who have always been my unwavering support since my birth. I would like to express my thanks to my family and best friends for their sincere encouragement during the challenging periods of my doctoral studies and for motivating me to overcome thesis-related obstacles.

Tu Tran Vo Minh

TABLE OF CONTENTS

	Page
.....	iii
ABSTRACT (THAI)	iii
.....	iv
ABSTRACT (ENGLISH).....	iv
ACKNOWLEDGEMENTS	v
TABLE OF CONTENTS.....	vi
LIST OF TABLES.....	x
LIST OF FIGURES	xi
CHAPTER 1 INTRODUCTION.....	14
CHAPTER 2 THEORIES AND LITERATURE REVIEWS.....	19
2.1 Hydrogel.....	19
2.1.1 General Introduction of Hydrogel	19
2.1.1 Classification of Hydrogel	20
2.1.1.1 Based on the source.....	20
2.1.1.2 Based on polymetric composition.....	20
2.1.1.3 Based on type of cross-linking.....	21
2.1.1.4 Based on the network electrical charge	21
2.1.2 Properties of Hydrogels	22
2.1.2.1 Swelling behavior.....	22
2.1.2.2 Mechanical Properties	23
2.1.2.3 Viscoelastic properties.....	23
2.1.2.4 Biodegradable properties	24
2.1.2.5 Biocompatibility and Cytotoxicity	24
2.1.3 Application of hydrogels in biomedical approach.....	25
2.2 Polymer based hydrogels	29

2.2.1 Natural polymer	29
2.2.2 Synthetic polymer hydrogel	31
2.3 Methods to synthesize hydrogel	32
2.3.1 Physically crosslinked hydrogels.....	33
2.3.2 Chemically crosslinked hydrogels.....	34
2.3.2.1 Gamma-irradiated chitosan hydrogels.....	34
2.3.2.2 Chitosan based-hydrogel through chemical reactions.....	40
2.4 Drug delivery systems (DDS)	46
2.4.1 Stimulants in DDS	47
2.4.1.1 pH-responsive systems	48
2.4.1.2 Ultrasound-responsive system	51
2.4.2 Mathematical models of drug release	55
2.4.3 Antibiotics	57
CHAPTER 3 EXPERIMENTAL PROCEDURES.....	59
3.1 Chemicals and Materials.....	59
3.2 Equipment and instruments.....	60
3.3 Preparation of chitosan-based hydrogels	61
3.4 Characterizations	63
3.4.1 Evaluation of gel contents.....	63
3.4.2 Swelling behavior.....	64
3.4.3 Chemical structure confirmation	64
3.4.3.1 Fourier transform infrared (FTIR)	64
3.4.3.2 ¹³ C Magic-angle spinning nuclear magnetic resonance (¹³ C MAS NMR).....	65
3.4.4 Scanning electron microscopy (SEM)	65
3.4.5 Thermogravimetric analysis (TGA).....	66
3.4.6 In vitro drug release test.....	66
3.4.7 Rheological properties of hydrogels	68
3.4.7.1 Gelation behavior of CS/EGDE solutions	68

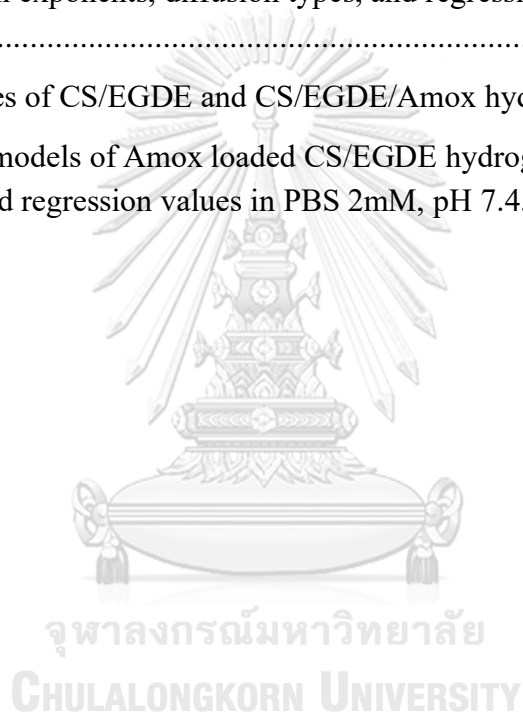
3.4.7.2 Viscoelastic behavior of CS/EGDE hydrogels and Amox-entrapped CS/EGDE hydrogels.....	69
3.4.8 Water content (WC) and density of hydrogels	69
3.4.9 In-vitro Amoxicillin release	70
3.4.9.1 Amoxicillin encapsulation in hydrogels	70
3.4.10 Fourier transform infrared (FTIR) and Scanning electron microscope (SEM).....	71
CHAPTER 4 RESULTS AND DISCUSSION.....	72
4.1 Gamma-irradiated CS/PVA hybrid hydrogels	72
4.1.1 Gel fraction.....	72
4.1.2 Swelling behavior	73
4.1.2.1 Swelling in DI water.....	73
4.1.2.2 Swelling indices in different pH solutions.....	75
4.1.3 Chemical structures of crosslinked CS hydrogels	76
4.1.3.1 FTIR spectra of unirradiated and gamma-irradiated CS/PVA hydrogels.....	76
4.1.4 Thermal analysis	81
4.1.5 Morphologies of the crosslinked CS hydrogels.....	83
4.1.6 In vitro amoxicillin release studies	84
4.2 Chitosan/Ethylene glycol diglycidyl ether/Amoxicillin hydrogels	89
4.2.1 Gelation behavior of aqueous CS/EGDE	89
4.2.2 Viscoelasticity of the resultant CS/EGDE hydrogels.....	91
4.2.3 Properties of CS/EGDE and CS/EGDE/Amox hydrogels.	92
4.2.4 US stimulated Amox release from CS/EGDE/Amox hydrogels	95
4.2.5 Kinetic models of Amox loaded CS/EGDE hydrogels	97
4.2.6 US influence on CS/EGDE/Amox hydrogels matrix	100
4.2.6.1 Evaluation of gelatious properties of polymeric hydrogels.....	100
4.2.6.2 Chemical structure confirmation of CS/EGDE hydrogels and Amox loaded CS/EGDE hydrogels.....	105
CHAPTER 5 CONCLUSION.....	107

REFERENCES..... 111
VITA..... 126



LIST OF TABLES

	Page
Table 2.1 Applications of hydrogel	26
Table 2.2 Prevalent epoxy crosslinkers	41
Table 4.1 Chemical shifts of C in the pure and blended hydrogels.....	79
Table 4.2 The kinetic models of CS/PVA irradiated hydrogel (50/50): drug-release rate constants, diffusion exponents, diffusion types, and regression values in diverse media	89
Table 4.3 Properties of CS/EGDE and CS/EGDE/Amox hydrogels.....	92
Table 4.4 Kinetic models of Amox loaded CS/EGDE hydrogels: diffusion exponents, diffusion types, and regression values in PBS 2mM, pH 7.4.....	98



LIST OF FIGURES

	Page
Figure 1.1 Schematic of Amoxicillin entrapped Chitosan/Ethylene glycol diglycidyl ether hydrogel for drug delivery systems	18
Figure 2.2 Disintegration of ⁶⁰ Co.....	35
Figure 2.3 Cross-linking of hyaluronic acid (HA) using ethylene glycol diglycidyl ether (EGDE)[106].....	43
Figure 2.4 The main cross-linking reaction of carboxymethyl cellulose with glycol diglycidyl ether[107]	44
Figure 2.5 The chemical crosslinking of GCS with PEGDE in water at 37 °C and optical images of GCS-PEG 1% (w/v) crosslinked with PEGDE 0.08% (mol/mol). In particular: a) just prepared GCS-PEG hydrogel; b) freeze dried GCS-PEG; c) swollen after freeze drying[102].	45
Figure 2.6 Physiological pH values in the human body[114].....	49
Figure 2.7 pH Sensitive Hydrogels in Drug Delivery[115].....	49
Figure 2.8 A core-shell pH-responsive drug-carrier based on chitosan-coated mesoporous silica nanospheres[118]	51
Figure 2.9 The scheme showing the fabrication of ORP NPs for immune stimulation as a nanovaccine and US-triggered release of ORP NPs from the NC gel[122].	53
Figure 2.10 (a) Ultrasound-triggered drug release of anticancer drug-loaded Gas-NPs in tumor-bearing mice; (b) In vitro US-responsible drug release profile of DOX-Gas-NPs were studied in PBS (pH 7.4); (c) After 4 h post-injection of 100 µL of Nile red-Gas-NPs and PLGA-NPs into SCC7 tumor bearing BALB/c male nude mice; (d) Anti-tumor therapeutic efficacy of DTX-Gas-NPs (10 mg/kg DTX) without or with the external US irradiation after 16 day post-treatment; (e) The tumor volumes of each sample treated tumor-bearing mice; (f) The representative images of excised tumors after 16 day post-injection of saline, free DTX, and DTX-Gas-NPs without or with the external US irradiation. (g) Histological analysis of the excised tumor tissue was evaluated via H&E staining (upper) and TUNEL assay (lower) [123].	54
Figure 3.1 The procedure to synthesize gamma-irradiated CS/PVA hydrogels.....	62
Figure 3.2 The process to synthesize CS/EGDE hydrogels.....	63
Figure 3.3 Fourier transform infrared spectrometer (Source: https://www.thermofisher.com/).....	65

Figure 3.4 Nuclear magnetic resonance spectroscopy (NMR) (Source: https://www.bruker.com/)	65
Figure 4.1 Effect of irradiation dose on the gel fraction (%) of CS/PVA at different compositions	73
Figure 4.2 Swelling ratio (g/g) vs. time (min) graph of the prepared hydrogels in deionized water at different polymer ratios a) and radiation doses of 50/50 CS/PVA b)	74
Figure 4.3 Swelling ratios of the 50/50 CS/PVA hydrogel discs at a pH 1–13.....	76
Figure 4.4 a) Fourier transform infrared spectra of pure PVA, neat CS, non-irradiated CS/PVA, and b) FTIR of crosslinked hydrogels irradiated at 10, 25, 30 kGy; c) solid-state ¹³ C nuclear magnetic resonance spectrum of pure CS, neat PVA before and after irradiation, and the 50/50 CS/PVA hydrogel.....	78
Figure 4.5 a) Typical TG and DTG curves of pure PVA, pure CS, and CS/PVA blended hydrogels at 25 kGy and b) 50/50 CS/PVA at 10, 25, and 30 kGy.	81
Figure 4.6 Scanning electron microscopy images of the crosslinked hydrogels: a) pure PVA, b–d) 25/75, 50/50, and 75/25 CS/PVA-based hydrogels crosslinked at 25 kGy, respectively; e, f) 50/50 CS/PVA-based hydrogel crosslinked at 10 and 30 kGy.	85
Figure 4.7a) Calibration curve for Amoxicillin using UV-vis spectroscopy, b) cumulative release of the 50/50 CS/PVA; the drug release profiles of CS/PVA 50/50 were calculated using the c) zero-order, d) first-order, e) Hixson-Crowell model, f) Higuchi model, and g) Korsmeyer-Peppas model.....	89
Figure 4.8a) Time change of G' and G'' and b) tan δ for the CS/EGDE solutions with various CS concentrations.....	91
Figure 4.9a) G' and G'' and b) tan δ at different strain % for the CS/EGDS hydrogels. These hydrogels were washed with large volumes of water and tested on samples with a pH of 7 in the water they contain.....	91
Figure 4.10a) UV-Vis spectra of CS/EGDE hydrogel, CS/EGDE/Amox hydrogel with 1.37 and 1.48 mm thickness, respectively, and Amox aqueous solution at 50 μg/ml, Amox chemical structure, and external appearance of CS/EGDE hydrogels without Amox; b) US experimental setup; c) Appearance picture of CS/EGDE/Amox hydrogels prepared with different CS percentages in absence and presence of US-triggered release at 35 W.....	93
Figure 4.11 Concentration of Amox released into aqueous PBS solution, pH 7.4 was measured against ultrasonic (US) exposure time. The US irradiation was conducted with a frequency of 43 kHz, power of 0-35 W, temperature of 25 °C at various CS contents with 1.5 % (a), 2 % (b), 2.5 % (c), and 3 % (d).....	95

Figure 4.12 Kinetic models of Amox release profile from CS/EGDE/Amox hydrogels (a, f) zero-order, (b, g) first-order, (c, h) Higuchi model, (d, i) Hixson-Crowell model, and (e, j) Korsmeyer-Peppas model of 1.5 %, 2 %, 2.5 %, and 3 % at 35 W/43 kHz; 0 W, 10 W, 20 W, and 35 W of 2 % CS/EGDE/Amox, respectively. 99

Figure 4.13 Cross-section SEM images of the Amox-entrapped CS/EGDE hydrogels before releasing (a), 2 % CS/EGDE hydrogels and 2 % CS/EGDE/Amox hydrogels after releasing Amox in absence and presence of US for 120 min (b) in x100, x1000, and x5000 magnification (left); EDS layered photo and S, C elements of those hydrogels (right). 100

Figure 4.14 Amox-trapped CS/EGDE hydrogels were subjected to strain sweep measurements (a, c, e, g) with corresponding $\tan \delta$ measurements (b, d, f, h), both with and without ultrasonic exposure (43 kHz, 35 W, 120 min). These hydrogels were made from CS solutions with concentrations of 1.5 wt% (a, b), 2 wt% (c, d), 2.5 wt% (e, f), and 3 wt% (g, h). The measurements were performed at a frequency of 1 Hz and characterized by G' (storage moduli), G'' (loss moduli), and $\tan \delta$, which is defined as the ratio of G'' to G' . The relation of G' at 0.1 % strain of Amox-CS/EGDE hydrogels at 1.5 % to 3 % of CS and US powers at 0, 10, 20, and 35 W. 105

Figure 4.15 Chemical structure confirmation of CS/EGDE hydrogels and Amox loaded CS/EGDE hydrogels before and after releasing with/without US exposure. 105



CHAPTER 1

INTRODUCTION

Drug delivery systems (DDS) are an integral part of modern medicine, allowing for the targeted and controlled release of therapeutic compounds. In the past decade, traditional DDS faces a sharp increase and decrease in drug levels in the blood after each administration, which can cause fluctuations in therapeutic effects. In addition, frequent administration of drugs is required to maintain therapeutic levels in the blood, which can be inconvenient for patients. Furthermore, traditional DDS may result in side effects due to the drug reaching toxic levels in the blood or being ineffective due to low drug levels. As a consequence, traditional DDS may not be optimal for drugs that have short biological half-lives or require long-term administration. Nowadays, an ideal DDS has two critical functions: targeting and controlling drug release. Targeting is essential to enhance drug efficacy and minimize adverse effects, particularly when dealing with anti-cancer drugs that can harm healthy cells. By selectively delivering the drug to the target area, the DDS can increase the concentration of the drug at the site of action, thus reducing the required dose and the likelihood of side effects.

Polymers are essential materials for creating drug delivery systems because they can be formulated into various physical shapes and compositions. Effective drug delivery can be accomplished with polymeric systems designed to serve as drug carriers that control release rates. Such systems typically involve combining a polymer with an active agent to form a homogeneous matrix. Under certain conditions, the active agent diffuses from the polymer matrix into the surrounding medium. Of all the polymers,

hydrogels have garnered considerable attention due to their specific properties such as biocompatibility and hydrophilicity. These properties enable hydrogels to absorb water and swell while maintaining their structural integrity, making them an attractive option for developing drug delivery systems. Furthermore, smart hydrogels can respond to external stimuli, such as changes in temperature, pH, light, or ultrasound, by undergoing reversible changes in their swelling behavior, structure, or permeability. These unique properties make them promising candidates for drug delivery systems (DDS), as they can provide a controlled and targeted release of drugs in response to specific stimuli. The development of smart hydrogels for DDS is challenging, as they require careful selection and design of the hydrogel composition, crosslinking density, and functional groups that can respond to the desired stimuli. Among these hydrogel compositions, polysaccharides are one of the most abundant classes of biomolecules found in nature and play a critical role in a variety of biological processes. In particular, chitosan is a versatile biomaterial that is produced by the deacetylation of chitin, resulting in a polymer with a cationic charge due to the presence of amino groups in its structure. Thus, chitosan possesses antimicrobial, antioxidant, and immunomodulatory properties which can provide a biocompatible and biodegradable platform for drug delivery, minimizing the risk of adverse effects and enabling safe and efficient drug delivery. However, physical chitosan hydrogels have lower mechanical strength compared to synthetic hydrogels. This can limit their use in DDS that require high mechanical stability. Pure chitosan hydrogels have a tendency to swell rapidly and can reach their maximum swelling capacity quickly leading to burst release in a short period of time. To overcome this obstacle, crosslinking chitosan hydrogel gained the attention of scientists through chemical

reactions with crosslinker agents or reinforced by synthetic polymers. Polyvinyl alcohol (PVA) is a water-soluble synthetic polymer that has been widely studied for its use in DDS due to its biocompatible and non-toxic. Because PVA can be easily dissolved in water making it easy to process and formulate into hydrogel-DDS.

There are two pathways to synthesizing hydrogel: physical and chemical crosslinking. The physical method involves the formation of a hydrogel network through non-covalent interactions between polymer chains. The most common physical method for preparing chitosan hydrogels is through the process of heating or cooling due to the helix formation, association of the helices, or creating junction zones. Additionally, physical cross-linking hydrogels are formed by ionic interaction, hydrogen bonding, and freeze-thawing. On the other hand, chemically cross-linked hydrogels can be obtained by (i) radical polymerization of low molecular weight monomers in the presence of crosslinking agents, (ii) chemical reaction of complementary groups: the presence of some hydrophilic functional groups in their structures, mainly hydroxyl (OH), amide (CONH₂), and amine (NH₂) can be crosslinked by aldehyde or epoxy, (iii) high energy radiation such as gamma, electron beams, or X-rays. The advantage of chemical crosslinks compared to physical crosslinks is to provide enhanced mechanical properties which are necessary for biomedical applications. Unfortunately, the most commonly used crosslinking agents for chitosan hydrogels, such as glutaraldehyde and formaldehyde, have some disadvantages for drug delivery applications. These agents can be toxic and their use can result in the formation of unexpected by-products, which can affect the properties of the hydrogel and potentially cause harm to the patient. Therefore, there is a need to develop alternative

crosslinking methods that are safer and more effective for use in drug delivery applications.

For this reason, the main aim of this study is to examine a drug delivery system that is activated externally and employs hydrogels as drug carriers. The two polymers chosen for the experiment were chitosan and polyvinyl alcohol, which were subsequently modified and characterized. Moreover, gamma irradiation and crosslinked by EGDE agent are considered as the green methods to fabricate the hydrogel matrix which plays a crucial factor for smart DDSs. In this current research, the model drug utilized was amoxicillin, which is an antibiotic similar to ampicillin. Amoxicillin is a semi-synthetic antibiotic that possesses a broad range of bacteriocidal activity against various gram-positive and gram-negative microorganisms, commonly prescribed for the treatment of bacterial infections as part of wound healing therapy. Several kinetic models, including the zero-order, first-order, Higuchi, Hixson–Crowell, and Korsmeyer–Peppas models, were employed to identify the drug release mechanism.

Objectives

1. To investigate the influence of the composition of CS, PVA, and gamma irradiation doses on chemophysical properties and to explore the pH-responsive behavior in the localized release of amoxicillin.
2. To study ultrasound-triggered DDSs based on amoxicillin-loaded CS/EGDE hydrogel and to measure the viscoelasticity of such hydrogels in the absence and in the presence of ultrasound.

The expected beneficial outcome(s) of this dissertation

Obtaining the crosslinked chitosan hydrogels matrix as antibiotic carriers for smart DDS under pH and ultrasound stimulation.

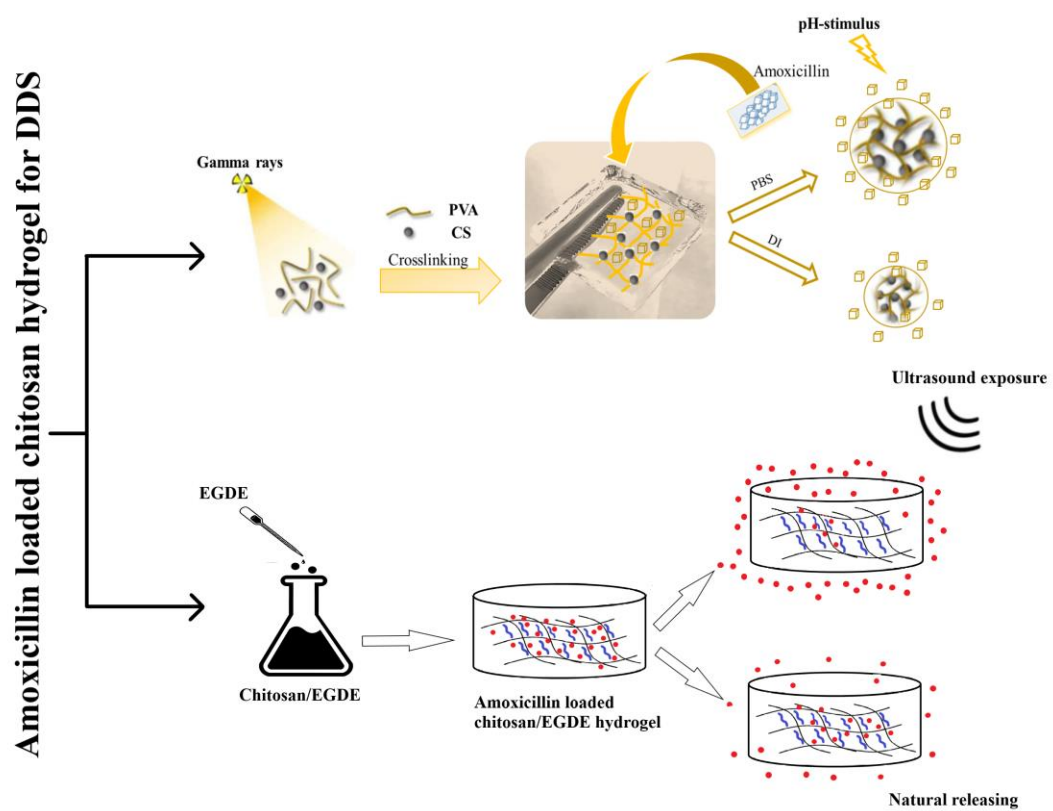


Figure 1.1 Schematic of Amoxicillin entrapped Chitosan/Ethylene glycol diglycidyl ether hydrogel for drug delivery systems

CHAPTER 2

THEORIES AND LITERATURE REVIEWS

2.1 Hydrogel

2.1.1 General Introduction of Hydrogel

Hydrogel materials are a class of cross-linked hydrophilic polymers that can absorb water and retain it within their three-dimensional networks [1]. In simple terms, a hydrogel is a flexible structure composed of a network of hydrophilic polymers that have been physically or chemically linked together including chemical crosslinker reagents, temperature, pH changes, freeze-thaw [2], irradiation [3], and enzymatic crosslinking. The hydrophilic polymer within the hydrogel contains water-attracting functional groups like carboxylic, hydroxyl, and amide groups, which enable the hydrogel to absorb and retain water. The cross-links between the polymer chains prevent the gel from dissolving when in contact with water. The cross-linking density affects the diffusion of water, ions, and small molecules in hydrogels [4].

The properties of hydrogels can be manipulated by varying the crosslinking density, polymer type, and concentration. For example, increasing the crosslinking density results in a stiffer hydrogel, while decreasing the polymer concentration can result in a softer and more elastic hydrogel. Hydrogels are attractive materials for drug delivery systems (DDS) due to their capacity to embed biologically active agents and their ability to absorb and retain water [5]. The utilization of hydrogels offers effective solutions to various challenges related to formulation and drug delivery, making them highly suitable for applications in drug delivery systems, tissue engineering, and wound management. The use of smart hydrogels in drug

delivery systems provides several benefits such as reducing the frequency of dosing, ensuring the maintenance of the desired therapeutic concentration with a single dose, and minimizing potential side effects [6].

Generally, the polymer in the cross-linking process can come from synthesis or natural sources. With more robust chemical properties, the synthesis polymer grants their hydrogel better mechanical strength, but on the other hand, the degradation rate also becomes slower [7, 8]. On the contrary, natural polymers present a high degradation rate but compromise on the mechanical properties [7]. To balance those two adverse characteristics, the current advanced technologies allow engineers to manipulate the hydrogel depended on polymer molecules weight, cross-linking density, polymer sources, etc [9].

2.1.1 Classification of Hydrogel

Hydrogels can be classified into many several types:

2.1.1.1 Based on the source

Based on the source of the original polymer, hydrogel can be classified as natural and synthesis hydrogel [10, 11].

2.1.1.2 Based on polymeric composition

Homopolymeric hydrogels: referring to the hydrogel with a single monomer making the structure of the network. The characteristic of the hydrogel will depend on the nature of the monomer and how they are cross-linking together [12].

Copolymeric hydrogels: referring to two or more monomers engaging in the chain of the polymer with at least one hydrophilic component. The species can arrange in block, alternative, or random along the network [13].

Multipolymer interpenetrating polymeric hydrogel (IPN): referring to the hydrogel that comprise of a network structure containing two distinct polymer components, which are cross-linked can be either synthetic or natural. In a semi-IPN hydrogel, one of the polymer components is cross-linked, while the other component is not cross-linked [14].

2.1.1.3 Based on type of cross-linking

Hydrogels can be categorized based on the cross-linking method employed to create their three-dimensional network structure. This classification involves two main types: physically cross-linked hydrogels and chemically cross-linked hydrogels. Physically cross-linked hydrogels are typically formed using multiblock copolymers or graft copolymers, where the cross-linking occurs through physical interactions. On the other hand, chemically cross-linked hydrogels rely on covalent and irreversible bonds between functional groups to maintain their structure. Various methods, including chemical cross-linking, grafting, and radical polymerization, can be utilized to prepare chemically cross-linked hydrogels. In the synthesis of hydrogels, a cross-linking agent is employed to facilitate the formation of a three-dimensional network through chemical cross-linking [15].

2.1.1.4 Based on the network electrical charge

By the basis of presence or absence of electrical charge on the cross-link network, hydrogels can be classified into three categories: ionic (anionic and cationic), amphoteric electrolyte, and zwitterionic [16].

2.1.2 Properties of Hydrogels

The physicochemical properties of hydrogels have a significant impact on the applications, making them important considerations in material engineering. This section is dedicated to delve into the spatial properties of hydrogel, which are primarily responsible for its behavior and its utilization.

2.1.2.1 Swelling behavior

The presence of the hydrophilic group in the network give hydrogel the ability to absorb, swell, and retain a high amount of aqueous solutions up to several thousand times of their own dried weight. To determine the swelling behavior of hydrogels, the sample is immersed in distilled water at room temperature and monitored by frequent weighing. To ensure accuracy, the swollen polymer is removed from the water and any surface moisture is wiped with tissue paper before weighing [12]. The swelling degree (SD) is used to express the ability of the hydrogel to swell, and is calculated using the equation (1). Where W_d is the weight of the dried hydrogel (g), W_t is the weight of the swollen hydrogels at time t (g).

$$SD = \frac{(W_t - W_d) \times 100}{W_d} \% \quad (1)$$

The swelling behavior of chitosan hydrogels is pH-dependent, influenced by the dissociation of $-\text{NH}_3^+$ ions, which is characterized by a dissociation rate constant known as pKa [17]. The swelling properties of chitosan-based superporous hydrogels are significantly impacted by the methods of drying and the density of crosslinking [18]. Furthermore, new pH-sensitive chitosan hydrogels have been developed and extensively studied to comprehend their swelling behavior and water states [19]. These investigations emphasize the importance of

comprehending the swelling characteristics of chitosan hydrogels under diverse conditions, as they hold potential for applications in drug delivery, tissue engineering, and other areas within the biomedical field. Chitosan hydrogels demonstrate significant swelling behavior under acidic conditions, while their swelling remains relatively stable within the pH range of 6 to 10 [19]. The high swelling observed at low pH is attributed to the electrostatic repulsion between ionized amino groups, causing the surface of the hydrogels to expand. This expansion facilitates the penetration of water and acidic substances into the hydrogel sample, contributing to its swelling behavior.

2.1.2.2 Mechanical Properties

Visually, hydrogel appears as a soft, rubbery, and transparent material. When mentioned about mechanical properties of hydrogels, many factors like shear module (G' and G''), viscoelasticity and tensile strength are appointed [20]. The mechanical properties of hydrogels from chitosan have been studied, and the results confirmed that hydrogels behave as elastic materials [21]. One the important factors impact on the mechanical property of the hydrogel is the degree of crosslinking [22]. Usually the denser the cross-linking gel requires a higher external force to deflect, leading to the fact that higher density crosslinking gel have better strength, hardness, or stiffness. Besides the density of crosslinking, polymer sources and type of crosslink also affect the mechanical properties of the hydrogel [23].

2.1.2.3 Viscoelastic properties

The viscoelastic property of hydrogels plays a crucial role as it provides insights into their specific flexible nature for application on the human body [24].

Hydrogels possess inherent viscoelasticity, meaning they exhibit both viscous and elastic behavior. However, due to their porosity and the presence of water, their viscoelastic behavior becomes complex. To assess and understand the viscoelastic properties of hydrogels, dynamic (oscillatory) rheology is employed. This technique allows for the characterization of the frequency-dependent mechanical properties of materials, enabling a comprehensive understanding of the viscoelastic behavior of hydrogels [25].

2.1.2.4 Biodegradable properties

Biodegradation refers to the capability of a material to decompose through enzymatic or chemical reactions caused by microorganisms when implanted in a living organism (in vivo). Under physiological conditions, labile bonds present in the polymer backbone or cross-links can be hydrolyzed, leading to the breakdown of the material [26, 27]. There are two methods that are commonly used to assess the rate of biodegradation in hydrogels: enzymatic degradation and microbial degradation.

2.1.2.5 Biocompatibility and Cytotoxicity

Biocompatibility and cytotoxicity are important characteristics for biomedical applications. Biocompatibility consists of two main elements: biosafety and bio-functionality. In vitro tests for biocompatibility are generally performed in two different ways. The first method involves positioning the hydrogels in direct contact with host environmental cells and incubating them for a specific period at 37°C. In the other method, the material is placed in a suitable physiological solution and incubated for a specified period of time at 37°C to allow for any leaching from the material. The obtained leachates are then used to conduct

biocompatibility tests in the presence of cells [28]. Cytotoxicity tests usually involve assessing cell viability and cell proliferation. Cell proliferation is visualized by microscopy and by carrying out the MTT assay, a colorimetric method that allows for the quantification of cell growth and proliferation [29].

Hydrogels are highly biocompatible due to their hydrophilic surface and low interfacial free energy, which results in low protein and cell adhesion [30].

2.1.3 Application of hydrogels in biomedical approach

Hydrogels have versatile applications due to their unique structures and compatibility with different conditions. Their water content provides flexibility, making them useful in various fields ranging from industrial to pharmaceutical. Moreover, their biocompatibility and non-toxic chemical behavior in biological environments extend their applications to medical sciences, are shown in Table 2.1.



Table 2.1 Applications of hydrogel

Biomedical Application	Hydrogels	Specific medical condition or target tissue	Advantages	Reference
Contact Lenses	Chitosan hydrogels	Correction of vision impairment with the ability of drug delivery	Electrochemical cross-linking has been found to enhance the transmittance and toughness of hydrogels without compromising their oxygen permeability.	[31]
	Poly(2-hydroxyethyl methacrylate-co-quaternary ammonium salt chitosan) hydrogel		p(HEMA-co-mHACC) hydrogel with tear protein deposition resistance and antimicrobial activity	[32]
	Polyacrylamide semi-interpenetrating network hydrogel including quaternized chitosan and tannic acid (PAM-QCS-TA)		Antibacterial and antioxidant properties, which relieved oxidative stress and protect cells	[33]
	Poly(vinyl alcohol) (PVA) soft hydrogel		A water content of 78 % and a tensile strength of 50 kg/cm ² , five times as strong as that of commercial poly(2-hydroxyethyl methacrylate) soft contact lens.	[34]
Tissue Engineering	CS-based injectable hydrogels	Bone and dental tissue	thermo/pH-response are advantageous in terms of their high-water imbibing capability, minimal invasiveness	[35]
	Dimethyl 3-3, dithio bis' propionimidate (DTBP)-crosslinked chitosan scaffolds	Skin tissue engineering	The toxicity of DTBP-crosslinked chitosan scaffolds is improved over glutaraldehyde - crosslinked scaffolds.	[36]
	Chitosan-hydroxyapatite system	Bone tissue	Positive cell encapsulation indicates possible application of prepared hydrogel as a cell carrier.	[37]
	Injectable chitosan hydrogel	Skin tissue regeneration	Good biocompatibility, non-toxicity, non-immunogenicity, good porosity, large surface volume ratio	[38]

	PVA/Dextran-aldehyde composite hydrogel	Skin Tissue regeneration	High fluid absorption (6 times of original weight), high tensile strength (5.6 MPa), interconnected porous networks (5–10 μm)	[39]
	PVA/Glucose hydrogels	Glucose in blood sensor	Rapid response (1s), high response current (μA level) to glucose, high specific surface area and porous structure	[40]
Biosensor	Chitosan-based hydrogels	Bioelectronic sensing	Biocompatibility, stimulus response, and tissue-like structure.	[41]
	Chitosan hydrogels	Mussel-inspired sensor	pH-responsive and adjustable adhesion, toughness and self-healing capability	[42]
Drug delivery	Chitosan-grafted-glycidyl methacrylate (CTS-g-GMA) and poly(ethylene glycol)diacrylate (PEGDA)	Amoxicillin	For gastric ulcer treatment with enhanced mechanical properties	[43]
	L-glutamic acid grafted chitosan (CH-g-GA) hydrogel prepare by gamma-irradiated graft copolymerization	Doxorubicin	High swelling ratio (426%) with extended period of drug release (81.33% in 144h)	[44]
	Carboxymethyl chitosan and poly(vinylpyrrolidone) based irradiation crosslinked hydrogels	Kanamycin	Good cell viability, cumulative drug release of more than 90% at 168 h at pH 7.4	[45]
	Core-shell chitosan cross-link hydrogels into a microcapsule	Poly(lactic-co-glycolic acid) (PLGA)	Acid triggering dissolve the chitosan shell, the drug load particles slowly release the drug.	[46]
	Drug loaded membrane by GG (guar gum), CS (chitosan) and PVA (polyvinyl alcohol)	Amoxicillin Doxycycline Hyalite	25 mg of drug was loaded on the membrane with high swelling ability for drug delivery	[47]

2.2 Polymer based hydrogels

Based on the origin polymer of hydrogel, hydrogels can be classified into three distinct categories namely natural polymer, semisynthetic polymer, and synthetic polymer. Each of those type of polymers carries a its own pros and cons. Based on their potential application, the specific type of hydrogels should be targeted and modified to balance the advantages and disadvantages of its properties.

2.2.1 Natural polymer

Natural polymers, derived from plants, microorganisms, and animals, provide structural support to living organisms and are composed of carbohydrates and proteins. The six primary types of natural polymers are proteins, polysaccharides, polynucleotides, polyisoprenes, polyesters, and lignin. Natural polymers offer economic advantages, as they are readily available, potentially biodegradable, and biocompatible due to their origin, making them a promising choice for various applications. Standing as the second most abundant polymer in the world (behind cellulose) [48], chitin and its derived – chitosan has been seen as the valuable material in making hydrogels. Chitosan is obtained by the partially deacetylation of natural chitin [48]. By the deacetylation, chitosan contains more amino groups compare to chitin, made it become more soluble. In other word, the more deacetylation from chitin to chitosan, the more biocompatibility and biodegradability chitosan become. Chitosan is a linear polysaccharide composed of randomly distributed N-acetyl-D-glucosamine and D-glucosamine units which can be found in crustaceans, insects, and fungi [49]. Chitosan has unique properties such as biodegradability, biocompatibility, low toxicity, and cohesion, making it a

promising material for various biomedical applications. Chitosan nanoparticles are effective in drug delivery and also enhance the therapeutic efficacy of the drugs. Due to their in-situ gelling properties and mucoadhesive character, chitosan nanoparticles was used in oral drug delivery as they open the tight junctions of the mucosal membrane and enhance absorption [50]. The porous nature of chitosan-based matrices allows for the encapsulation and controlled release of drugs, providing sustained therapeutic levels over an extended period [51]. Chitosan can be solubilized by protonation of the amino group (-NH₂) present in its D-glucosamine units. This protonation occurs in an acidic environment, transforming the chitosan polysaccharide into a polyelectrolyte. The solubility of chitosan increases with a higher degree of protonation. The solubility features of chitosan are influenced by both its molecular weight and degree of deacetylation. Molecular weight refers to the size of the chitosan polymer chain, with higher molecular weight chitosan typically having lower solubility. On the other hand, the degree of deacetylation refers to the extent of acetyl group removal from the chitin precursor, resulting in a higher proportion of amino groups available for protonation. Higher degrees of deacetylation lead to increased solubility of chitosan [52]. However, chitosan are still facing with some obstacles like high degree of variability in natural materials derived from animal sources and structurally more complex causing low mechanical properties of natural polymer based-biomaterials [53]. It is necessary to improve this drawback of chitosan-based biomaterials by facilitating through chemical reactions. By utilizing the protonated amino groups, chitosan can effectively interact with other polymers, resulting in enhanced mechanical properties. This capability opens up opportunities to optimize the performance of

composite materials and improve their mechanical strength in various applications [54].

2.2.2 Synthetic polymer hydrogel

In order to overcome the disadvantage of natural polymer, synthesis polymer had been chosen as an alternative to enhance the mechanical properties of the hydrogel. Polyvinyl alcohol (PVA) is a water-soluble synthetic polymer that has been widely studied and utilized in various biomedical applications. For examples, ophthalmic solutions containing 1.4% polyvinyl alcohol of tear replacement solutions without experiencing any ocular discomfort [55]. Tramadol–Dexketoprofen combination loaded in PVA film was formulated with high drug release effectiveness up to 80 % of drug-entrapped in PVA film [56]. The crosslinked structure of poly(vinyl alcohol co-vinyl acetate) exhibits intriguing physical and chemical properties that have yet to be fully explored and understood for their potential in tissue engineering applications. By combining two key attributed of this scaffold, namely controlled molecule delivery and support for cell growth, a smart scaffold is created [57]. Being well-known for its excellent biocompatibility, non-toxicity, and adjustable properties, PVA stands out as a suitable candidate for creating composite hydrogels with natural polymers [58]. A promising drug delivery system for COVID-19 treatment involves the use of a hydrogel based on Laponite® RD (Lap) trapped within a poly(vinyl alcohol) (PVA) matrix, which is obtained through the freezing/thawing method. These Rif-loaded PVA/Lap hydrogels offer potential as effective drug delivery systems for COVID-19 treatment. They aim to achieve a synergistic therapeutic effect by dual targeting of the viral 3CLpro enzyme and S proteins, thereby enhancing the efficacy of the treatment approach

[59]. Additionally, PVA has a high degree of hydrophilicity, which enables the formation of strong hydrogen bonding with natural polymers, such as chitosan, resulting in a more stable and efficient network. However, neat synthetic polymers may not always be suitable for biomedical applications due to their lack of biocompatibility and biodegradability. Therefore, a combination of both synthetic and natural polymers can result in a composite hydrogel with superior mechanical and biological properties. In recent years, the development of composite hydrogels has gained significant attention in the field of biomaterials due to their potential for use in various biomedical applications, especially in drug delivery. The combination of natural and synthetic polymers can result in hydrogels with improved properties such as enhanced mechanical strength, increased stability, and prolonged drug release kinetics [60].

2.3 Methods to synthesize hydrogel

The properties of hydrogels including their porosity, swelling capacity, mechanical strength, and biodegradability, can be influenced by the method of crosslinking [61]. Therefore, the selection of preparation techniques may significantly impact the biological functions of the produced hydrogels. Hydrogels can be classified as physical or chemical gels based on the primary interactions involved in forming the network. Physically crosslinked hydrogels are created by secondary interactions which involve electrostatic attraction, hydrogen bonding, and hydrophobic interaction [62]. Meanwhile, the chemical crosslinked hydrogels are created through covalent bonds that occur between the functional groups of crosslinkers and chitosan [63].

2.3.1 Physically crosslinked hydrogels

The polymeric chain in the hydrogels is mainly connected by entanglement or physical interaction including electrostatic interaction and hydrogen bonding.

Electrostatic Interactions: Chitosan, being a positively charged polysaccharide, is capable of eliciting electrostatic interactions with molecules that possess a negative charge (with low molecular weight (MW) ion such as sulphates [64], citrates [65]). The strength of these ionic interactions is influenced by the degree of deacetylation (DDA) and MW, and concentration of chitosan, as well as the size, density, and ionic charge of anionic groups [66]. In addition, chitosan can combine with anionic polymers to form polyelectrolyte complexes (PECs) through electrostatic interactions between polyions with opposite charges. Various anionic polysaccharides like alginate, pectin, dextran, and gellan gum, proteins such as silk fibroin protein and collagen, as well as synthetic polymers like poly(acrylic acid), poly(L-lactide), and polyphosphate, can all create PECs when combined with chitosan [63]. A novel and versatile method has been developed to create dynamic hydrogels through the controlled interactions between positively charged biopolymers and polyoxometalate (POM) anions. By immersing primary networks in aqueous solutions of POMs with different nuclearity and charges, hydrogels were formed. The integration of pre-dispersed chitosan in this process resulted in the formation of double network (DN) hydrogels. These DN hydrogels exhibited significantly higher toughness, surpassing the toughness of previous composite hydrogels by 2-3 orders of magnitude [67].

Hydrogen bonding: hydrogen bonding involves the attraction between a hydrogen atom attached to a molecule and a highly electronegative atom on another

molecule [68]. The most common hydrogen bonding sites within hydrogels are amine, amide, alcohol, and carboxylic acid groups [69]. A self-healing hydrogel based on chitosan has been successfully created using noncovalent interactions, specifically hydrogen bonding between acrylamide segments and chitosan backbone. This autonomous hydrogel has the ability to spontaneously repair itself due to the reversible nature of the hydrogen bonds formed between the polymer segments and chitosan [70].

Therefore, physically crosslinked chitosan hydrogels have been explored extensively in drug delivery applications, owing to their minimal toxicity, and good biocompatibility without chemical modification. Nevertheless, the nature of reversible and unstable network produced the limitation of physical crosslinking.

2.3.2 Chemically crosslinked hydrogels

The primary interactions that create the network in chemically crosslinked hydrogels are covalent crosslinks between various reactive amino and hydroxyl groups of chitosan and the functional groups present in the crosslinker. The chemical crosslinkers can be added during the gelation process, and their concentration and reactivity can be adjusted to control the degree of crosslinking.

2.3.2.1 *Gamma-irradiated chitosan hydrogels*

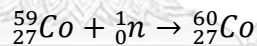
Gamma radiation

Radiation chemistry is a field of chemistry that studies the chemical changes that occur due to the absorption of high-energy ionizing radiation. This type of radiation may come in the form of electromagnetic radiation with a short wavelength between 10-100 nm and an energy of approximately 10-100 keV, such as X-rays, γ -rays, or particulate radiation like electrons and protons [71]. The most

commonly utilized source of γ -rays for chemical studies in industry, medicine, and research is cobalt-60.

Gamma radiation, also referred to as gamma ray, was first identified by French scientist Paul Villard in 1900 and named by Ernest Rutherford in 1903. This type of radiation is ionizing and originates from the nucleus of a radioactive atom. The wavelength of gamma radiation is incredibly small, measuring less than 0.01 nm, which makes it the shortest wavelength in the electromagnetic spectrum. Due to this short wavelength, gamma radiation has the highest frequency, which is approximately 10^{19} Hz. Furthermore, gamma radiation has the greatest energy of all electromagnetic radiation types [72].

The radionuclide cobalt-60 can be created in a nuclear power reactor by irradiation of cobalt-59 with neutrons as displayed in Equation 1 [73].



Cobalt-60 is an unstable atom due to the excess neutron it contains [74]. As illustrated in Figure 2.1, it undergoes radioactive decay and transforms into a stable nickel-60 by emitting photons with energies of 1.17 and 1.33 MeV [75].

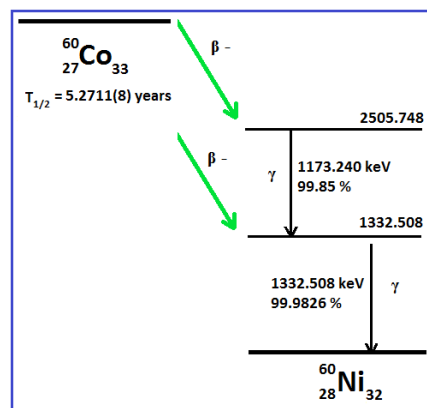


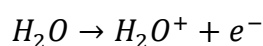
Figure 2.2 Disintegration of ${}^{60}\text{Co}$

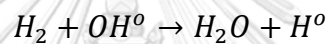
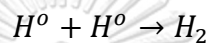
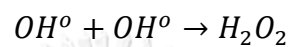
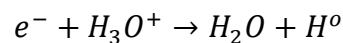
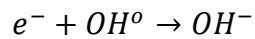
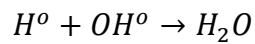
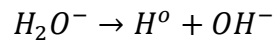
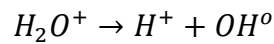
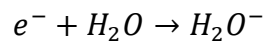
Radiation effects on materials that have been exposed to radiation can be classified into two categories: direct and indirect effects. Direct effects refer to the decomposition of chemical bonds caused by the energy of the radiation [76]. This energy can cause molecules to become ionized or excited to a higher energy state. Indirect effects, on the other hand, are also important in the overall action of radiation. They occur through the continuous reactions of radiolytic products, particularly hydroxyl radicals ($\text{OH}\cdot$), solvated electrons (e_{aq}^-), hydrogen radicals ($\text{H}\cdot$), hydrogen peroxide (H_2O_2), and hydroperoxyl radicals (HO_2°).

Effect of Ionizing Radiation in Aqueous Solutions

Hydrogel was successfully synthesized by polymer crosslinking using ionizing radiation [77]. Polymers used in this research were chitosan and polyvinyl alcohol (PVA). Both polymers could be crosslinked by the irradiation method. Chitosan is an important component of naturally occurring organic compounds widely distributed in marine species and generally occurs in nature associated with water. PVA is a synthetic water-soluble polymer that is commonly used in biomedical applications due to its high tensile strength and can form a three-dimensional hydrogel network.

The initial steps of radiolysis involve the generation of reactive species when aqueous solutions are exposed to radiation [78]. Solvated electrons, which react slowly with carbohydrates, and -OH radicals and atoms, which react more easily, are examples of these reactive species. Polymers can have their carbon-bound hydrogen atoms removed by both $\text{OH}\cdot$ and $\text{H}\cdot$. Figures (a) and (b) depict the radiolysis of water and the incorporation of free radicals [79], respectively.





Secondary stages of polymer crosslinking reactions [80]

Hydroxyl and hydrogen radicals are highly reactive species that can interact with a variety of molecules, including polymers like CS and PVA. When these radicals come in contact with the polymer chain, they can abstract a hydrogen atom from the carbon backbone, leaving behind a carbon-centered radical. This can lead to the formation of new covalent bonds and crosslinking between polymer chains.



Gamma sterilization [81]

Definition of sterilization is a process or method that eliminates all forms of life, especially microorganisms such as viruses, bacteria, and fungi. A gamma irradiation dose of 25 kGy can sterilize devices and materials and it is recommended for medical purpose [82].

Advantages of gamma sterilization [83, 84] are

- 1) Good certainty of product sterilization, which is better than filtration and aseptic processing.
- 2) No waste or residue, which is better than chemical process such as EtO.
- 3) More penetrating, which is better than e-beam.
- 4) Ability to process at low temperature.
- 5) Simple validation process.

There are frontier researchers on the fabrication of CS hydrogel and their composites using gamma irradiation applied for biomedical applications. According to Safiya Nisar and partners, chitosan-based hydrogel beads were prepared using L-glutamic acid as a monomer and gamma-irradiated graft copolymerization technique. These hydrogel beads were loaded with the anti-cancer drug Doxorubicin and showed potential as an anti-cancer drug delivery system with high swelling ratio (426%) and drug release (81.33% in 144 hours). The system demonstrated effective MCF-7 cancer cell toxicity and exhibited effective cancer cell toxicity of about 78.18%, thus it can be used as a potent anti-cancer drug carrier [44]. Cs/Au nanocomposites, consisting of gold nanoparticles and chitosan, were created by irradiating Cs/Au solutions with varying doses. The spherical-shaped gold nanoparticles formed were free of aggregation. These nanocomposites were tested as an anticancer agent and found to be more effective in inhibiting the proliferation of HepG-2 and CACO-2 cells compared to neat chitosan. The concentration required to inhibit 50% of the cells was lower for Cs/Au nanocomposites than for chitosan on both cell lines [85]. A new hydrogel was created by physically mixing CH and P407 and then cross-linking it with

gamma irradiation, called CH-P, which was evaluated for its wound-healing properties. The hydrogel has the ability to gel and reverse at low temperatures, making it easy to apply to wounds. CH-P also maintains its antimicrobial/antifungal properties through its acidic pH and CH characteristics. CH-P 7 demonstrated the highest wound-closure rate in the first week of testing on mice [86]. Hydrogels composed of chitosan (CS), gelatin (Gel), and polyvinyl alcohol (PVA) were created using gamma irradiation for use as wound dressings. These hydrogels demonstrated good pH sensitivity, swelling capacity, and water evaporation rate. The swelling ratios of all hydrogels decreased when the pH values of PBS exceeded 6.0. Despite this, these hydrogels have great potential as wound dressings [87]. Wenhui Guo's study describes an effective method for producing PVA-based composite hydrogels, which are double cross-linked using gamma radiation-induced chemical crosslinking and physical crosslinking between polyvinyl alcohol (PVA), chitosan (CS), and tannic acid (TA). The hydrogels are first prepared using gamma radiation and then immersed in TA solution to form a second physical network, resulting in a composite hydrogel with improved mechanical properties. Furthermore, the inclusion of TA creates a strong physical crosslinking network and gives the composite hydrogels antibacterial properties, making them a promising material for use in biomedical applications and soft devices [88]. A Hybrid polymer network (HPN) consisting of chitosan (CS) and poly(vinyl alcohol) (PVA) was created using radiation-degraded chitosan. During irradiation, the chemical structure of chitosan underwent chain scission reactions that reduced its molecular weight and altered its hydrophilicity. The study demonstrates that the molecular weight of chitosan decreases sharply with the

lowest molecular weight of 5.53×10^4 g/mol observed in the sample irradiated at 100 kGy compared to 25 kGy. The radiation-degraded chitosan was then utilized in the dissolution casting method to produce the HPN, and the study examined how the molecular weight of chitosan influenced the structural, thermal, and surface characteristics of HPN [89]. The process of radiation grafting chitosan with 2-acrylamido-2-methyl propane sulfonic acid (AMPS) was carried out successfully. The hydrogel formed from chitosan-AMPS had the highest equilibrium degree of swelling (38.6 g/g) and gel percentage (94.7 %) when the AMPS content was at 40% and the absorbed dose was 10 kGy. The hydrogel contained poly-electrolytes that acted as sorbents and ion exchangers, which could help purify wastewater. The chitosan-AMPS hydrogel was synthesized using gamma irradiation for use in the sorption of dyes or metal ions from wastewater [90]. The method of creating chitosan-poly(ethylene glycol) diacrylate (CS-PEGDA) beads through radiation-induced crosslinking was used. The CS-PEGDA beads had maximum porosity (97.50 ± 0.73 %) and swelling degree (48.32 ± 4.90 %) when irradiated with gamma radiation at 25 kGy. The concentration of PEGDA and radiation dose were important factors in controlling the porosity and swelling degree of the beads. To load peppermint oil into the CS-PEGDA beads, a concentration of 0.25 mg/ml was used, resulting in an encapsulation efficiency of 93 ± 0.51 %. The release of peppermint oil from the beads was controlled for approximately ten days (230 h).

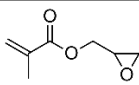
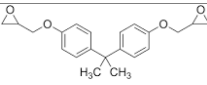
2.3.2.2 Chitosan based-hydrogel through chemical reactions

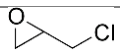
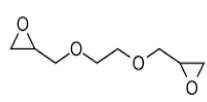
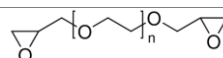
Typical crosslinkers for crosslinking hydrogel include epoxy [91], carbodiimides [92], aldehydes [93], and genipin [94]. Among them, hydrogels can be produced by crosslinking polysaccharides with epoxy groups via a process called epoxy-

amine crosslinking [95]. This process involves the reaction of the amine groups present in a polysaccharide with the epoxy groups present in a crosslinker molecule, which is generally a bifunctional epoxy compound. The resultant network of crosslinked bonds forms a hydrogel that can absorb water and expand, while still retaining its structural integrity. Epoxy groups are highly reactive and can form covalent bonds with a variety of functional groups, including amine and hydroxyl groups on polysaccharides. This allows for efficient crosslinking and the formation of stable hydrogels [96]. The degree of crosslinking can be controlled by adjusting the concentration of the epoxy compounds. This allows for the mechanical and swelling properties of the hydrogel to be tailored to biomedical application [97].

Some common epoxy compounds used for crosslinking polysaccharides including glycidyl methacrylate (GMA), diglycidyl ether of bisphenol A (DGEBA), epichlorohydrin (ECH), ethylene glycol diglycidyl ether (EGDE), and polyethylene glycol diglycidyl ether (PEGDGE) that were summarized in Table 1.

Table 2.2 Prevalent epoxy crosslinkers

Crosslinker	Composition	Chemical structure	Advantage	Disadvantage	References
Glycidyl methacrylate (GMA)	An epoxy group and a methacrylate group		-Highly reactive	-Cytotoxicity	[98, 99]
Diglycidyl	Two epoxy		-Highly reactive	-Endocrine	[100]

ether of groups bisphenol A (DGEBA)			-Excellent mechanical properties for hydrogel	disruption and toxicity -High viscosity	
Epichlorohydrin (ECH)	An epoxy group and a chlorohydrin group		-Highly reactive	-Potential health concerns: carcinogenicity and mutagenicity	[101]
Ethylene glycol diglycidyl ether (EGDE)	Bifunctional epoxy		-Highly reactive -EGDE-crosslinked hydrogels have good swelling properties	-Flammability	[96]
Polyethylene glycol diglycidyl ether	Bifunctional epoxy		-Low toxicity	-High viscosity -Longer reaction times	[102]

(PEGDGE)

Additionally, EGDE is a less toxic compound with bifunctional epoxy groups that are reactive towards hydroxyl, carboxyl, amino, and sulfhydryl groups [103]. This property makes it a popular choice for crosslinking biopolymers like DNA, proteins, and polysaccharides [104]. Compared to other dialdehydes, EGDE has a lower toxicity level and has been widely used for crosslinking. The reaction of EGDE occurs under alkaline conditions, i.e., pH above 7 [105].

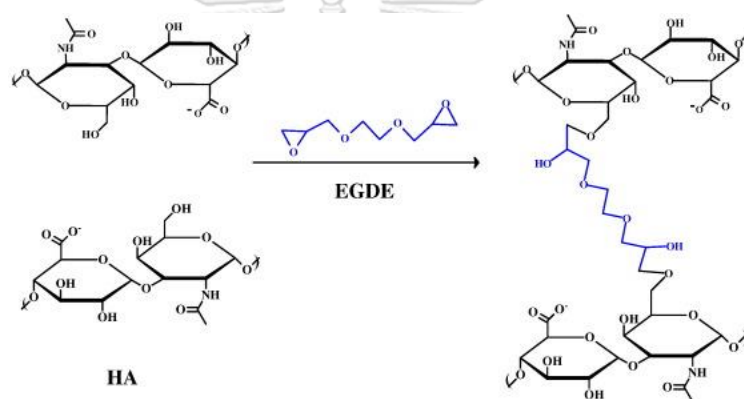


Figure 2.3 Cross-linking of hyaluronic acid (HA) using ethylene glycol diglycidyl ether (EGDE)[106]

To create hydrogels that have strong mechanical properties and are based on hyaluronic acid, a biomacromolecule with specific biological functions. To achieve this, hyaluronic acid was crosslinked in aqueous solutions using the cross-linker EGDE. The resulting hydrogels displayed a compressive modulus of 0.9 MPa and were able to sustain compressive stresses of 19.4 MPa. These strong mechanical properties and high water content, which makes them an excellent material for biomedical applications where stress-bearing is needed [106]. Olayide S. Lawal et al., focused on creating hydrogels through the cross-linking of carboxymethyl cellulose using di- or polyfunctional glycidyl ether. The process involves the

reaction of polysaccharides with di- or poly-epoxy compounds, which begins with the formation of polysaccharide alkoxides following the addition of NaOH. When the epoxy compound is introduced, the ring opens and a new macromolecular epoxy is produced. This new macromolecular epoxy then undergoes a reaction with other polysaccharide carbonyl anions, leading to the formation of a bridge between chains. A representative reaction scheme is depicted in Fig 2 to illustrate the process. The research findings suggest that hydrogels made with difunctional epoxy group cross-linkers exhibit higher swelling properties than those made with multifunctional epoxy group cross-linkers. Additionally, the study revealed that swelling increases with an increase in the chain length of the cross-linker, but decreases as the number of epoxy groups increases. Therefore, it is possible to produce carboxymethyl cellulose hydrogels with desired swelling properties by carefully selecting the appropriate cross-linkers [107].

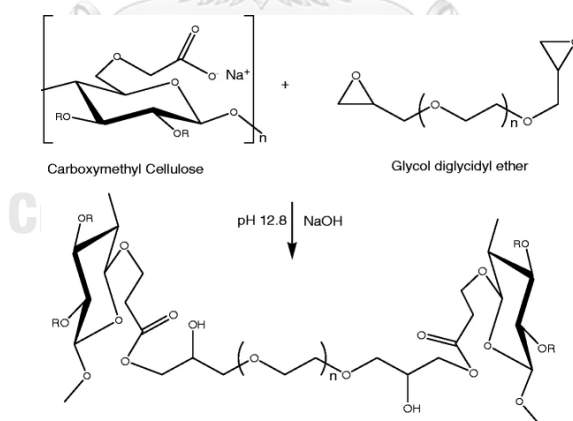


Figure 2.4 The main cross-linking reaction of carboxymethyl cellulose with glycol diglycidyl ether[107]

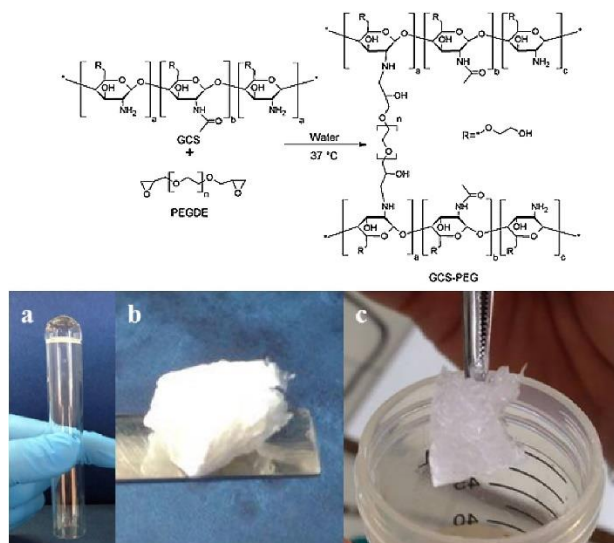


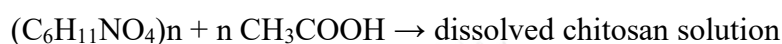
Figure 2.5 The chemical crosslinking of GCS with PEGDE in water at 37 °C and optical images of GCS-PEG 1% (w/v) crosslinked with PEGDE 0.08% (mol/mol). In particular: a) just prepared GCS-PEG hydrogel; b) freeze dried GCS-PEG; c) swollen after freeze drying[102].

The study proposes a straightforward method to create a chemical crosslinking of glycol-chitosan (GCS) through a one-step process that takes place in water at 37 °C. GCS is a derivative of chitosan that is water-soluble in physiological conditions and has advantageous biological properties, which make it potentially useful for tissue engineering applications. It is non-toxic and can stimulate chondrocyte growth at low concentrations. Thus, the proposed method for creating chemical crosslinking in GCS is an efficient and practical approach to leverage the desirable characteristics of GCS for tissue engineering applications [102].

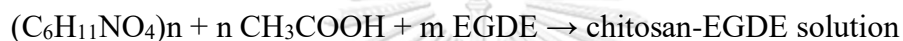
The properties of cross-linked chitosan products are largely dependent on the characteristics of the cross-linking agent used. Recently, there has been considerable interest in using ethylene glycol diglycidyl ether (EGDE) as a successful alternative for modifying chitosan due to its desirable features, including non-toxicity, water solubility, and bifunctional diepoxy groups. EGDE

contains two epoxide functional groups located at both ends of each molecule, which are highly reactive compared to other ethers. The reaction between the epoxide groups of EGDE and the amino groups (-NH₂) of D-glucosamine units in the polymeric matrix of chitosan results in successful cross-linking [108].

Firstly, chitosan is typically insoluble in water at neutral pH, so it needs to be dissolved in an acidic solution such as acetic acid.



Secondly, EGDE is added to the chitosan solution dropwise while stirring.



Finally, crosslink the chitosan hydrogel in NaOH solution, the reaction between chitosan and EGDE is initiated by the addition of NaOH, which acts as a catalyst.



2.4 Drug delivery systems (DDS)

A drug delivery system (DDS) refers to a product or tool that facilitates the administration of a medicinal substance to the body. It enhances the effectiveness and safety of the drug by regulating the timing, location, and pace of its release within the body [109]. Drug delivery systems (DDS) have been evolving over time, starting from traditional large-scale systems to more advanced controlled, targeted, and responsive nanoscale systems. The modern era of drug delivery technology began with the development of Spansule® sustained-release capsules in 1952, which could provide drug release for up to 12 hours after oral ingestion [110]. Oral and transdermal formulations were the primary DDSs used until the 1980s. In the period between 1980 and 2010, also known as the second-generation era of DDSs, significant advancements were made, but their clinical applications

were not particularly impressive [111]. Currently, smart drug delivery system (SDDS) have focused on the preparation of drug carrier from natural polymers, which enable the introduction of a therapeutic substance into the body that improves its efficacy and safety by controlling the rate, time, and place of release of drugs into the body.

2.4.1 Stimulants in DDS

Smart drug delivery system (SDDS) are also known as stimuli-sensitive delivery systems, and they can be triggered by chemical or physical stimuli. The stimulants can be categorized as exogenous and endogenous stimulants. The term "exogenous" refers to external stimuli such as temperature, electric fields, light, ultrasound, and magnetic fields that can trigger drug release in drug delivery systems. In contrast, "endogenous" stimuli refer to internal chemical processes such as pH changes, enzyme activity, and redox changes that can also trigger drug release in targeted areas [112]. Endogenous stimuli-based drug delivery systems have the advantage of being more specific and targeted to the site of action, as they respond to changes in the body's natural environment. On the other hand, exogenous stimuli-based drug delivery systems, can be more easily controlled and manipulated, as the external stimuli can be applied and removed as needed [113]. The two types of drug delivery systems, endogenous and exogenous stimuli-based, have undergone significant research and development, and their efficacy is determined by the particular application and the intended result. Ultimately, the decision to utilize endogenous or exogenous stimuli-based drug delivery systems will depend on the individual requirements of the patient and the therapeutic goal.

2.4.1.1 pH-responsive systems

Unique pH-responsive materials possess high biocompatibility, and nontoxicity, and targeted drug delivery. Such materials are of pronounced interest owing to the change of swelling capacity or polymer degradation which promote the medicine release faster from the polymer matrix in the specific conditions to achieve targeted drug delivery. In particular, the majority of human tissues have a physiological pH range of approximately 7 to 7.4, with a few exceptions. Notably, the pH in the stomach is between 1 and 3, while the pH in the small intestine falls between 4 and 7. The pH of blood ranges from 7.3 to 7.45, shown in Figure 2 [114]. These variations in pH levels are significant because they can be exploited to design drug delivery systems that selectively release drugs in response to changes in pH (Figure 3). pH-responsive drug delivery systems can take advantage of these differences in pH to enhance drug efficacy and minimize unwanted side effects. pH-sensitive swelling in ionic hydrogels is caused by the presence of charge-carrying pendant groups and is influenced by various factors, including the ionic charge, pKa or pKb values of ionizable groups, degree of ionization, hydrophilicity, polymer concentration, and pH of the swelling medium. The key factors that control the properties of pH-sensitive hydrogels are pH and the nature of the functional groups. For example, cationic hydrogels like chitosan swell in acidic media (low pH) due to the protonation of amino/imine groups. The positively charged moieties on the polymer chains repel each other, leading to swelling. Such hydrogels can be used for drug delivery to the stomach during ulceritis or as carriers for an injectable drug delivery system. By releasing drugs in response to changes in pH, these systems can target specific tissues or organs while

avoiding non-target areas [115]. Additionally, chitosan is a natural, biodegradable, and biocompatible polymer that can be easily modified to have pH-responsive properties. Therefore, chitosan-based hydrogels have been used for controlled, localized drug delivery to improve the effectiveness of the treatment.

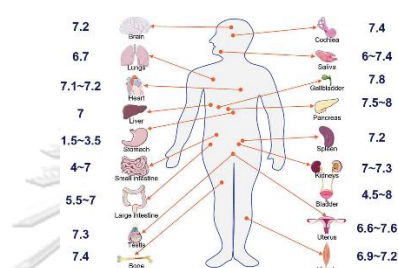


Figure 2.6 Physiological pH values in the human body[114]

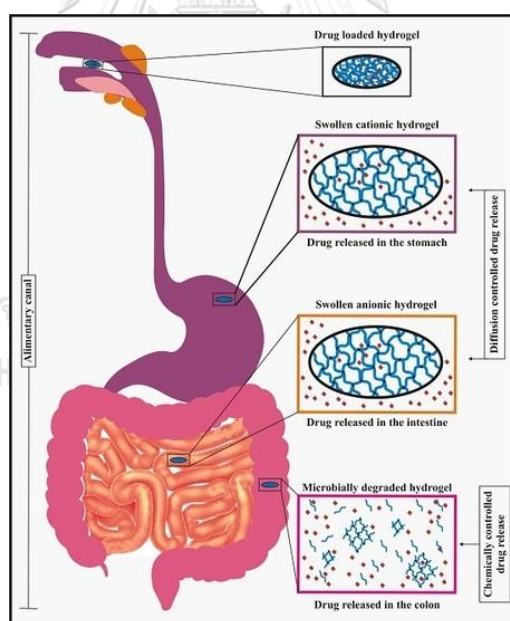


Figure 2.7 pH Sensitive Hydrogels in Drug Delivery[115]

In the previous studies, the synthesized pH-responsive compounds using chitosan and hyaluronic acid was applied to observe changes in various properties of a polymer-based drug delivery system for traditional Chinese medicine Cortex

Moutan (CM). The highest cumulative drug release (86.5%) after 5 days under mild acidic conditions (pH 6.4). These findings suggest that the pH-responsive compounds synthesized from chitosan and hyaluronic acid could be used to enhance the drug-release behavior of polymer-based drug delivery systems for CM, potentially leading to more effective treatments with reduced side effects [116]. Another study prepared a pH-responsive nanocomposite hydrogel based on chitosan grafted with acrylamide monomer and gold nanoparticles. The study found that the hydrogel exhibited pH-responsive swelling and drug release behavior [117]. A pH-responsive drug delivery system based on chitosan-coated mesoporous silica nanoparticles for the controlled release of ibuprofen (Figure 4). It was indicated that the drug was released due to protonation of the amino group on chitosan when the pH was below its isoelectric point (6.3) [118]. As a result, chitosan hydrogel responds to the environmental pH of a tissue, which, when existing within a certain acidic range, can lead to structural and chemical changes of the drug delivery system so they can deliver drugs in a targeted and controlled manner, which makes them suitable for overcoming the shortcomings of conventional drug formulations.

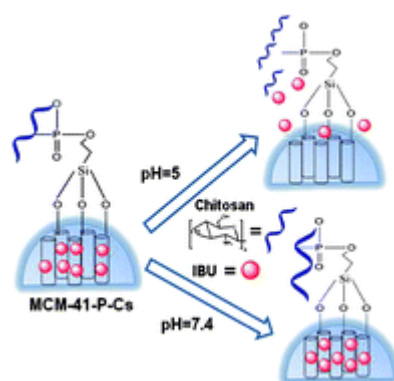


Figure 2.8 A core-shell pH-responsive drug-carrier based on chitosan-coated mesoporous silica nanospheres[118]

2.4.1.2 Ultrasound-responsive system

Ultrasound (US) has emerged as a powerful and non-invasive technology for drug delivery systems (DDS), with a wide range of applications. It can be used to achieve controlled drug release and activation in DDS, and is an attractive option due to its precision, low toxicity, and non-invasive nature. US has shown potential in biomedical imaging for implantable drug delivery systems, enabling sustained drug release. In addition, it can be utilized to target and modulate drug release in advanced drug delivery systems. Smart US-responsive drug delivery systems have been developed that can release drugs at the tumor site upon demand. Although the use of US in drug delivery systems is a relatively new concept, recent studies have demonstrated promising results, highlighting its potential as an innovative and effective approach [119].

Ultrasound, which can be classified as low frequency (<100 kHz) or high frequency (>100 kHz and MHz range), is a widely used physical factor in disease diagnosis and therapy. Research has shown that ultrasound can enhance the permeability of agents into living cells since the mid-1990s. The delivery efficiency of drugs can be improved through thermal and non-thermal effects induced by ultrasound sonication. Thermal effects are produced by the absorption of acoustic energy in biological tissues. Ultrasound can increase the temperature of the target area, causing the drug to release faster due to increased molecular mobility and solubility. The increase in temperature can also increase the permeability of the cell membrane, allowing for faster drug uptake by the cells.

Meanwhile, non-thermal effects are mainly generated by ultrasound pressure, acoustic streaming, shockwaves, liquid microjet, and ultrasound-induced oscillation or cavitation. The non-thermal effects of ultrasound can bring about alterations in the structure of the drug delivery system, leading to improved drug release kinetics. Ultrasound has the ability to create cavitation, which results in the formation and collapse of gas bubbles within the drug delivery system, thus leading to the temporary creation of pores or holes. This allows for a faster drug release. These effects have been widely studied and are considered promising for various applications in drug delivery systems [120]. In the previous researches, the development of telechelic Dopa-modified polyethylene glycol-based hydrogels was investigated that was responsive to ultrasound (US). The hydrogels are formed through Fe^{3+} -induced cross-linking of four-arm polyethylene glycol-dopamine precursors, with the molar ratio of Fe^{3+} to Dopa in the precursor solution determining the relative amounts of H bonds, coordination bonds, and covalent bonds within the hydrogels. The study finds that Fe^{3+} -[PEG-Dopa]₄ hydrogels with higher concentrations of coordination bonds are more mechanically robust and have a decreased susceptibility to US-mediated disintegration at lower intensities. However, Fe^{3+} -[PEG-Dopa]₄ hydrogels with lower concentrations of coordination bonds are more susceptible to rapid disintegration upon exposure to US, and their disintegration can be controlled through pulsed US exposure. Additionally, sustained US energy can also stabilize the hydrogels through the formation of additional cross-links via free radical-mediated coupling of pendant catechols. Overall, the study demonstrates that Fe^{3+} -[PEG-Dopa]₄ hydrogels offer a

promising class of stimulus-responsive polymers with applications ranging from smart drug delivery to transient medical implants [121].

A new self-healing hydrogel system (Fig. 5) that responds to ultrasound has been developed for personalized cancer immunotherapy. The hydrogel can release nanovaccines in response to ultrasound treatment and then self-heal into a gel. Mice injected with the nanovaccine-loaded gel and subjected to ultrasound treatments exhibited antitumor immune responses, which, when combined with immune checkpoint blockade, effectively inhibited established tumors and prevented postoperative tumor metastases and recurrence. This personalized nanovaccine system shows promise as a potential treatment option for cancer [122].

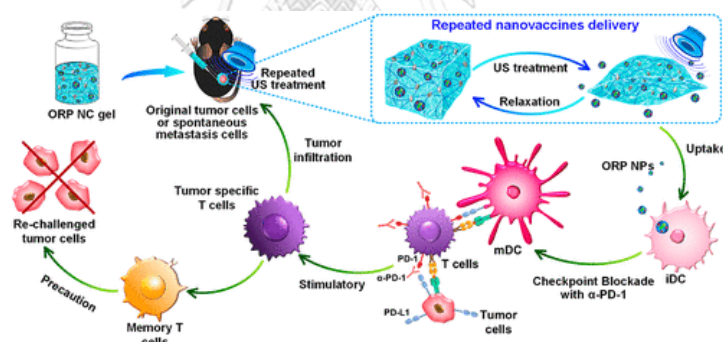


Figure 2.9 The scheme showing the fabrication of ORP NPs for immune stimulation as a nanovaccine and US-triggered release of ORP NPs from the NC gel[122].

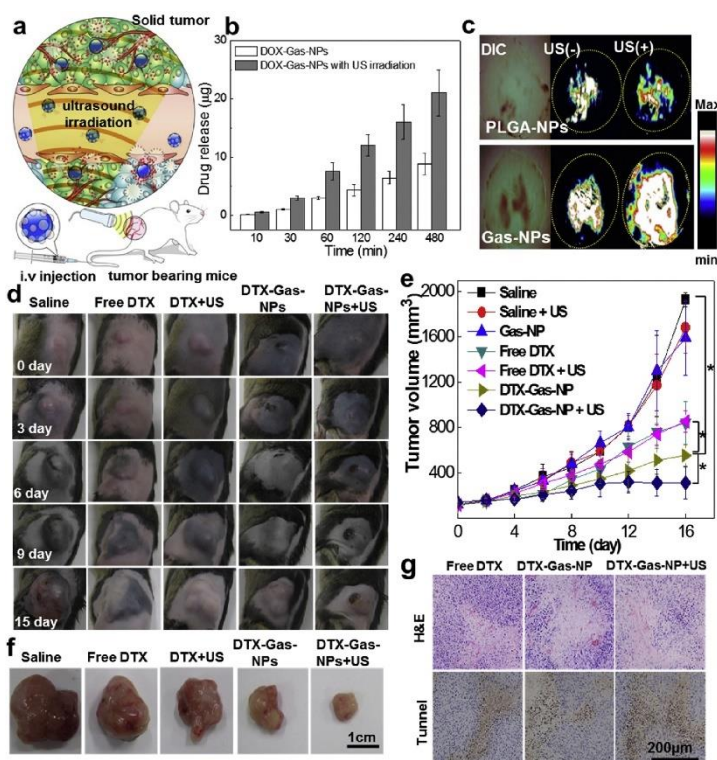


Figure 2.10 (a) Ultrasound-triggered drug release of anticancer drug-loaded Gas-NPs in tumor-bearing mice; (b) In vitro US-responsible drug release profile of DOX-Gas-NPs were studied in PBS (pH 7.4); (c) After 4 h post-injection of 100 µL of Nile red-Gas-NPs and PLGA-NPs into SCC7 tumor bearing BALB/c male nude mice; (d) Anti-tumor therapeutic efficacy of DTX-Gas-NPs (10 mg/kg DTX) without or with the external US irradiation after 16 day post-treatment; (e) The tumor volumes of each sample treated tumor-bearing mice; (f) The representative images of excised tumors after 16 day post-injection of saline, free DTX, and DTX-Gas-NPs without or with the external US irradiation. (g) Histological analysis of the excised tumor tissue was evaluated via H&E staining (upper) and TUNEL assay (lower) [123].

The researchers have created a novel theranostic nanoparticle that can generate CO₂, which has potential applications in both ultrasound imaging and cancer treatment. This nanoparticle allows for real-time ultrasound imaging while simultaneously providing site-specific and timing-specific drug delivery. In detail, to confirm the ability of Gas-NPs to generate gas, the nanoparticle dispersion by using external US irradiation destroyed the bubbles. The Gas-NPs and Sonovue® were dispersed at a concentration of 10 mg/mL and administered into an agar gel

phantom. US images were obtained for 2 minutes, followed by the application of high US power using the US destruction mode (40 MHz, 100% power) for 2 minutes using the Vevo770® software. The samples were then incubated for 10 minutes to allow for regeneration of bubbles. Using this time interval of 2 minutes on and 10 minutes off, US images and intensities were recorded for up to 1 hour. The Gas-NPs have been loaded with anti-cancer drugs and when exposed to external ultrasound, can trigger drug release leading to improved therapeutic efficacy *in vivo*, shown in Fig. 6. This unique approach of US-triggered imaging and therapy can expand the clinical applications of ultrasound from intravascular imaging to theranostic applications [123].

2.4.2 Mathematical models of drug release

In the field of drug delivery, controlled release dosage forms have seen significant advancements over the past 30 years. Drug release is a crucial aspect of therapeutic systems as it is responsible for absorption and availability of the active agent to the body. In order to achieve specific drug release profiles, it is essential to understand the mass transport mechanisms involved and quantitatively predict the resulting drug release kinetics. Modified release systems can control drug release through various methods, including dissolution, diffusion, partitioning, osmosis, swelling, and erosion. Differences in solubility of drugs, factors affecting solubility, and participation of different processes contribute to varying drug release behaviors of the same active agent incorporated in the polymeric matrix. Mathematical models, such as zero order, first order, Higuchi, Hixson-Crowell, and Korsmeyer-Peppas, can be used to describe the release profile [124].

Zero order: $C_t/C_0 = k_0t$

First order: $\log C_t/C_0 = -k_1t/2.303$

Higuchi: $C_t/C_0 = k_{ht}^{0.5}$

Korsmeyer - Peppas: $\log (C_t/C_0) = \log(k) + n \log(t)$

Hixson-Crowell: $C_0^{1/3} - C_t^{1/3} = k_{hc}t$

where C_t denotes the quantity of drug released at time t ; C_0 defines the initial concentration of drug in the hydrogel; k_0 , k_1 , k_h , k_{hc} and k are the release rate constant, and n is the release exponent which indicates the release mechanism. Zero-order kinetics is suitable for identifying the drug dissolution in certain types of controlled-release pharmaceutical doses, such as transdermal systems or osmotic systems. First-order kinetics is appropriate for studying the solubility of drugs in pharmaceutical doses, particularly those containing water-insoluble drugs in porous matrices. The drug release rate is directly proportional to the initial concentration and increases linearly with an increase in the drug concentration. The Higuchi model is used to describe the diffusion process based on Fick's diffusion law for the release of water soluble or poorly soluble drugs in insoluble and swellable porous matrices. This indicates that the release mechanism is controlled by diffusion. The equation assumes that the dissolution rate controls the drug release behavior and that there is a change in the surface area and/or diameter of particles. The Korsmeyer–Peppas model is useful for investigating the drug release mechanism from hydrogel or the existence of multiple release phenomena. In this model, a variety of parameters that contribute to polymer swelling, erosion, matrix porosity, and drug diffusion rates in swelling systems were investigated. Literature indicates that if n is less than 0.45, solvent penetration into hydrogels

follows the Fickian process. In addition, when n is between 0.45 and 0.89, drug release is governed by diffusion and polymer network relaxation. This process is referred to as non-Fickian. However, several n values greater than 0.89 represent drug release as a function of the expansion or relaxation of the polymer gel system [124].

2.4.3 Antibiotics

Antibiotics are drugs used to treat bacterial infections. Classes of antibiotics include beta-lactam, glycopeptides and lipoglycopeptides, glycyclines, tetracyclines, lincosamides, macrolides, oxazolidinones, and sulfonamides. The principle governing the use of antibiotics is to ensure that the patient receives one to which the target bacterium is sensitive, at a high enough concentration to be effective but not cause side effects, and for a sufficient length of time to determine the significance of any unpleasant reaction people have to an antibiotic [125]. Among these antibiotics, Amoxicillin is a penicillin antibiotic that fights bacteria. It is used to treat many different types of bacterial infections, such as tonsillitis, bronchitis, pneumonia, and infections of the ear, nose, throat, skin, or urinary tract. Amoxicillin may cause side effects such as diarrhea, nausea, vomiting, and allergic reactions. Amoxicillin is available in various forms such as capsules, tablets, and chewable tablets. Nowadays, DDS can help maintain sufficient concentrations of antibiotics in the target area, which can be difficult to achieve with topical therapy. Hence, it is imperative to develop a drug carrier that is biocompatible and allows for controlled and targeted drug release, minimizing the potential side effects of antibiotics on the body. With this crucial objective in mind, this study aims to explore a drug delivery system that can be externally activated and employs

hydrogels as carriers for drugs. The two polymers chosen for the experiment, chitosan and polyvinyl alcohol, were carefully selected and subsequently modified and characterized. Additionally, environmentally friendly techniques such as gamma irradiation and crosslinking with the EGDE agent were investigated to create the hydrogel matrix, which plays a vital role in smart drug delivery systems. In this particular investigation, amoxicillin, an antibiotic similar to ampicillin, was employed as the model drug. Amoxicillin is a semi-synthetic antibiotic known for its wide range of bacteriocidal activity against various gram-positive and gram-negative microorganisms. It is commonly prescribed in wound healing therapy and for the treatment of bacterial infections, including those caused by the *Helicobacter pylori* (*H. pylori*) bacteria that lead to inflammation. To understand the mechanism of drug release, several kinetic models were utilized, including the zero-order, first-order, Higuchi, Hixson-Crowell, and Korsmeyer-Peppas models. These models were employed to analyze and gain insights into the release of the drug from the hydrogel carriers.

CHAPTER 3

EXPERIMENTAL PROCEDURES

In this chapter, the experimental design is divided into two main parts.

Part A

Firstly, the “green” synthesis method to fabricate the hydrogel by using gamma radiation and its physicochemical properties are investigated. Secondly, pH stimulation amoxicillin release from γ -irradiated CS/PVA hydrogel in DI water and PBS buffer at different pH values are carried out.

Part B

First of all, the gelation behavior of aqueous CS/EGDE and the viscoelasticity of CS/EGDE hydrogels were measured. Secondly, the Amox-entrapped CS/EDGE hydrogel matrix and US-stimulated amoxicillin release are investigated. The viscoelastic behaviors of Amox-loaded CS/EDGE hydrogel matrix before and after US exposure are characterized and US-triggered Amox release characteristics are discussed.

3.1 Chemicals and Materials

Part A

1. High molecular weight (M_w) CS (M_w of 700 kDa and degree of deacetylation of 80%) was provided by Seafresh Chitosan (Lab) Co., Ltd., Thailand.
2. PVA (M_w of 145,000 g/mol) was purchased from CT Chemicals Ltd., Thailand

3. Glacial acetic acid was obtained from Merck Co., Ltd., Germany
4. Amoxicillin trihydrate was procured from Siam Bheasach Co., Ltd., Thailand

Part B

5. Chitosan (Degree of deacetylation = 80 %) was supplied from KATOKICHI CO., Ltd., Japan
6. Ethylene glycol diglycidyl ether (EGDE) was provided by TCI Chemicals Co., Ltd., Japan
7. Sodium hydroxide was provided by Nacalai Tesque, INC., Japan
8. Amoxicillin trihydrate was supplied by TCI Chemicals Co., Ltd., Japan

3.2 Equipment and instruments

Part A

4. Gamma irradiator (^{60}Co gamma MARK I irradiator)
5. Fourier-transform infrared spectroscopy (Nicolet™ iS50 FTIR Spectrometer)
6. ^{13}C Magic-angle spinning nuclear magnetic resonance (^{13}C MAS NMR; AVANCE III 400 WB spectrometer - Bruker, Billerica, MA, USA)
7. Scanning electron microscopy (SEM; Hitachi SU5000)
8. Ultraviolet-visible spectroscopy (UV 9100 Series, LabTech, Hopkinton, MA, USA)
9. Thermogravimetric analyzer (TGA/DSC3p STARe System, Mettler Toledo, Columbus, OH, USA)
10. Freeze-drying machine (Beta 1-8 LD plus, Martin Christ, Germany)
11. Mechanical stirrer

Part B

12. Rheometer (Physica MCR 301, Anton Paar, Austria)
13. Fourier-transform infrared spectroscopy (JASCO FT/IR-4100, Japan)
14. Scanning electron microscopy and an energy dispersive spectrometer (EDS) (JSM-5300 LV, JEOL, Japan)
15. Ultraviolet-visible spectroscopy (UV 9100 Series, LabTech, Hopkinton, MA, USA; JASCO V-570 UV/VIS/NIR spectrophotometer)
16. Multifunction balance (GX-200, A&D Company Limited, Japan)
17. A sonoreactor device, a US water bath (ϕ 86 mm x 65 mm) was equipped with a Langevin-type transducer (HEC-45242M, Honda electrics Co. Ltd., Japan) using a wave factory (WF1943B multifunction synthesizer, NF, Japan)
18. Gold coater (Sanyu Denshi K.K., Japan)

3.3 Preparation of chitosan-based hydrogels

Part A

To begin the experiment, a high-molecular-weight CS powder was mixed with a 1% acetic acid solution at room temperature, while PVA was dissolved in DI water at a temperature of 90 °C to create a clear solution consisting of 1.5% CS and 5% PVA. The next step involved blending different ratios of CS/PVA (100/0, 25/75, 50/50, 75/25, and 0/100) to create homogeneous polymer blend solutions. It is worth noting that higher concentrations of the CS solution were not possible due to its high viscosity. Finally, 6 g of the blended solutions were added to 2.5 x 2.5 cm containers with lids and sealed tightly. These containers were then exposed to

gamma rays at doses of 10, 25, and 30 kGy, with a dose rate of 1.04 kGy/h using a ^{60}Co gamma MARK I irradiator.

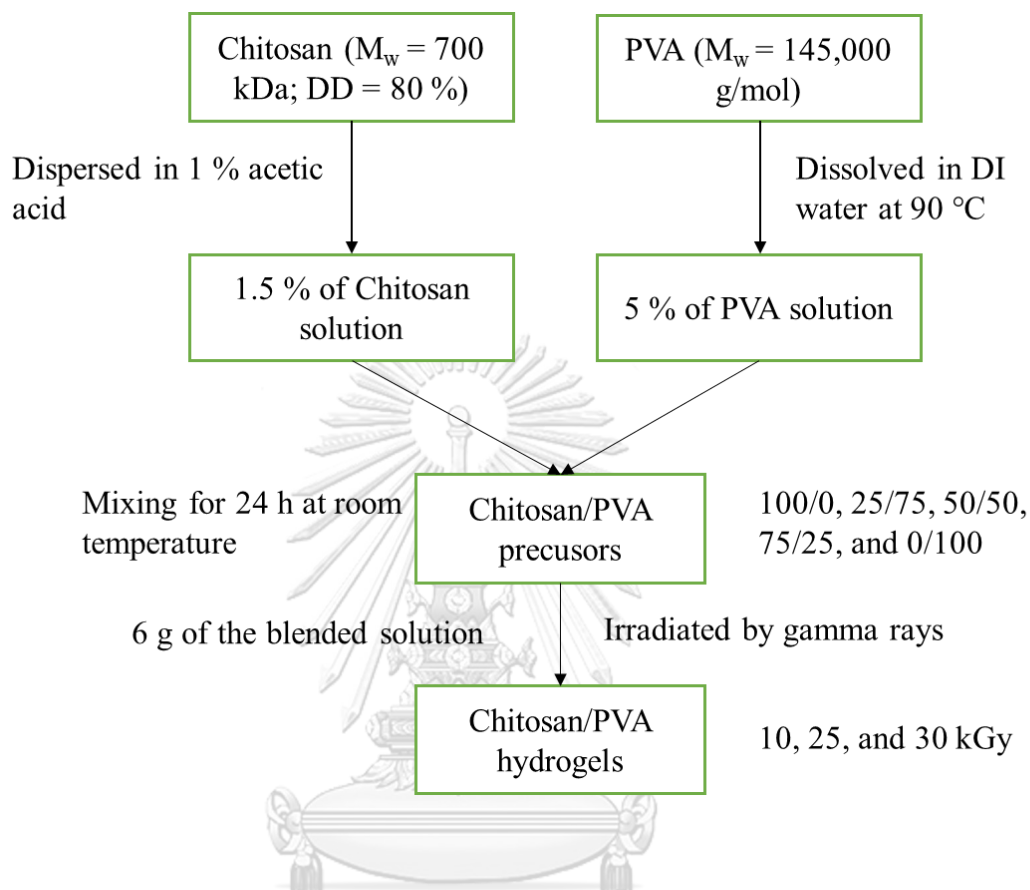


Figure 3.1 The procedure to synthesize gamma-irradiated CS/PVA hydrogels

Part B

The process of hydrogelation in chitosan-EGDE involved mixing chitosan in aqueous solution with a concentration ranging from 1.5% to 3% in 3% acetic acid. The crosslinker agent, EGDE, was then added dropwise under constant stirring to the chitosan solution in a 1:1 molar ratio for 24 hours. This mixture was then placed into 3.5 cm-diameter petri dishes. The chitosan/EGDE precursor was then crosslinked in an alkaline medium (1 M NaOH) for 12 hours to form a stable gel. To remove the sodium hydroxide, the gel was extensively rinsed with deionized

water until neutrality was achieved. Finally, the gel was stored in deionized water before testing.

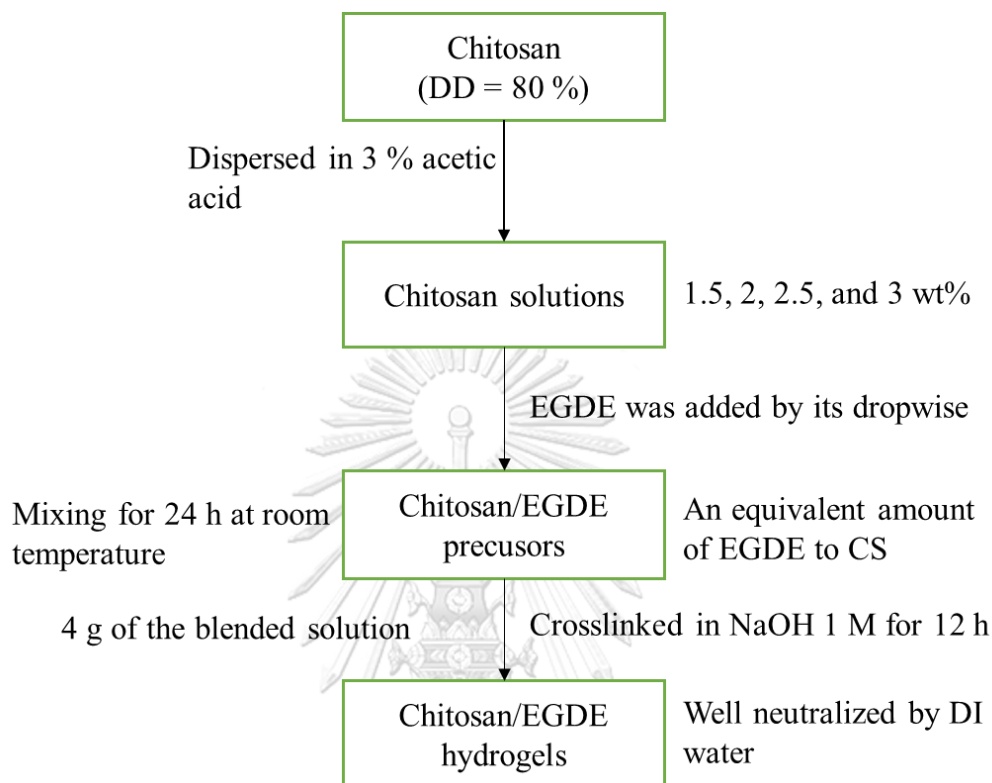


Figure 3.2 The process to synthesize CS/EGDE hydrogels

3.4 Characterizations

Part A

3.4.1 Evaluation of gel contents

Following irradiation, the hydrogels underwent a drying process at a temperature of 60 °C for a duration of 48 hours. They were then weighed precisely (W_0) using a highly precise electronic analytical balance with four decimal places. To remove any un-crosslinked portions, the dried hydrogels were submerged in deionized (DI) water for 24 hours, followed by another drying process in a vacuum oven at 60 °C until a stable weight (W_1) was achieved. This procedure was repeated three times

to ensure accuracy. The gel fraction was determined using the subsequent equation:

$$\text{Gel fraction (\%)} = (W_1/W_0) \times 100$$

3.4.2 Swelling behavior

The swelling ratio (SR) is a parameter that indicates the ability of a hydrogel to absorb water. In order to determine the SR, the hydrogel samples were subjected to measurements in deionized (DI) water as well as solutions with various pH values (1, 4, 7, 10, and 13). Initially, the dry samples were accurately weighed and then immersed in water at room temperature until they reached equilibrium swelling. After removing any excess surface water using filter paper, the fully swollen samples were weighed again. The SR was subsequently calculated using the following equation:

$$\text{SR} = (W_s - W_d)/W_d$$

where W_s is the weight of the swollen sample at equilibrium and W_d is the weight of the dry sample. Experiments were conducted in triplicate.

3.4.3 Chemical structure confirmation

3.4.3.1 Fourier transform infrared (FTIR)

The chemical compositions of the hydrogels were analyzed through ATR-FTIR spectroscopy, employing a Nicolet™ iS50 FTIR Spectrometer. The spectral range investigated was from 4000 cm^{-1} to 500 cm^{-1} , with a resolution of 4 cm^{-1} . To ensure accuracy, an average of 32 scans were collected for each measurement.



Figure 3.3 Fourier transform infrared spectrometer (Source: <https://www.thermofisher.com/>)

3.4.3.2 ^{13}C Magic-angle spinning nuclear magnetic resonance (^{13}C MAS NMR)

To examine the chemical structures of the crosslinked hydrogels, the spectra of neat CS (chitosan), pure PVA (polyvinyl alcohol), and CS/PVA gel beads were obtained using an AVANCE III 400 WB spectrometer manufactured by Bruker in Billerica, MA, USA. The spectrometer operated at a frequency of 400 MHz.



Figure 3.4 Nuclear magnetic resonance spectroscopy (NMR) (Source: <https://www.bruker.com/>)

3.4.4 Scanning electron microscopy (SEM)

In order to examine the morphologies and characteristics of the hydrogel networks, the structure of freeze-dried samples was analyzed using a scanning electron microscope (SEM). The SEM used for this investigation was the Hitachi SU5000, with a magnification of 1000 times. To prepare the samples for observation, hydrogel samples with dimensions of 5 mm × 5 mm were fabricated and coated with a layer of gold (Au).



Figure 3.5 Scanning electron microscopy (SEM)

3.4.5 Thermogravimetric analysis (TGA)

The thermal properties of the hydrogels were examined utilizing a thermogravimetric analyzer (TGA/DSC3p STARe System) manufactured by Mettler Toledo in Columbus, OH, USA. The analysis involved heating samples of approximately 5 mg from 50 to 600 °C at a rate of 10 °C/min under a nitrogen (N₂) atmosphere. The maximum temperature at which thermal degradation occurred was determined by analyzing the data from thermal mass loss (TG) and derivative thermogravimetric (DTG) measurements.

3.4.6 In vitro drug release test

To incorporate the model amoxicillin drug into the CS/PVA irradiated hydrogel, the post-loading method was employed. The process involved the following steps: Firstly, the hydrogel was immersed in a solution containing the model drug with a concentration of 1 mg/ml at room temperature for 24 hours, allowing the hydrogel to fully swell and absorb the drug.

Secondly, the amoxicillin-loaded hydrogels were subsequently placed in an oven set at 37 °C for 24 hours to ensure complete drying.

Thirdly, the dried hydrogels were weighed, and the amount of drug uptake was determined using Peppas's equation, which allows for the examination of drug release kinetics.

The calculation of drug uptake was performed using a standard curve that relates the measured values to the known drug concentrations.

Drug uptake = The amount of amoxicillin – Loaded hydrogel / The initial weight of hydrogel ($\mu\text{g}/\text{mg}$)

In vitro investigations were conducted to study the release of drugs from the polymer hydrogels in buffer solutions with pH values of 2.1 and 7.4, as well as in deionized water (DI). The drug-loaded hydrogels were immersed in 10 ml of the respective buffer solutions at a temperature of 37 °C, and the release of the drug was monitored over time. At specific time intervals, 3 ml samples of the surrounding media were collected, and the volume was maintained by adding an equal amount (3 ml) of appropriate buffer solution. The concentration of amoxicillin in the collected media was determined using a UV-Vis spectrophotometer (UV 9100 Series, LabTech, Hopkinton, MA, USA) at a wavelength of 272 nm, utilizing a calibration curve for amoxicillin (shown in Figure 7a). The results are presented in terms of drug release as a function of time. After completion of the experiment, the hydrogels were removed from the drug-release system and dried in a vacuum oven at 37 °C. The trials were conducted three times, and the average results were calculated for analysis.

Drug release (%) = $(C_t/C_0) \times 100$

The quantity of amoxicillin released from the hydrogels at specific time intervals is represented by C_t , while C_0 refers to the initial amount of amoxicillin absorbed into the hydrogels. To investigate the drug release kinetics from the hydrogel networks, the following mathematical models were utilized [126]:

$$\text{Zero order: } C_t/C_0 = k_0t$$

$$\text{First order: } \log C_t/C_0 = -k_1t/2.303$$

$$\text{Higuchi: } C_t/C_0 = k_h t^{0.5}$$

$$\text{Korsmeyer - Peppas: } \log (C_t/C_0) = \log(k) + n \log(t)$$

$$\text{Hixson-Crowell: } C_0^{1/3} - C_t^{1/3} = k_{hc}t$$

where C_t denotes the quantity of drug released at time t and C_0 is the initial concentration of drug in the hydrogel. The release rate constant for zero-order, first-order, Higuchi model, Korsmeyer–Peppas model, and Hixson-Crowell model are k_0 , k_1 , k_h , k_{hc} and k , respectively, and n is the release exponent which indicates the release mechanism for Korsmeyer–Peppas model.

Part B

จุฬาลงกรณ์มหาวิทยาลัย
CHULALONGKORN UNIVERSITY

3.4.7 Rheological properties of hydrogels

3.4.7.1 Gelation behavior of CS/EGDE solutions

To examine the gelation behavior of alkaline aqueous solutions of CS/EGDE, the changes in dynamic viscoelasticity, specifically the storage modulus G' and loss modulus G'' , were monitored using a rheometer (Physica MCR 301, Anton Paar, Austria) at room temperature. For the analysis of the hydrogel properties, a time-sweep oscillation was conducted using a rheometer (Physica MCR 301, Anton Paar, Austria). The measurement involved applying a strain of 1% and oscillating

at a frequency of 1 Hz for a duration of 2000 seconds to observe the changes in the storage modulus G' and loss modulus G'' over time.

3.4.7.2 Viscoelastic behavior of CS/EGDE hydrogels and Amox-entrapped CS/EGDE hydrogels

The viscoelastic properties of the CS/EGDE hydrogels and CS/EGDE/Amox hydrogels were assessed using the Auto Paar-Reoplus equipment from Anton Paar Japan, Tokyo. The measurements were conducted at a constant frequency of 1 Hz and at room temperature. In the case of the hydrogels triggered by ultrasound (US), an amplitude sweep was performed both before and after a 120-minute exposure to US. The relationship between the storage modulus G' and loss modulus G'' was recorded in response to strain ranging from 0.1% to 1000%. This analysis aimed to evaluate the viscoelastic behavior of the hydrogels and to observe any changes induced by the US exposure. $\tan \delta$ (tan delta) values, representing the ratio of G'' to G' , were also recorded at each strain rate.

3.4.8 Water content (WC) and density of hydrogels

The water content (WC) of the hydrogels prepared was determined using the following formula:

$$WC = (W_0 - W_1)/W_1 \times 100\%,$$

where W_0 represents the weight of the hydrogel in its wet state, and W_1 represents the weight of the hydrogel in its dry state. Before measuring the value of W_0 , the surface of the hydrogel was carefully wiped by tissue paper to remove the water on the surface and the matrices were subjected to vacuum drying at 50 °C for 24 hours to ensure complete drying. The density of the Amox-entrapped CS/EGDE

hydrogels was measured at 25 °C using a multifunction balance (GX-200, A&D Company Limited, Japan), with three samples being taken for accurate results.

3.4.9 In-vitro Amoxicillin release

3.4.9.1 Amoxicillin encapsulation in hydrogels

The amount of Amox (amoxicillin) entrapped within the hydrogels was assessed using a previously established technique with slight modifications []. In order to accomplish this, the Amox-entrapped hydrogel was cut into small pieces and immersed in 15 ml of distilled water. The mixture was stirred for 2 hours, 24 hours, and 48 hours at room temperature to facilitate the release of the entrapped Amox into the aqueous medium. To ensure the reliability of the results, the experiment was repeated with three separate specimens.

In the Amox releasing experiments, the release of Amox from the Amox-entrapped CS/EGDE hydrogel was measured in US water bath as depicted in Figure . The hydrogel matrix, with dimensions of 25 mm in diameter and 3 mm in height, was placed in a sample holder along with 30 ml of phosphate buffer solution (PBS) 2 mM at pH 7.4. A sonoreactor device was utilized, consisting of a US water bath with a diameter of ϕ 86 mm and a height of 65 mm. The water bath was equipped with a Langevin-type transducer (HEC-45242M, Honda electrics Co. Ltd., Japan) and operated at a temperature of 25 °C. The ultrasound (US) power output was controlled using a wave factory (WF1943B multifunction synthesizer, NF, Japan) and set within the range of 0 to 35W.

The release of Amox into the PBS solution within the US water bath was monitored by measuring the intensity of the absorption peak at 273 nm using a JASCO V-570 UV/VIS/NIR spectrophotometer.

To explore the drug release mechanism from the hydrogel or exist in more than one sort of release phenomenon, the mathematical models were utilized to determine drug release kinetics from CS/EGDE/Amox hydrogel network according to previous reports [], shown in section 3.4.6.

3.4.10 Fourier transform infrared (FTIR) and Scanning electron microscope (SEM)

The FTIR spectra of the Amox-entrapped CS/EGDE hydrogels were analyzed using a JASCO FT/IR-4100 spectrometer (JASCO Corporation, Japan) in the range of 4000–500 cm^{-1} . The resolution was set at 4 cm^{-1} , and an average of 16 scans was obtained to enhance the spectral quality.

For observation of the hydrogel morphology, a scanning electron microscope (SEM) model JSM-5300 LV from JEOL, Japan, was utilized. The morphology of Amox-entrapped CS/EGDE hydrogels, prepared with a 1.5 %, 2 %, and 3 % CS/EGDE hydrogels were obtained. Additionally, 2 % CS/EGDE/Amox hydrogels were exposed to ultrasound at both 0 and 35 W before measuring SEM. These hydrogels were frozen using liquid nitrogen, and the water within the frozen matrix was removed through freeze-drying.

To confirm the dispersion of Amox within the hydrogel matrix, cross-sections of the hydrogels were observed using an energy dispersive spectrometer (EDS). The hydrogel samples were coated with gold using a fast cool coater from Sanyu Denshi K.K., Japan, and then the cross-sections were examined and photographed for analysis.

CHAPTER 4

RESULTS AND DISCUSSION

This chapter is managed into two main parts composing part A and part B following the experiments described in Chapter 3. Part A optimized the fabrication parameters of CS/PVA hybrid hydrogels using gamma irradiation. High molecular-weight CS was chosen to prevent rapid degradation. The physical properties, crosslinking mechanisms, and morphology of the hydrogels were investigated. The pH-responsive behavior of the hydrogels makes them suitable for drug delivery systems, with potential applications in localized amoxicillin release. Part B studied ultrasound-triggered DDSs based on Amoxicillin-loaded CS/EGDE hydrogel. For the purpose of exploring the CS/EGDE hydrogel properties of US, the effect of US on the Amox-entrapped hydrogel drugs was investigated using a sonoreactor, which can measure the Amox releasing from such hydrogels under US irradiation.

Part A

4.1 Gamma-irradiated CS/PVA hybrid hydrogels

4.1.1 Gel fraction

Gel fraction analysis was conducted to evaluate the degree of crosslinking in irradiated hydrogels. The effects of radiation doses and CS/PVA ratios on the gel fractions were studied. The gel fraction increased with increasing radiation dose until it reached a maximum at 25 kGy, after which it started to decrease due to chain scission becoming dominant over crosslinking. At 10 kGy and 30 kGy, the 75/25 CS/PVA ratio did not form a gel, while at 25 kGy, approximately 20% gel fraction was achieved. The 50/50 CS/PVA hydrogel showed a significantly higher change in gel fraction compared to the 75/25 CS/PVA hydrogel at 25 kGy. The

increase in PVA content led to a higher fraction of the insoluble part due to the formation of more PVA radicals and subsequent 3D network formation. However, the gel fraction decreased with an increase in CS content as a higher amount of CS hindered radical recombination. Water in the polymer solution played a crucial role in achieving maximum crosslinking by increasing the number of free radicals. Radical crosslinking and chain scission were simultaneous reactions during irradiation.

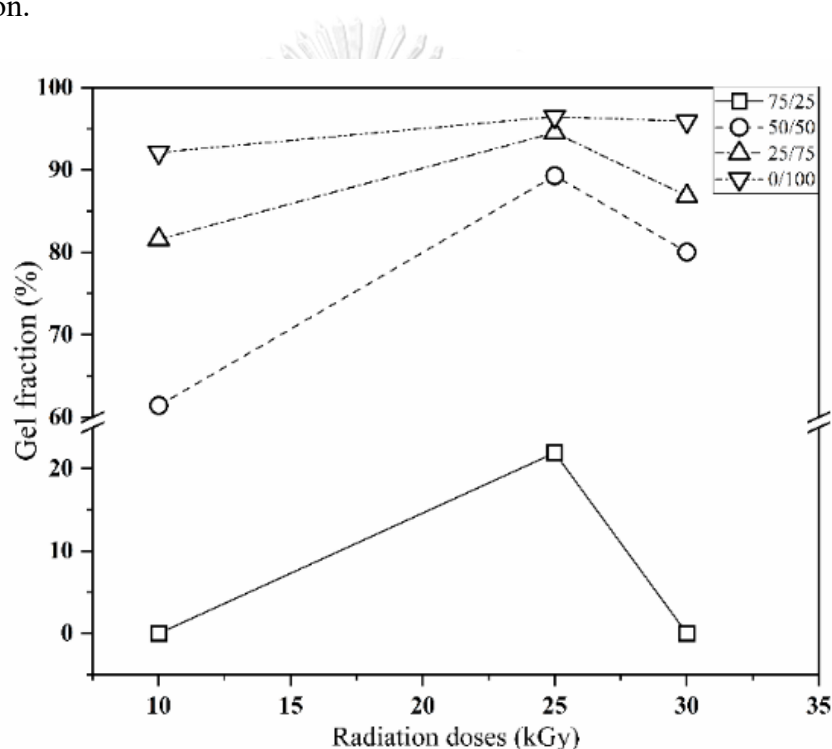


Figure 4.1 Effect of irradiation dose on the gel fraction (%) of CS/PVA at different compositions

4.1.2 Swelling behavior

4.1.2.1 Swelling in DI water

The ability of a hydrogel to retain water or biological fluid is crucial for its suitability in biomaterial applications. The swelling rate of the hydrogel can be tailored for controlled drug release in specific pH environments. In deionized (DI) water, the crosslink density primarily determines the swelling abilities of

hydrogels. The swelling ratios (SRs) of hydrogels at different radiation doses and CS/PVA content over time were analyzed. Hydrogels prepared at 10 kGy exhibited different swelling rates compared to those fabricated at higher radiation doses (25 and 30 kGy). After 24 hours, the equilibrium swelling degrees of the 50/50 CS/PVA hydrogel were 8.4-fold, 4.7-fold, and 5.2-fold compared to the dried state at 10, 25, and 30 kGy, respectively. At 25 kGy, the higher crosslinking of polymer chains resulted in a stronger network with increased resistance to expansion, leading to a reduced swelling degree compared to 10 kGy. However, at 30 kGy, due to predictable polymer chain scission and a decrease in crosslinking density, the swelling degree slightly increased compared to 25 kGy. The amount of absorbed water in the gel network increased significantly before reaching a plateau. Additionally, the SR decreased with an increase in PVA content. As the concentration of PVA in the hydrogels increased, the crosslink density increased, resulting in a decrease in the SR.

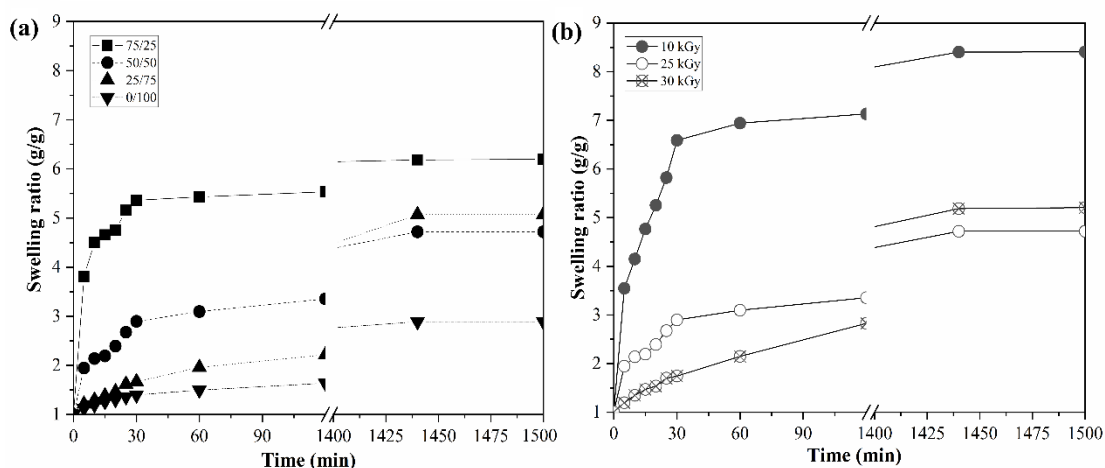


Figure 4.2 Swelling ratio (g/g) vs. time (min) graph of the prepared hydrogels in deionized water at different polymer ratios a) and radiation doses of 50/50 CS/PVA b)

4.1.2.2 Swelling indices in different pH solutions

The swelling mechanism of hydrogels is a complex process consisting of three consecutive steps. First, the solvent diffuses into the network, followed by chain relaxation within the hydrated gels, and finally, the network expands. This expansion is primarily driven by electrostatic repulsion caused by functional groups present within the gel. The presence of more free amino groups in the network enhances the electrostatic repulsion between polymer chains, leading to a faster swelling rate [127]. The pH sensitivity of hydrogels is attributed to the variation in their swelling behavior in buffer solutions with different pH values. In the study, it was found that a hydrogel made of 50% chitosan (CS) and 50% polyvinyl alcohol (PVA) irradiated at 25 kGy had a lower swelling ratio (SR) at pH 7, 10, and 13 compared to pH 1 and 4. The hydrogel's swelling degree at pH 1 was approximately twice as high as that at pH 13, reaching around 7 (g/g). The swelling degree of the hydrogel can also be influenced by the ionic strength of the solution. High molecular weight (Mw) chitosan (CS) offers better opportunities for chemical or physical crosslinking, resulting in the formation of a 3D network structure with increased entanglement. This, in turn, reduces the repulsive force and promotes intramolecular interaction at pH 5.5-6 in CS/PVA blended hydrogels. The amino groups of high Mw CS can be protonated (NH_3^+) in acidic fluids at low pH, leading to electrostatic repulsions that enhance the hydrophilicity of the hydrogel and expand its network. Conversely, swelling decreases under neutral (pH 7) and alkaline (pH 10 and 13) conditions due to the deprotonation of these amino groups. The pH-sensitive swelling behavior of hydrogels holds promise for controlled drug delivery applications that require precise regulation of

drug release. Also, the advantageous nature of these behaviors in the context of drug delivery had been explored [128].

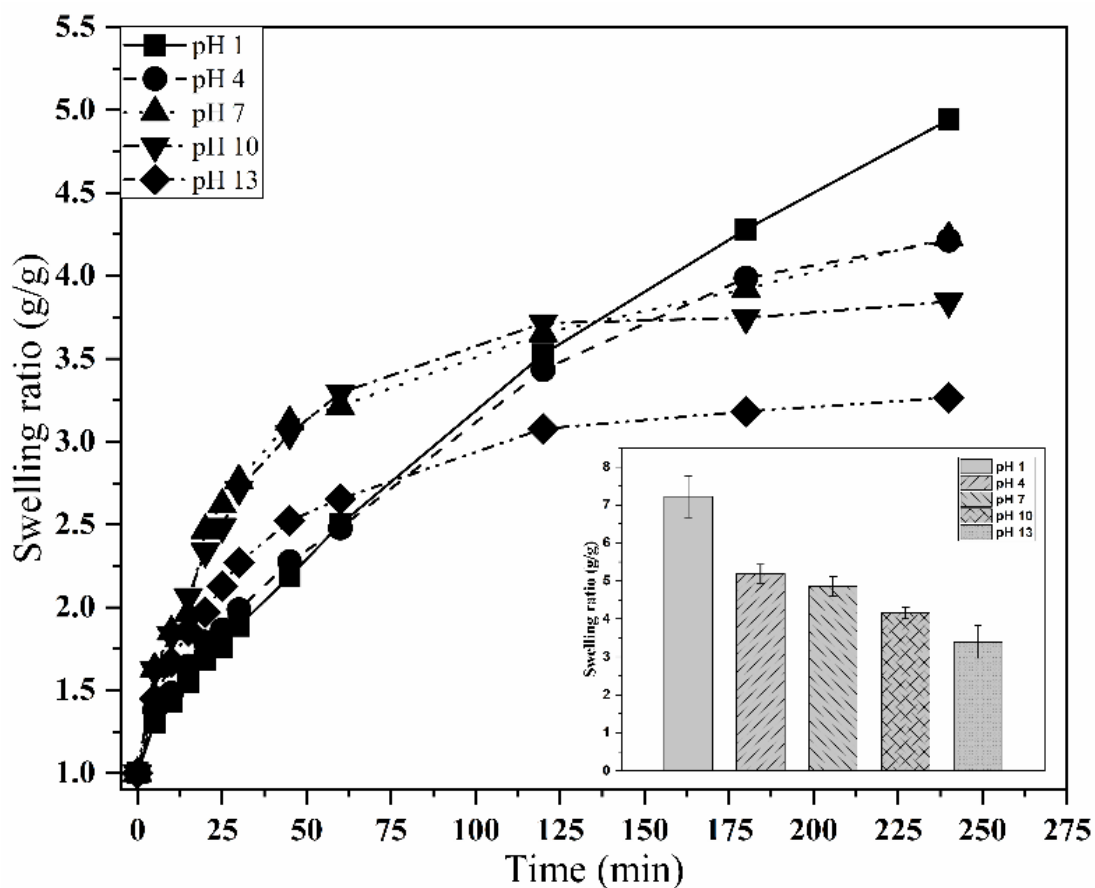


Figure 4.3 Swelling ratios of the 50/50 CS/PVA hydrogel discs at a pH 1–13

4.1.3 Chemical structures of crosslinked CS hydrogels

Distinctive functional groups and newly formed bonds between neat CS, pure PVA, and CS/PVA hybrid hydrogels were assessed via FTIR absorption spectroscopy and solid-state ^{13}C NMR spectroscopy.

4.1.3.1 FTIR spectra of unirradiated and gamma-irradiated CS/PVA hydrogels

The Fourier Transform Infrared (FTIR) spectrum of pure polyvinyl alcohol (PVA) reveals certain characteristic absorption bands. A broad absorption band at 3301 cm^{-1} corresponds to the stretching and bending vibrations of the hydroxyl ($-\text{OH}$)

group. Peaks at 2923, 1433, and 1090 cm^{-1} indicate the stretching of alkyl groups, bending of alkyl groups, and stretching of the carbonyl-oxygen (C=O) group, respectively [129]. Neat chitosan (CS) exhibits specific absorption peaks in its FTIR spectrum. The peak at 3330 cm^{-1} is attributed to the vibrational stretching of intermolecular and intramolecular hydrogen bonds involving the nitrogen-hydrogen (N-H) and oxygen-hydrogen (O-H) groups. The stretching vibration absorption peak of the C-H group in the CS chain occurs at approximately 2879 cm^{-1} . Furthermore, absorption peaks at 1645 cm^{-1} (amide I), 1567 cm^{-1} (amide II), and 1387 cm^{-1} (amide III) can be observed. These peaks arise from the stretching vibration of the C-O bond, the vibration of the N-H bond, and the stretching vibration of the C-N bond, respectively [130]. Characteristic peaks related to the saccharide backbone of the CS molecule are also evident. The peaks at 1141 cm^{-1} and 1021 cm^{-1} correspond to the antisymmetric stretching of the C-O-C bridge and the C-O vibration of the ring, respectively [131]. The FTIR spectrum of the hybrid hydrogel displays characteristic peaks associated with both CS and PVA hydrogels. In the non-irradiated samples, the peaks shifted from 3304 cm^{-1} to 3291 cm^{-1} , 3279 cm^{-1} , and 3287 cm^{-1} compared to the irradiated samples. This shift can be attributed to the formation of intermolecular hydrogen bonds between CS and PVA. These hydrogen bonds act as connectors between the two polymers. Furthermore, the data indicates that there was no significant degradation of CS in the 50/50 hydrogel samples irradiated at different radiation doses as the intensity of the peak at 1567 cm^{-1} slightly increased [132].

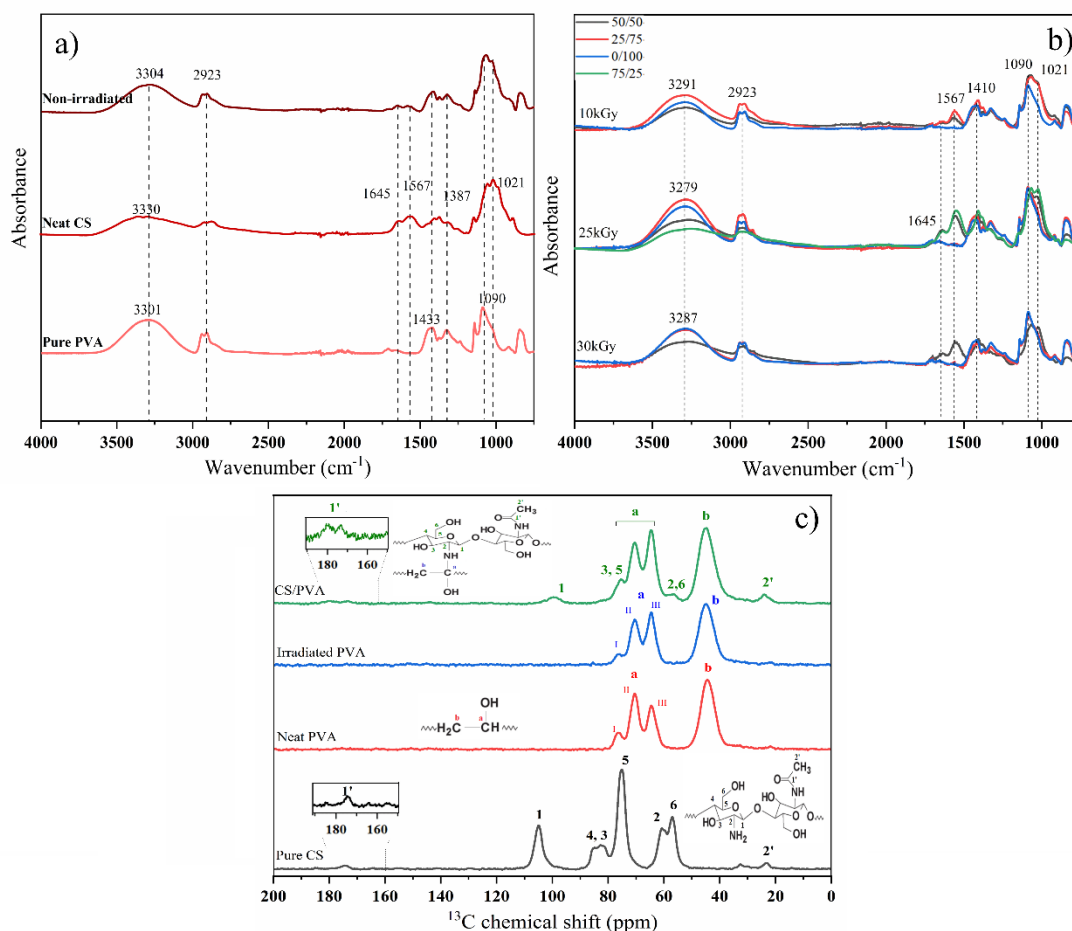


Figure 4.4 a) Fourier transform infrared spectra of pure PVA, neat CS, non-irradiated CS/PVA, and b) FTIR of crosslinked hydrogels irradiated at 10, 25, 30 kGy; c) solid-state ¹³C nuclear magnetic resonance spectrum of pure CS, neat PVA before and after irradiation, and the 50/50 CS/PVA hydrogel.

The chemical structures of hydrogels were confirmed using solid-state ¹³C NMR spectroscopy. Table 2 provides the integrals of NMR signals corresponding to specific functional groups found in pure chitosan (CS) before and after the irradiation of pure polyvinyl alcohol (PVA) and the CS/PVA hydrogel. The assignments for these signals are as follows: 0-49 ppm for alkyl carbon (C), 49-62 ppm for N-CH, 62-94 ppm for O-alkyl C, 94-110 ppm for O-C-O anomeric C, and 160-188 ppm for COO and N-C-O groups [133]. The ¹³C magic angle spinning (MAS) NMR spectra clearly display a peak at 44.80 ppm, corresponding to

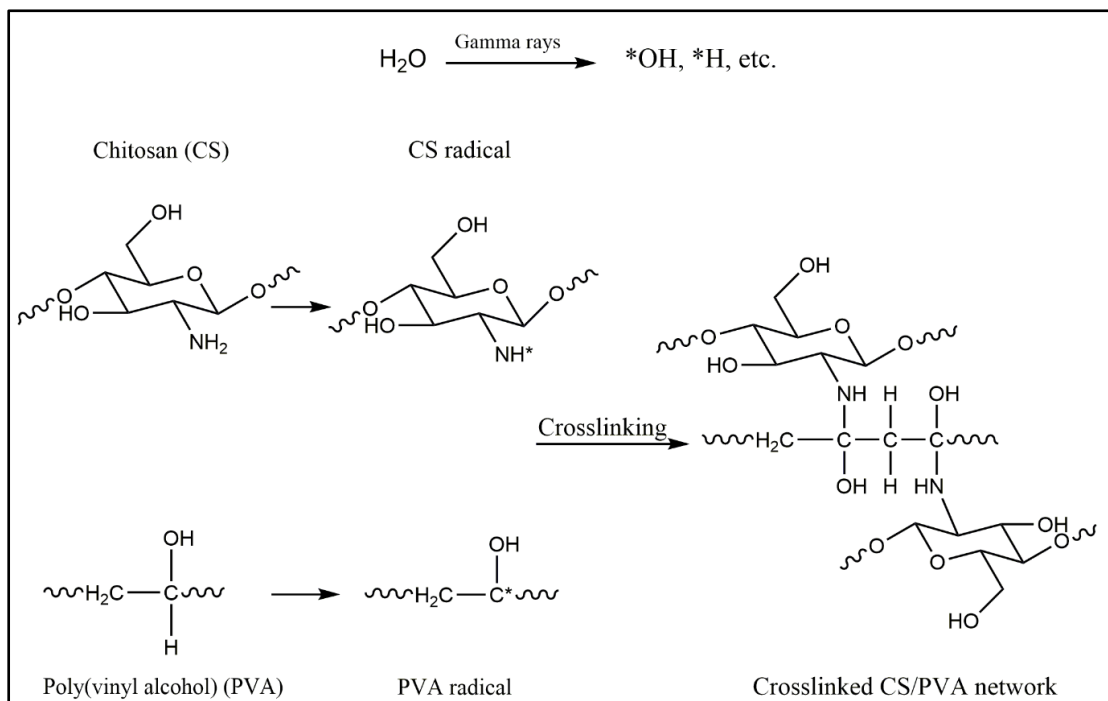
methylene C (-CH₂-) and resonances at 64.53, 70.48, and 75.32 ppm, corresponding to methine C (-CH-). The peak at 44 ppm represents methylene carbon in both non-irradiated and irradiated PVA spectra. The peaks at 64, 70, and 76 ppm are attributed to carbons connected to OH groups [134]. Peaks I and II are associated with the isotactic structure having two intramolecular hydrogen bonds, while Peak III corresponds to the syndiotactic structure with no intervening intramolecular hydrogen bonds. Comparison of the spectra of neat PVA before and after irradiation with those of the equivalent dry gels reveals that the gelation process breaks the network of intramolecular hydrogen bonds, based on previous NMR studies on PVA [135]. In the blended hydrogel (Fig. 4c), the combination of PVA and CS peaks is observed. Additionally, the overlapping peaks at 75.32 ppm (C3 and C5) result from the intramolecular hydrogen bond (Wang et al., 2019). In the pure CS spectrum, various C peaks are observed: C=O at 174 ppm, C1 at 104 ppm, C4/C3 at 85-82 ppm, C5 at 75 ppm, C2 at 60 ppm, C6 at 58 ppm, and CH₃ at 23 ppm. The C1 peak exhibits minor low-field shifts after irradiation of the hybrid hydrogel compared to pure CS, indicating the formation of intramolecular/intermolecular hydrogen bonds around C2, C3, C5, and C6 during crosslinking, which slightly shifts the corresponding peaks to lower fields, consistent with previous literature [136].

Table 4.1 Chemical shifts of C in the pure and blended hydrogels

Chemical shift (ppm)	Assignment	References
23.96	-CH ₂ - carbon of residual acetate	[134]
44.80	-CH ₂ -	[134]

56.54	C2	[134]
64.53	C6, Peak I	[134]
70.48	Peak II	[137]
75.32	Peak I	[137]
99.98	C1	[138]
173.20	C=O (ester)	[138]
180.61	C=O (amide)	[138]

Scheme 1 illustrates the proposed mechanism of crosslinking in CS/PVA hydrogel through gamma irradiation. When exposed to gamma radiation, the water present in the aqueous solution absorbs most of the energy. Indirect interaction with water molecules leads to the formation of radiolytic products, primarily including $\cdot\text{OH}$ radicals, e^- (aqueous electrons), and $\cdot\text{H}$ radicals [139]. Among these reactive species, the $\cdot\text{OH}$ radicals play a key role by extracting hydrogen from polymer chains, resulting in the generation of radicals in both CS and PVA, as well as water molecules. In the final step of the process, covalent bonds between polymer chains form as the macro radicals, specifically PVA-CS, PVA-PVA, and CS-CS radicals, recombine with each other.



Scheme 1 Proposed crosslinking process of CS/PVA hydrogel under gamma irradiation

4.1.4 Thermal analysis

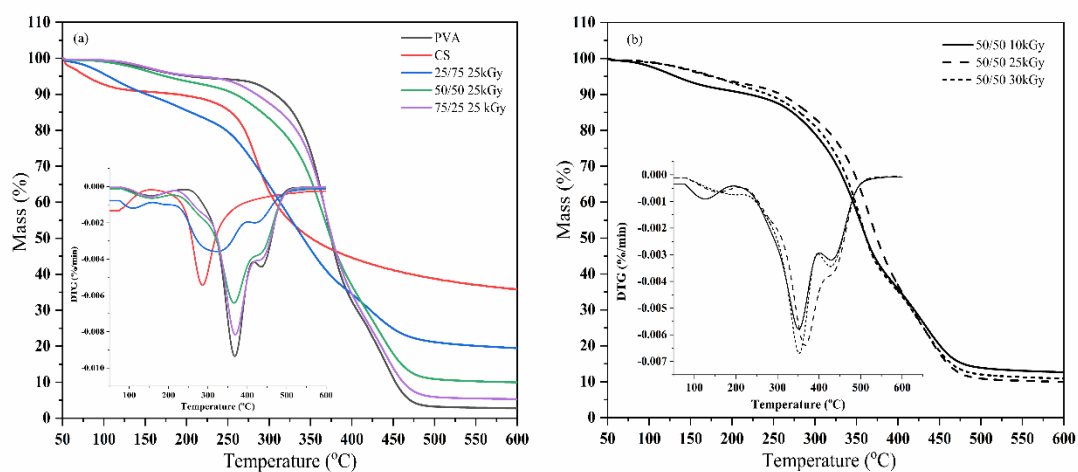


Figure 4.5 a) Typical TG and DTG curves of pure PVA, pure CS, and CS/PVA blended hydrogels at 25 kGy and b) 50/50 CS/PVA at 10, 25, and 30 kGy.

Thermogravimetric analysis (TGA) was performed to gain deeper insights into the thermal behavior of the hydrogels. Figure 5a presents the weight loss (TG) and

derivative (DTG) curves for pure PVA, neat CS, and blended CS/PVA hydrogels with varying CS and PVA contents, as well as different radiation doses. The TGA data revealed a two-stage degradation process for CS. The initial signs of degradation were observed at 60 °C, leading to a 10% weight loss attributed to the evaporation of water molecules. The subsequent weight loss of 49% between 280 and 350 °C was attributed to thermal and oxidative degradation of CS. This decomposition phase involved the breakdown of key components in CS, particularly the degradation of the pyranose ring and the fracture of the b-glycosidic bonds that connect the glucosamine and N-acetylglucosamine moieties [140]. Additionally, the main decomposition (as indicated by the DTG curve) occurred between 300 and 414 °C, associated with the dehydroxylation of PVA, which marked the onset of polymeric chain decomposition. Subsequent decomposition took place between 414 and 475 °C, involving the continuation of the polyene structure and the generation of carbon and hydrocarbons [141]. The decomposition temperatures (T_d) for CS, PVA, and blended hydrogels were found to be 223, 267, and 240-266 °C, respectively (Fig. 5a). Consequently, PVA exhibited the highest T_d and the greatest thermal stability due to the presence of intramolecular and intermolecular hydrogen bonding within its chains. Furthermore, the hybrid hydrogels containing 50-75% PVA displayed greater thermal stability compared to those with 25% PVA. This enhanced thermal stability was attributed to the high degree of crosslinking induced by gamma radiation, resulting in the formation of a network structure. When the radiation dose was increased from 10 to 30 kGy, the T_d of the 50/50 CS/PVA hydrogel

showed a slight increase, indicating higher crosslink densities at higher radiation doses (Fig. 5b).

4.1.5 Morphologies of the crosslinked CS hydrogels

The migration of drugs within a three-dimensional (3D) network relies on the absorption and release processes, making the morphology and interconnectivity of the pores crucial factors. To investigate the network topologies of hydrogels with different CS/PVA ratios, scanning electron microscopy (SEM) was employed. SEM images were taken with a 1000x magnification to determine the average diameter of 50/50 CS/PVA hydrogels at radiation doses of 10, 25, and 30 kGy. Twenty random locations were selected and measured using ImageJ software for each sample. At 10 kGy, the hydrogel framework exhibited fewer holes and larger pore sizes, approximately 8.83 μm , indicating limited crosslinking points between the polymers. As the radiation dose increased to 25 and 30 kGy, a more extensively crosslinked network structure was formed. The average pore sizes of the samples decreased to 3.59 μm when the radiation dose was increased from 10 to 25 kGy, and slightly expanded to 4.63 μm at 30 kGy (Fig. 6). Further increasing the radiation dose resulted in minor changes to the porous structure. With an increase in PVA concentration, a greater number of interconnected chains were formed, leading to a reduction in the average pore size. Notably, the morphology of neat PVA, which exhibited a significantly inferior porous pattern, differed from that of the hybrid hydrogels. The interconnected porous mesh structure provided excellent permeability, enhancing the transport of drugs through the hydrogels. The blended hydrogels, with their highly interconnected porous structure and

moderate pore size, showed promise for drug loading and release due to their superior swelling characteristics compared to other hydrogels [142].

4.1.6 In vitro amoxicillin release studies

The objective of localized release systems is to concentrate the concentration of medicine in the targeted organ, thereby reducing side effects resulting from unfocused release points (Fig. 7a) [143]. In this study, CS/PVA gels exhibited an amoxicillin uptake of 11.133 ± 0.231 $\mu\text{g}/\text{mg}$ polymer under these conditions. To assess the release of amoxicillin in vitro, UV spectrophotometry was employed at 37 °C. The release of amoxicillin from the hydrogel networks was monitored over 1440 minutes following pH changes in phosphate-buffered saline (PBS) medium and deionized (DI) water. Figure 7b presents the results of the drug release study. Notably, a rapid release of amoxicillin occurred in all samples at different pH values within the first 300 minutes. The percentage of amoxicillin released from the hydrogel at 1440 minutes was estimated to be 85 % at pH 2.1 and 7.4 in PBS media, and 34 % at pH 5.5 in DI water. In acidic conditions, the release of the drug from the hydrogel was enhanced due to electrostatic repulsion resulting from the protonation of amino groups. This repulsion created a larger surface area, facilitating drug release. Additionally, the porous structure of the hydrogel played a vital role in drug release by enhancing drug permeation [144]. The results indicate that the release of amoxicillin was higher in the physiological environment of phosphate-buffered saline (PBS) compared to deionized (DI) water. This could be attributed to the solubility of amoxicillin, which is influenced by pH and ionic strength.

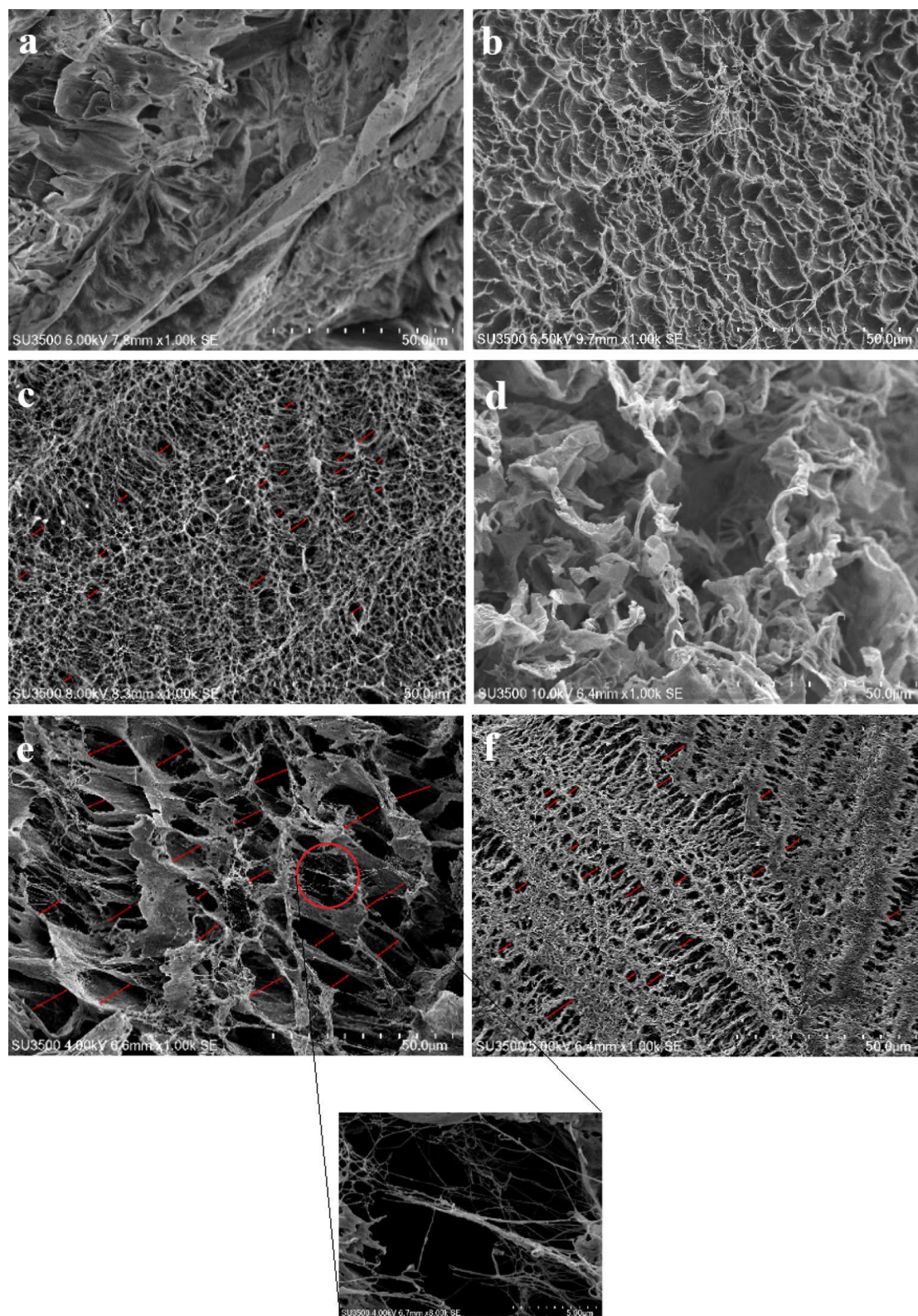


Figure 4.6 Scanning electron microscopy images of the crosslinked hydrogels: a) pure PVA, b–d) 25/75, 50/50, and 75/25 CS/PVA-based hydrogels crosslinked at 25 kGy, respectively; e, f) 50/50 CS/PVA-based hydrogel crosslinked at 10 and 30 kGy.

Higher percentages of released drugs from CS/PVA hydrogel might be due to the impact of pH and ionic strength on amoxicillin solubility. Moreover, higher ionic strengths were expected to weaken the molecular structure of the polymer by increasing repulsive electrostatic interactions between charged polymer molecules [145].

The utilization of mathematical modeling is highly advantageous in achieving the goal of controlled drug release as it allows for the estimation of release kinetics prior to developing release systems. This modeling approach involves measuring crucial physical characteristics such as drug diffusion coefficient and experimental release data [143]. Various model-linked techniques, including zero-order, first-order, Hixson-Crowell, Higuchi, and Korsmeyer-Peppas models, were employed to investigate the optimal drug release kinetic mechanism and explain the solution profile, as summarized in Table 3.

In the zero-order model, drug elimination remains constant regardless of concentration, while the first-order model shows drug elimination increasing proportionally with concentration [146]. The fitting of the zero-order and first-order equations to the amoxicillin release data in PBS at pH 2.1 and 7.4 resulted in r^2 values of approximately 0.76 and 0.90, indicating a less satisfactory fit. On the other hand, the zero-order kinetics provided a better fit with an r^2 value of up to 0.97 for drug release in DI water. It is worth noting that drug release in DI water is governed by the relaxation of polymeric chains and exhibits a constant release rate irrespective of drug concentration.

Higuchi drug release follows a diffusion-based method according to Fick's law, suggesting that matrix swelling and evaporation have minor or insignificant effects and exhibit a square-root time dependency [147]. The correlation coefficients obtained for the Hixson-Crowell model (0.79-0.91) were lower compared to those obtained for the Higuchi model, indicating that the Hixson-Crowell model was not suitable for describing the release mechanism. Diffusion-controlled release was identified as the primary mechanism governing drug kinetics, rather than changes in surface area and particle diameter.

To explore the drug release mechanism from the hydrogel or identify multiple release phenomena, the Korsmeyer-Peppas model was employed. This model investigates a range of parameters including polymer swelling, erosion, matrix porosity, and drug diffusion rates in swelling systems [143]. The literature suggests that if the value of n is less than 0.45, solvent penetration into the hydrogels follows the Fickian process. Additionally, if n falls between 0.45 and 0.89, drug release is controlled by diffusion and polymer network relaxation, indicating a non-Fickian process. However, values of n greater than 0.89 indicate drug release as a function of polymer gel system expansion or relaxation. In this study, amoxicillin release followed a non-Fickian process with n values ranging from 0.61 to 0.72 for different pH environments, and the r^2 values for all conditions were greater than 0.95, as shown in Table 3. Therefore, drug release occurs as a result of both diffusion and swellable porous matrix.

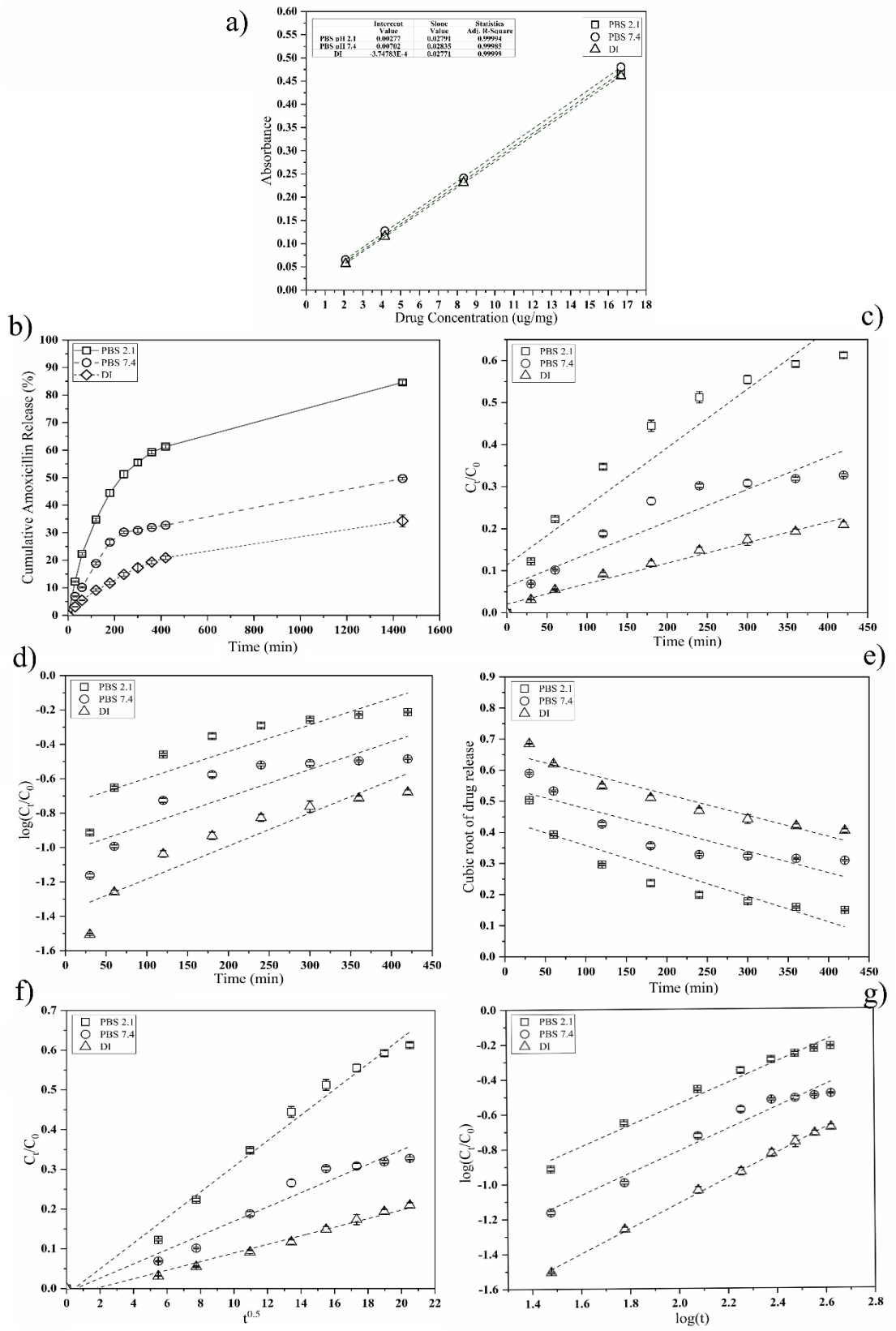


Figure 4.7a) Calibration curve for Amoxicillin using UV-vis spectroscopy, b) cumulative release of the 50/50 CS/PVA; the drug release profiles of CS/PVA 50/50 were calculated using the c) zero-order, d) first-order, e) Hixson-Crowell model, f) Higuchi model, and g) Korsmeyer-Peppas model.

Table 4.2 The kinetic models of CS/PVA irradiated hydrogel (50/50): drug-release rate constants, diffusion exponents, diffusion types, and regression values in diverse media

Drug loaded in CS/PVA gels (µg/mg polymer)		Kinetic models						
		Zero-order	First-order	Hixson-Crowell	Higuchi	Korsmeyer-Peppas		
Releasing media		r^2	r^2	r^2	r^2	k	n	r^2
11.4	pH 2.1; PBS	0.9015	0.7850	0.8355	0.9878	0.0175	0.61±0.04	0.9782
11.0	pH 7.4; PBS	0.8656	0.7630	0.7968	0.9618	0.0084	0.63±0.05	0.9630
11.0	pH 5.5; DI	0.9743	0.8675	0.9192	0.9818	0.0023	0.72±0.01	0.9981

Part B

4.2 Chitosan/Ethylene glycol diglycidyl ether/Amoxicillin hydrogels

4.2.1 Gelation behavior of aqueous CS/EGDE

The gelation of CS/EGDE solutions at various concentrations ranging from 1% to 3% CS was investigated using dynamic viscoelasticity analysis. The time-dependent variations in the G' and G'' moduli within this concentration range are depicted in Figure 1(a). The viscoelastic tests were carried out at 1 Hz strain and 1% mechanical oscillation. As the CS concentration in the CS/EGDE solution grew from 1% to 3%, both G' and G'' values increased with time. Furthermore, when concentrations grew, the initial values of G' and G'' increased due to the increasing viscosity of the CS/EGDE solution. However, at 1% CS concentration, the G' to G'' levels remained reasonably consistent throughout the testing period,

indicating that cross-linking gelation did not occur within that time frame. G' began to grow at roughly 200 s, 30 s, 11 s, and 10 s for concentrations of 1.5%, 2%, 2.5%, and 3%, respectively. These findings imply that gelation of CS/EGDE solutions occurs more quickly at higher CS concentrations. For the 1.5% CS/EGDE solution, for example, the G' value grew during the gelation process from 25 Pa at 30 s to 102 Pa at 2000 s. The temporal fluctuation of \tan , which indicates the ratio of G'' to G' (Figure 1(b)), confirmed this tendency. In particular, the \tan value suddenly dropped at a certain point before stabilizing. The aqueous CS/EGDE solution began to solidify as a result of gel formation at $\tan = 1$. For CS concentrations of 1.5%, 2%, and 3%, respectively, the decrease in gelation time was shown at 254 s, 70 s, and 40 s, showing quicker gelation at higher CS concentrations. The number, however, kept dropping even after achieving $\tan = 1$ and moving into the solidified state, demonstrating that gelation persisted until \tan reached a constant value. Higher CS concentrations resulted in the value remaining almost constant for 800 s. It dropped to 1600 s for the 1.5% concentration and was about 1000 s for the 2% CS concentration.

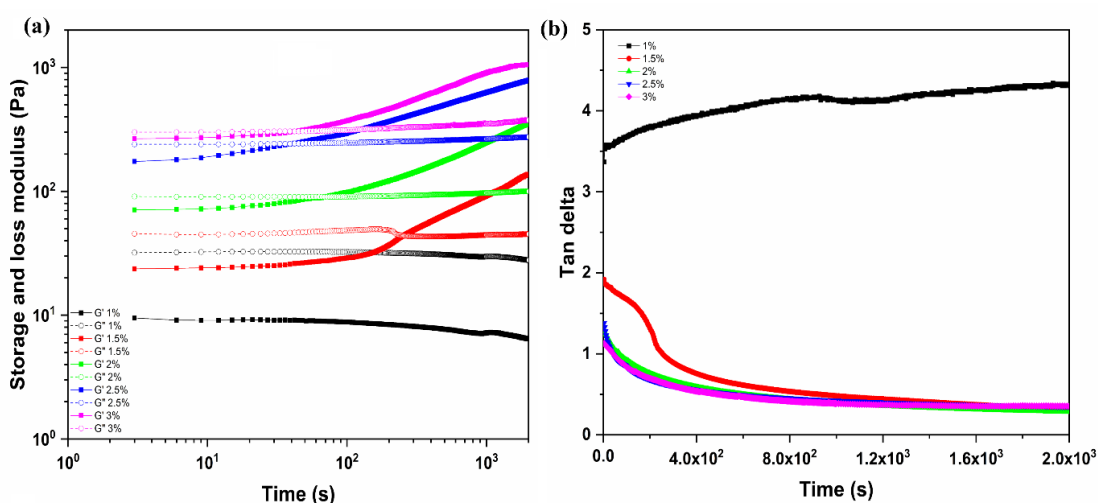


Figure 4.8a) Time change of G' and G'' and b) $\tan \delta$ for the CS/EGDE solutions with various CS concentrations.

4.2.2 Viscoelasticity of the resultant CS/EGDE hydrogels

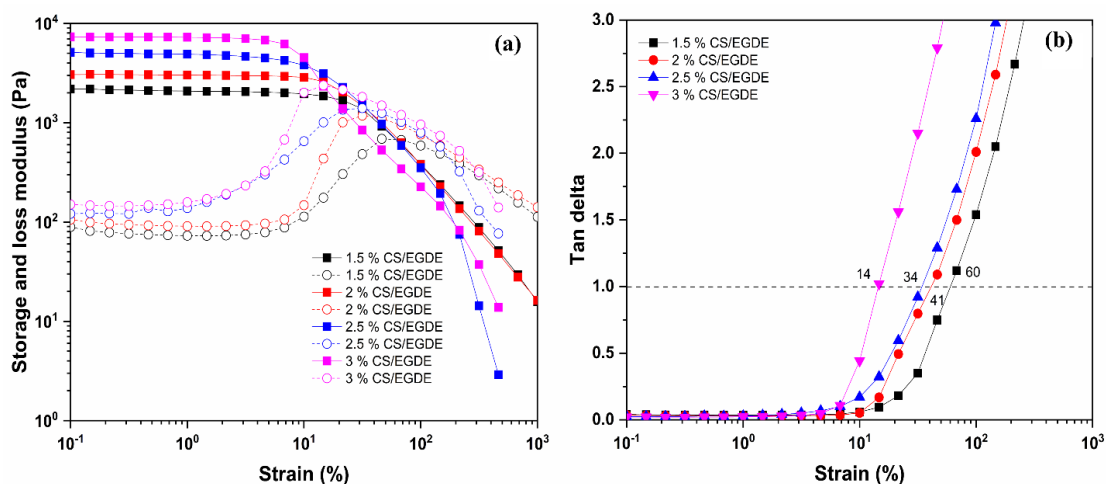


Figure 4.9a) G' and G'' and b) $\tan \delta$ at different strain % for the CS/EGDS hydrogels. These hydrogels were washed with large volumes of water and tested on samples with a pH of 7 in the water they contain.

Figure 2a shows the relationship between G' and G'' moduli and strain%, whereas Figure 2b shows the \tan values for the CS/EGDE hydrogels at each strain%. The G' value was greater for hydrogels with higher CS concentrations at a strain of 0.1%. For example, the G' value for the 3% CS/EGDE hydrogel was 7.3×10^3 Pa and 2.2×10^3 Pa for the 1.5% CS/EGDE hydrogel, demonstrating that higher CS concentration resulted in a stiffer gel. In terms of the \tan /strain relationship, the strain% at which \tan hit 1 was 60% for the softer 1.5% CS/EGDE hydrogel and 14% for the tougher 3% CS/EGDE hydrogel. This implies that the harder CS/EGDE hydrogels exhibited less deformation-induced collapse of the gel structure compared to the softer ones.

4.2.3 Properties of CS/EGDE and CS/EGDE/Amox hydrogels.

Table 1 compares the characteristics of these hydrogels when entrapped with Amox to those of CS/EGDE without Amox. Before the medication was entrapped, the soft 1.5% CS/EGDE hydrogel had lower densities than the hard 3% CS/EGDE hydrogel in the Amox-free CS/EGDE. In contrast, the former had a water content of 2929 24%, showing more water retention than the later, which had a water content of 1814 21%. After Amox was absorbed into these gels matrix by immersing these hydrogels in 0.1% Amox solution for 24 hours, the water content of those CS/EGDE/Amox hydrogels was somewhat enhanced. The water contents of hydrogels irradiated with 1.5% CS/EGDE/Amox, 2% CS/EGDE/Amox, 2.5% CS/EGDE/Amox, and 3% CS/EGDE/Amox, on the other hand, were 3149 42%, 2686 25, 2261 35, and 1957 30, respectively, when the 35 W US was applied for 120 min. A modest increase in water retention after US irradiation was seen when the water content in Table 1 was compared to the values obtained after post-ultrasonic irradiation. For cellulose hydrogels 42 and chitin hydrogels 15, a comparable pattern was seen. For the flexible 1.5% and 2% CS/EGDE/Amox, this tendency was noticeable, but not for the stiff 3% CS/EGDE/Amox hydrogel; instead, the moisture content dropped. This might be due to the dehydration of amino groups that were hydrogen bonded to water in the dense chitosan environment to the outside of the hydrogel by US irradiation.

Table 4.3 Properties of CS/EGDE and CS/EGDE/Amox hydrogels.

Samples	Gelation time (s)	G' strain	at 0.1 % strain	Amox encapsulated amount (µg/g)	Density (g/cm ³)	Water content (%) basis			
						Before	US	After	Dry US

	(Pa)	hydrogel)		exposure	exposure
1.5%CS/EGDE	254	2210	-	0.936 ± 0.004	2929 ± 24
2%CS/EGDE	70	3100	-	0.940 ± 0.003	2480 ± 26
2.5%CS/EGDE	40	5010	-	0.941 ± 0.003	2134 ± 17
3%CS/EGDE	40	7310	-	0.950 ± 0.002	1814 ± 21
1.5%CS/EGDE/Amox	-	2200	188 ± 16	0.939 ± 0.006	3010 ± 38
2%CS/EGDE/Amox	-	2950	252 ± 28	0.944 ± 0.001	2600 ± 58
2.5%CS/EGDE/Amox	-	3950	211 ± 22	0.945 ± 0.003	2268 ± 24
3%CS/EGDE/Amox	-	5520	208 ± 14	0.952 ± 0.000	1984 ± 27

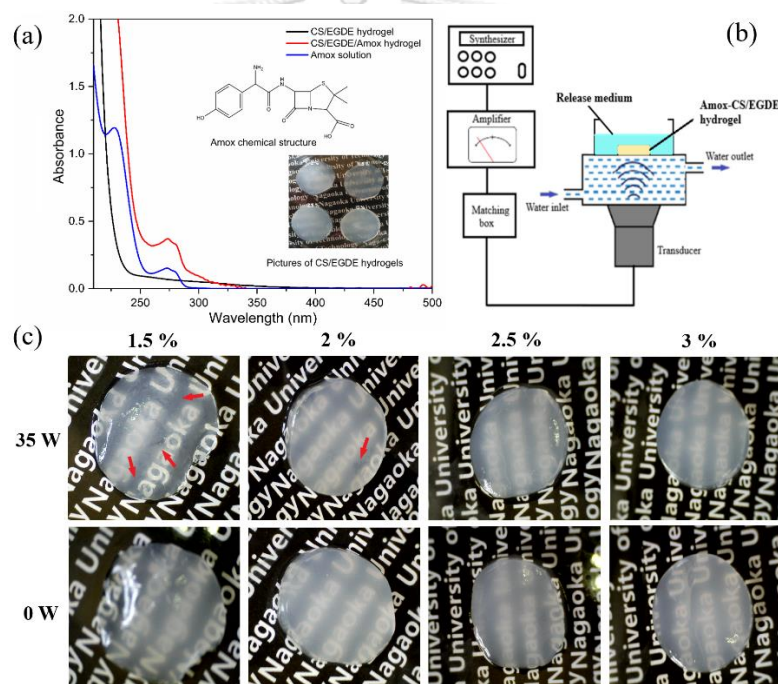


Figure 4.10a) UV-Vis spectra of CS/EGDE hydrogel, CS/EGDE/Amox hydrogel with 1.37 and 1.48 mm thickness, respectively, and Amox aqueous solution at $50 \mu\text{g/ml}$, Amox chemical structure, and external appearance of CS/EGDE hydrogels without Amox; b) US experimental setup; c) Appearance picture of CS/EGDE/Amox hydrogels prepared with different CS percentages in absence and presence of US-triggered release at 35 W.

Amox exhibits an absorption peak at 273 nm ascribed to the $\pi\text{-}\pi^*$ transition, as shown in Figure 3a. The band was found in the 2% CS/EGDE hydrogel,

confirming the existence of Amox with aromatic ring with π - π^* transition. The existence of a peak at 273 nm in the CS/EGDE/Amox hydrogel confirmed Amox incorporation. The produced hydrogel was exposed to US to evaluate US-triggered Amox release activity from CS/EGDE/Amox hydrogels using the experimental setup shown in Figure 3b. The hydrogels were placed in a US water tank and 43 kHz US was exposed from the bottom. In the water bath, the Amox triggered by US and released from the CS/EGDE/Amox hydrogel was estimated by absorbance change at 273 nm. As seen in Figure 3c, the appearance pictures of Amox-entrapped CS/EGDE hydrogels in presence and absence of US almost resembled the Amox free one that retained a great deal of water.

SEM images of Amox-loaded 1.5% CS/EGDE, 2% CS/EGDE, and 3% CS/EGDE are shown in Figure 6a. When the CS concentration was raised from 1.5% to 3%, the interior structure of these hydrogels was magnified by 1000x and 5000x, revealing a sponge network of CS forming a dense structure. This structural difference at 5000x is assumed to be the reason why the 3% CS/EGDE, with its dense CS mesh structure, had a lower water content because the hydrogel that absorbed the water did not have enough area to keep the water. However, there was ample room to store water in 1.5% CS/EGDE, suggesting that swelling was promoted. Also as shown on the right the EDS patterns of sulfur S and carbon C were exhibited as red and blue dots. The Amox-derived S was found to be widely distributed within the inner sponge structure of the gel after immersion of each hydrogel in Amox solution.

4.2.4 US stimulated Amox release from CS/EGDE/Amox hydrogels

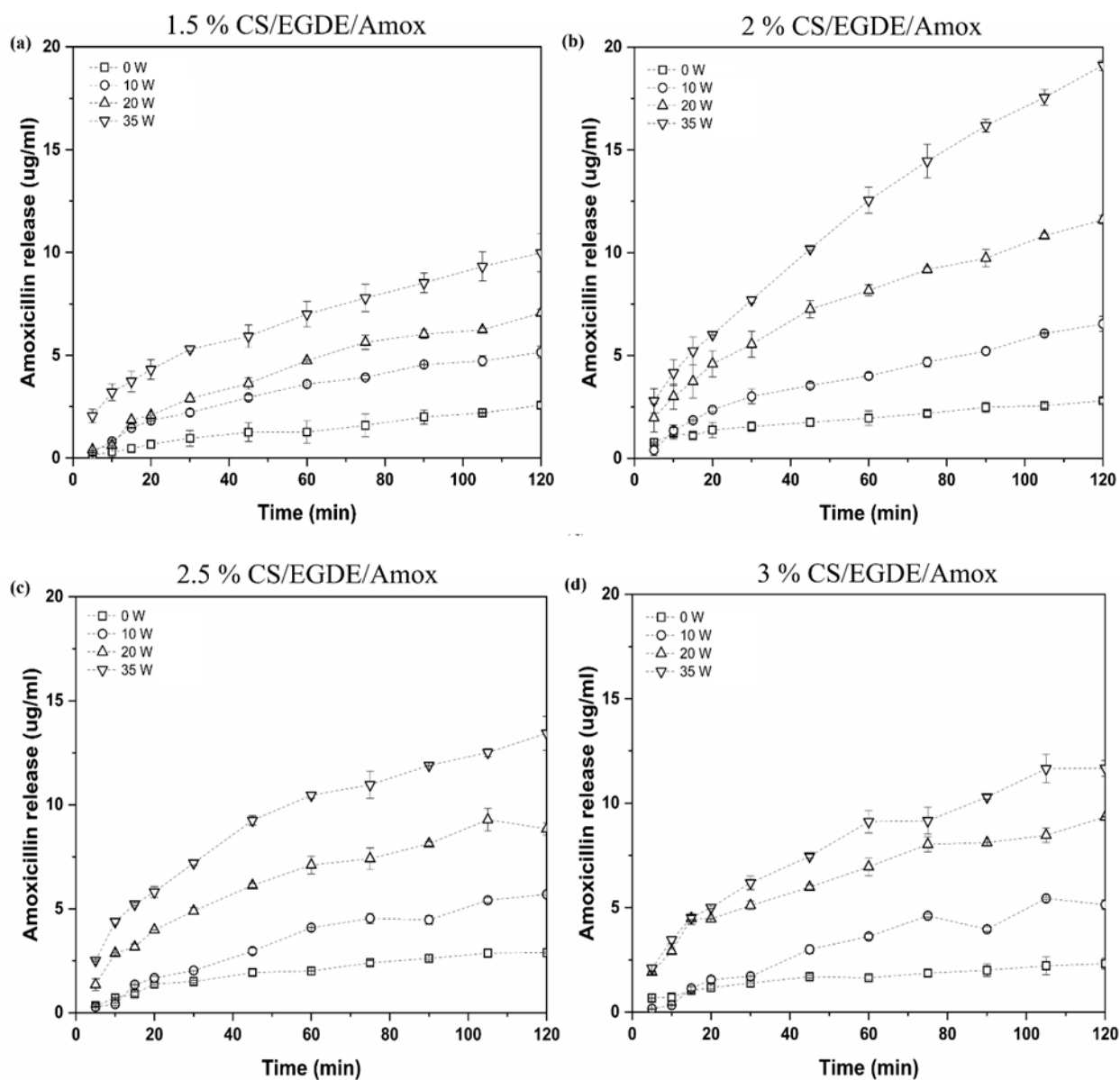


Figure 4.11 Concentration of Amox released into aqueous PBS solution, pH 7.4 was measured against ultrasonic (US) exposure time. The US irradiation was conducted with a frequency of 43 kHz, power of 0-35 W, temperature of 25 °C at various CS contents with 1.5 % (a), 2 % (b), 2.5 % (c), and 3 % (d).

Figure 4 displays the time course of Amox release quantities for hydrogels made of (a) 1.5% CS/EGDE/Amox, (b) 2% CS/EGDE/Amox, (c) 2.5% CS/EGDE/Amox, and (d) 3% CS/EGDE/Amox during US exposure with 0, 10, 20, and 35 W. The

Amox release with and without US altering the output powers of 10 W, 20 W, and 35 W at 43 kHz allowed for comparison. Despite the fact that the US was not exposed to radiation as it was in 0 W, it was shown that the amount of Amox released grew with the passage of time. Comparing findings with and without the US, all samples in the US system exhibited higher release. Additionally, when US power rose from 10 W to 35 W, the Amox release quantities increased along with the exposure period. The largest sustained release of Amox from those Amox-entrapped hydrogels was noted with 2% CS/EGDE/Amox. Approximately 19 g/ml at 35 W for 120 min, 10 g/ml at 20 W, and 5 g/ml at 10 W were the concentrations. In contrast, 1.5%, 2.5%, and 3% CS/EGDE/Amox had lower sustained releases than 2% CS/EGDE/Amox. Similar results were observed for cellulose hydrogels [148] and chitin [149], causing that the initial drug contents inside hydrogels influenced the quantity of amounts of drug released, when US exposure was operated. The entrapped Amox in the 2% CS/EGDE/Amox hydrogel was 252.28 g/g hydrogel. However, the amount of Amox entrapped in the 1.5% CS/EGDE/Amox hydrogels was 188.16 g/g hydrogel, and 208.14 g/g hydrogel for the 3% CS/EGDE/Amox hydrogels, as shown in Table 1. The variation in the trapped Amox quantities observed in the hydrogels formed with different CS concentrations can be attributed to the density of CS. As a result, in the instance of 1.5% CS/EGDE/Amox, where the amount of drug in the gel matrix was modest, the amount of sustained release was similarly reduced. Amox loading was lower in 3% CS/EGDE/Amox than in 2% CS/EGDE/Amox, but higher in 1.5% CS/EGDE/Amox. The changes in entrapped Amox levels in the hydrogels were caused by variations in Amox density and crosslink density, as Amox was

entrapped during the process of immersing the hydrogel matrix in an aqueous Amox solution. The explanation for this is because at 2% CS/EGDE, high porosity with intermediate matrix density was formed, allowing for additional area for Amox loading in the CS/EGDE network. The hydrogel matrix containing 2% CS/EGDE in the presence of US was loosen and roughed, as seen in SEM images in Figure 6b. Furthermore, due to the hydrogel pores being impacted by external US power and collapsing after releasing Amox during US exposure, the morphology of 2% CS/EGDE/Amox was slightly reduced and roughened by US irradiation. As a consequence, after 35 W US exposure after 120 minutes of release, a significant reduction in Amox from 2% CS hydrogel matrix was seen, but red color spots were still visible in EDS images in the event of spontaneous release without US stimulus. The outcome was consistent with medication release data, Amox might release with greater efficacy in response to US response.

4.2.5 Kinetic models of Amox loaded CS/EGDE hydrogels

To further understand the drug release behavior of the hydrogel, zero-order, first-order, Hixson-Crowell, Higuchi, and Korsmeyer-Peppas models were fitted to Figure 5 data. Table 2 lists the physical parameters found for the release exponent (n) and correlation coefficient (r^2). It was discovered that it conformed to both the Higuchi and Korsmeyer-Peppas models, which assumed that Amox release from the hydrogel matrix entrapped with drug follows occurred by diffusion. It was therefore proposed that the impact of US may promote the diffusion of Amox from the inside of the gel matrix to the outside. In addition, the rate of drug release has a linear relationship with the square root of time. The Korsmeyer-Peppas model [150] made the assumption that a combination of diffusion-controlled and

relaxation-controlled processes was responsible for drug release. The kinetic data was noted in Table 2. When US was operated at 35 W/43 kHz, amox release followed a non-Fickian distribution with n values ranging from 0.45 to 0.70, and the r^2 value for all situations was more than 0.95, indicating excellent fitting. However, when the US powers of the 2% CS/EGDE/Amox sample were changed from 10 W to 35 W, the n values were 0.54, 0.55, and 0.61, respectively. As a result of both diffusion and relaxation of the porous hydrogel matrix, drug release occurs. However, the n -value of 2% CS hydrogel in the absence of US was 0.38, which was lower than 0.45, indicating that Amox release from this hydrogel followed the Fickian process, which signifies Amox release exclusively through diffusion.

Table 4.4 Kinetic models of Amox loaded CS/EGDE hydrogels: diffusion exponents, diffusion types, and regression values in PBS 2mM, pH 7.4.

Parameters	Kinetic models						
	Zero-order	First-order	Higuchi	Hixson-Crowell	Korsmeyer-Peppas		
	r^2	r^2	r^2	r^2	n	r^2	
Chitosan concentration (%) at 35 W, 43 kHz	1.5	0.934	0.855	0.999	0.904	0.48	0.995
	2	0.972	0.887	0.994	0.933	0.61	0.998
	2.5	0.926	0.795	0.998	0.851	0.50	0.986
	3	0.936	0.811	0.998	0.868	0.52	0.989
US powers (W) for 2 % CS/EGDE/Amox	0	0.907	0.882	0.993	0.919	0.38	0.974
	10	0.962	0.899	0.996	0.941	0.54	0.992
	20	0.949	0.840	0.999	0.892	0.55	0.998
	35	0.972	0.887	0.994	0.933	0.61	0.998

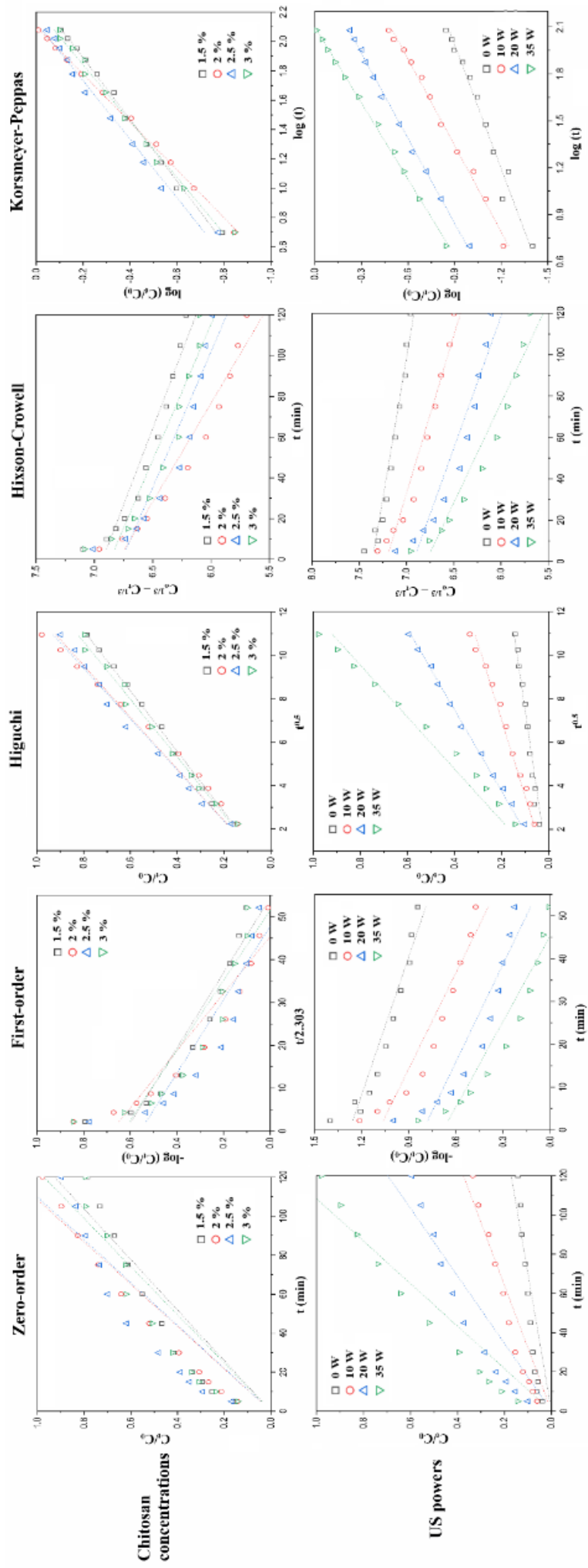


Figure 4.12 Kinetic models of Amox release profile from CS/EGDE/Amox hydrogels (a, f) zero-order, (b, g) first-order, (c, h) Higuchi model, (d, i) Hixson-Crowell model, and (e, j) Korsmeyer-Peppas model of 1.5 %, 2 %, 2.5 %, and 3 % at 35 W/43 kHz; 0 W, 10 W, 20 W, and 35 W of 2 % CS/EGDE/Amox, respectively.

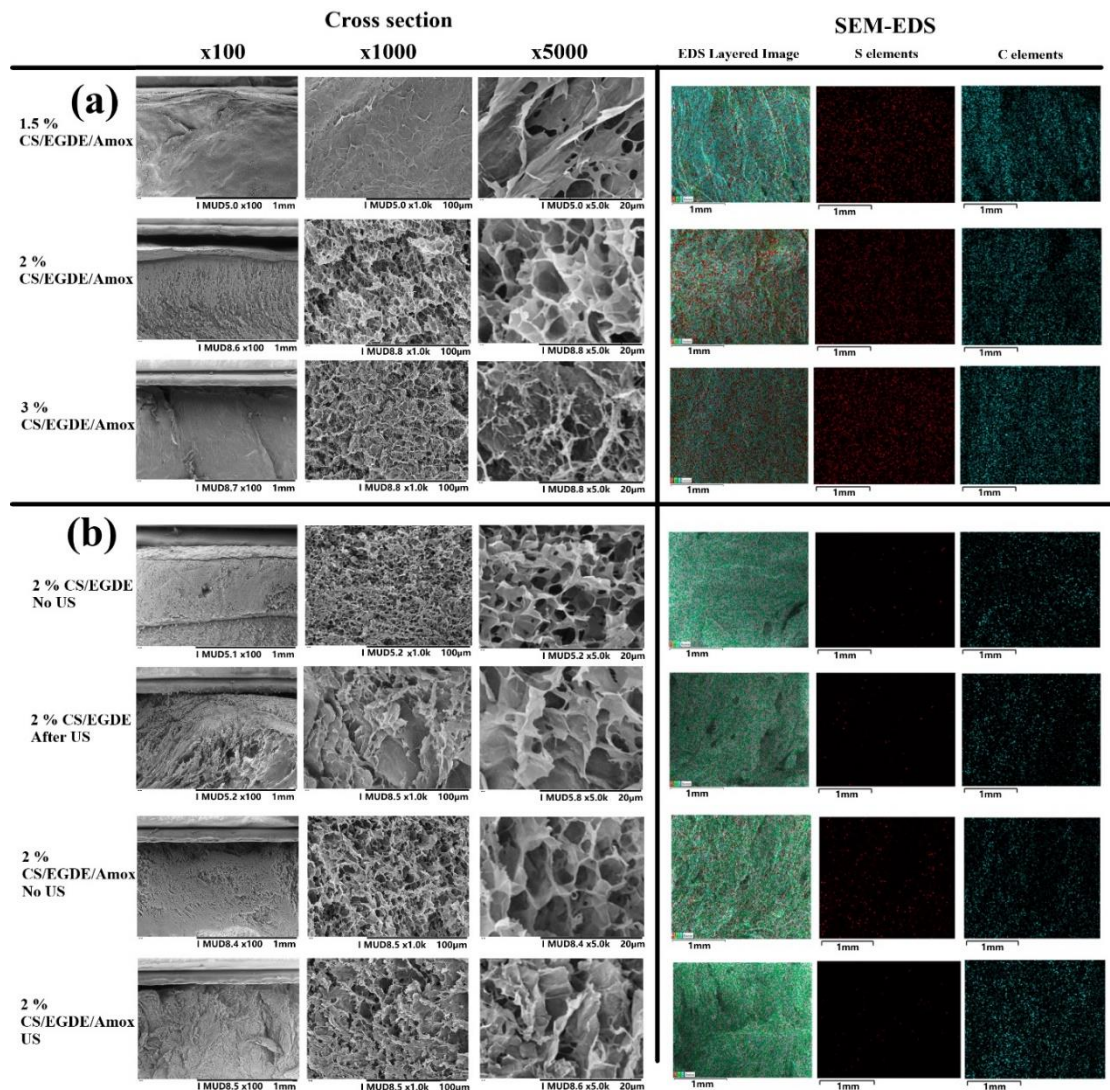


Figure 4.13 Cross-section SEM images of the Amox-entrapped CS/EGDE hydrogels before releasing (a), 2 % CS/EGDE hydrogels and 2 % CS/EGDE/Amox hydrogels after releasing Amox in absence and presence of US for 120 min (b) in x100, x1000, and x5000 magnification (left); EDS layered photo and S, C elements of those hydrogels (right).

4.2.6 US influence on CS/EGDE/Amox hydrogels matrix

4.2.6.1 Evaluation of gelatious properties of polymeric hydrogels

Viscoelasticity information, as is well known, is useful in evaluating the gelatious characteristics of polymeric hydrogels [151]. Figures 7 (a), (c), (e), and (g) show the G' and G'' values of those CS/EGDE/Amox hydrogels before and after 120 minutes of US irradiation. When CS/EGDE and CS/EGDE/Amox G' values were

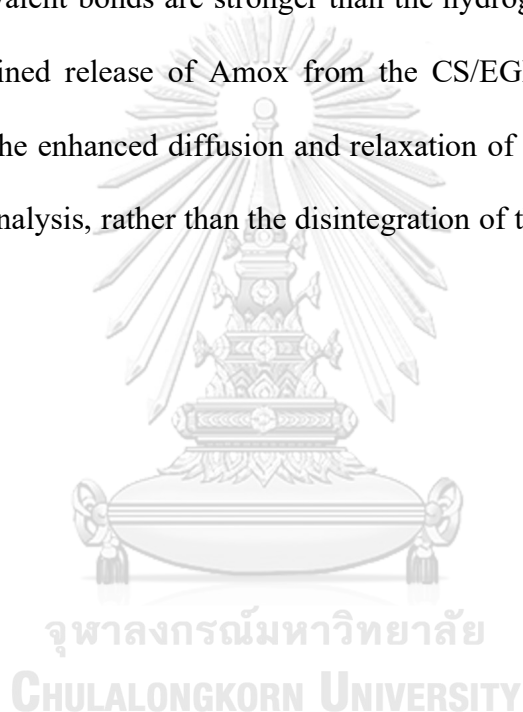
compared in Table 1, the G' values at 0.1% strain tended to decrease when Amox was entrapped. However, the G' value at 0.1% strain rose when the hydrogels were changed from 1.5% CS/EGDE/Amox to 3% CS/EGDE/Amox. The drop in G' caused by Amox entrapment appears to be due to Amox incorporation via amino group interaction. However, the increase in G' with increasing CS concentration from 1.5 % to 3 % could be attributed to the dense gel network in addition to the increase in density.

Figure 7 depicts the change in G' and G'' at strain% after each CS/EGDE hydrogel was exposed to 35W US. The G' value remained nearly constant at 2200, 2950, 3950, and 5520 Pa for the 1.5% CS/EGDE/Amox, 2% CS/EGDE/Amox, 2.5% CS/EGDE/Amox, and 3% CS/EGDE/Amox, respectively. Furthermore, when the strain% grew, the G' dropped, suggesting that the hydrogel structure crumbled and liquefied. The values of G'' were consistent for all hydrogels up to around 10% strain, then rapidly grew and approached the value of G' . When $G' = G''$, the transition from solid gel to liquid gel happened at the strain%. At 0 W, the results for 1.5% CS/EGDE/Amox, 2% CS/EGDE/Amox, and 3% CS/EGDE/Amox were 100%, 99%, and 71% strain, respectively. As a result, the harder 3% CS/EGDE/Amox hydrogel produced a lower strain% of gel structure collapse owing to mechanical stress than the softer 1.5% CS/EGDE/Amox hydrogel. This might be because a tougher hydrogel cannot absorb the mechanical shear force generated by the rheometer. The same experiments with 35 W US irradiation produced nearly the same strain% change as the unirradiated 0 W findings; for 2% CS/EGDE/Amox, US intensities of 10 W and 20 W were also obtained with the 35W results. However, when the US intensity grew, so did the G' values in the

0.1% - 30% strain range. In the instance of 2% CS/EGDE/Amox, the strain% at $G' = G''$ was also altered from roughly 127% to around 90% as the US intensity rose. When US was applied, this research showed that, in addition to mechanical deformation, US shear forces distorted hydrogels and expedited the collapse of the gel structure. As a result, the drop in G' after US irradiation was thought to be caused by the collapse of the hydrogel under mechanical strain imposed by the US. Figure 7i depicts the impact of different US powers on G' value at 0.1% strains of 1.5%, 2%, 2.5%, and 3% CS/EGDE/Amox hydrogels. Due to the softening impact of US, the G' values were going lower when the US output power was increased from 0 W to 35 W for 1.5% and 2% CS/EGDE/Amox. The G' value at 0.1% strain at 0 W, 10 W, 20 W, and 30 W for 2% CS/EGDE/Amox hydrogel was 2950 Pa, 2680 Pa, 2010 Pa, and 1800 Pa, respectively. This indicated that when the US power increased, the gel softened due to gel structural deformation and the significant quantity of Amox released from hydrogels during US irradiation, resulting in a fall in the G' value. Furthermore, the stimulatory impact of US on the hydrogel matrix was demonstrated independent of chitosan concentration differences across different hydrogel systems. The reduction trend of G' value were not significant seen for higher CS contents at 2.5 % and 3 % CS/EGDE/Amox because US force might not effective in the case of dense covalent crosslinking network.

There were prior examples of viscoelastic changes in hydrogels upon US irradiation in cellulose hydrogels [152], in which the mechanical shear force of the rheometer combined with the shear force of US resulted in higher degree of the change than that of CS/EGDE hydrogels. The change of strain % at $G' = G''$ was

also greater for the cellulose hydrogels [153]. In the case of cellulose hydrogels, gelation was mainly due to hydrogen bonding and entanglement of the molecular chains, but no covalent crosslinking like CS/EGDE. In the cellulose hydrogel, hydrogen bond disruption contributed to the softening of the gel due to a decrease in viscoelasticity. In contrast, in the case of CS/EGDE, gelation is due to covalent bonding between CS and EGDE, so US softening of the gel was unlikely to occur because the covalent bonds are stronger than the hydrogen bonds. As a result, the enhanced sustained release of Amox from the CS/EGDE hydrogels might have contributed to the enhanced diffusion and relaxation of hydrogel matrix suggested by the kinetic analysis, rather than the disintegration of the gel matrix by ultrasonic shear forces.



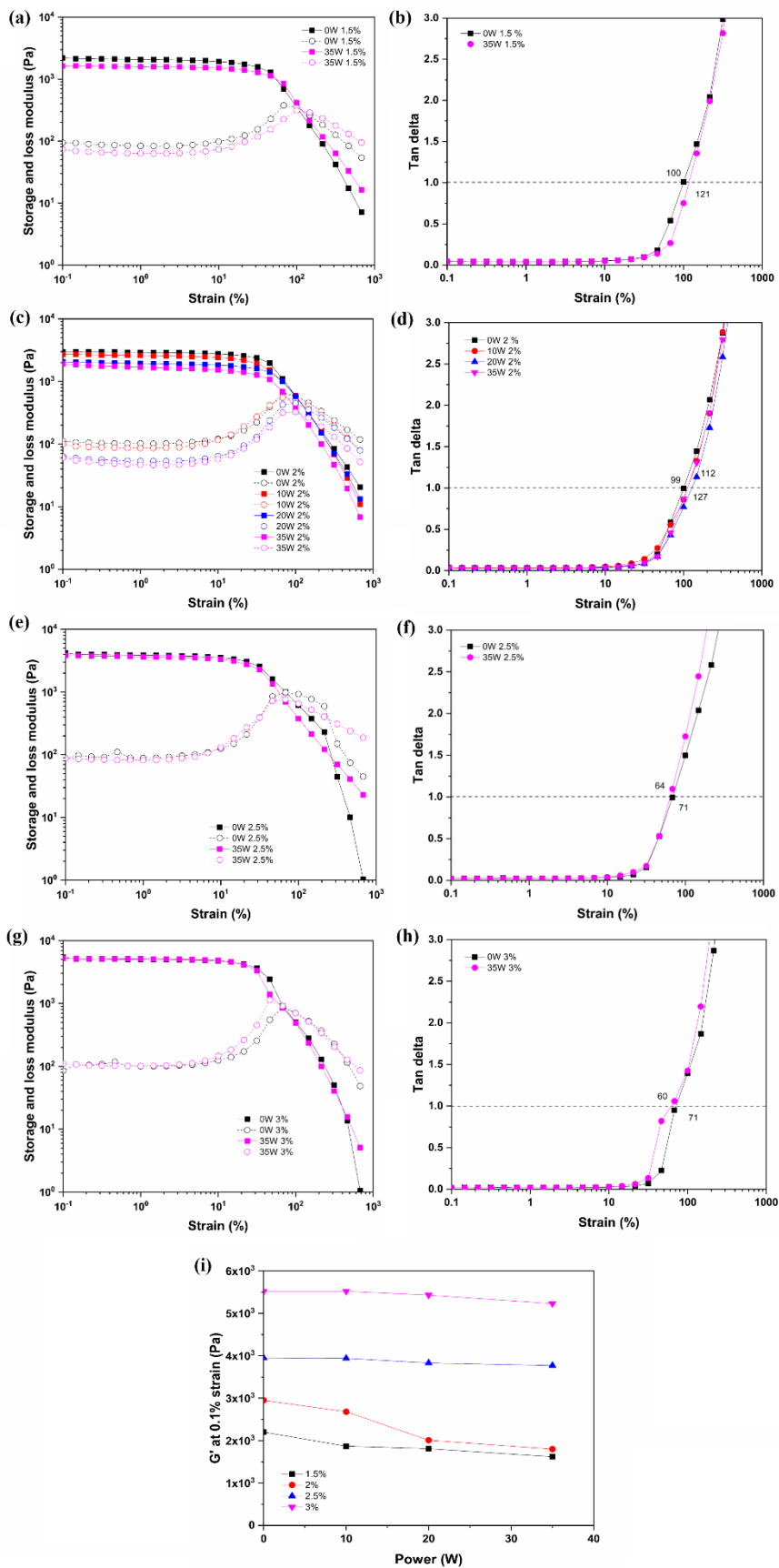


Figure 4.14 Amox-trapped CS/EGDE hydrogels were subjected to strain sweep measurements (a, c, e, g) with corresponding $\tan \delta$ measurements (b, d, f, h), both with and without ultrasonic exposure (43 kHz, 35 W, 120 min). These hydrogels were made from CS solutions with concentrations of 1.5 wt% (a, b), 2 wt% (c, d), 2.5 wt% (e, f), and 3 wt% (g, h). The measurements were performed at a frequency of 1 Hz and characterized by G' (storage moduli), G'' (loss moduli), and $\tan \delta$, which is defined as the ratio of G'' to G' . The relation of G' at 0.1 % strain of Amox-CS/EGDE hydrogels at 1.5 % to 3 % of CS and US powers at 0, 10, 20, and 35 W.

4.2.6.2 Chemical structure confirmation of CS/EGDE hydrogels and Amox loaded CS/EGDE hydrogels

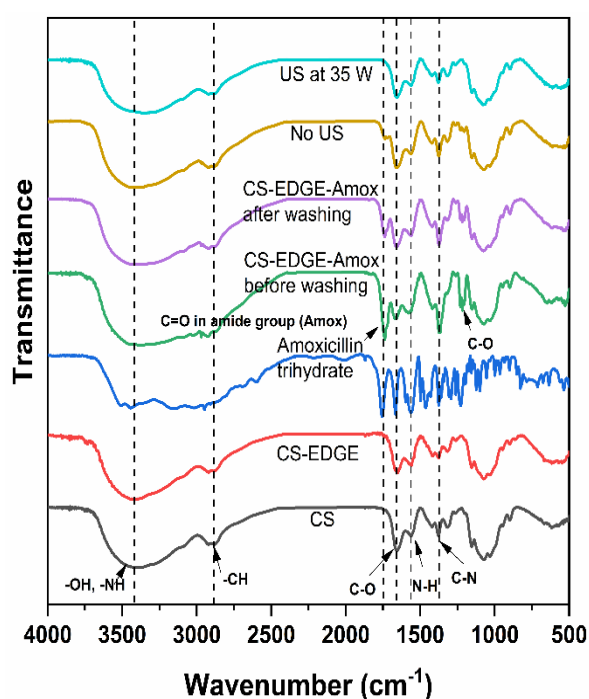


Figure 4.15 Chemical structure confirmation of CS/EGDE hydrogels and Amox loaded CS/EGDE hydrogels before and after releasing with/without US exposure.

The absorption bands of the Amox-derived C=O group were detected at 1750 cm^{-1} and O-C-O at 1240 cm^{-1} in the FTIR spectra presented in Figure 8, suggesting that Amox was certainly in the 2% CS/EGDE/Amox hydrogel. The distinctive bands in the Amox spectra were 1759 cm^{-1} and 1241 cm^{-1} . As a consequence of the comparison between Amox and CS/EGDE/Amox, the C=O band peak in the CS/EGDE/Amox migrated toward the low wavenumber side, resulting in

interaction of the Amox molecule with CS. Similarly, C=O band peaks in the spectra of the 2% CS/EGDE/Amox before and after water washing following immersion in Amox aqueous solution were seen. Specifically, even after washing with water, the observed Amox band was preserved in the hydrogel due to its interaction with CS. The vibrational stretching overlapping peaks of N-H and O-H intermolecular and intramolecular hydrogen bonds were found at 3330 cm^{-1} in the CS. When compared to the CS/EGDE, which did not include Amox, the overlapped peak top seemed to broaden. At about 2879 cm^{-1} , the stretching vibration absorption peak of C-H along the CS chain was identified. Furthermore, the absorption peaks of CS were identified at 1645 (amide I), 1567 (amide II), and 1387 cm^{-1} (amide III), which can be attributed primarily to the stretching vibrations of the C-O, N-H bond, and C-N bond, respectively, and those peaks of the 2% CS/EGDE/Amox were appeared at 1750 cm^{-1} , 1387 cm^{-1} , and 1215 cm^{-1} . Even though the peaks of Amox-entrapped CS/EGDE shifted somewhat when compared to the Amox spectra, this indicated a CS-Amox interaction. Two peaks were found for the distinctive saccharide backbone at 1141 and 1021 cm^{-1} , which corresponded to the antisymmetric stretching of the C-O-C bridge and the ring's C-O vibration. Figure 8 also displays the observed spectra following a 120-minute exposure to US radiation at 35W. The presence of Amox's distinctive C=O in this spectrum indicated that its sustained release was virtually complete. The hydrogel's residual spectrum was nearly identical to that of the hydrogel before Amox got trapped in it. This implied that the hydrogel did not decompose even after 120 minutes of sonication.

CHAPTER 5

CONCLUSION

This research aims to investigate chitosan-based hydrogels as the antibiotic carriers matrix for drug delivery systems to enhance the effectiveness of the medicine and minimize the side effects of the antibiotic by providing targeted and controlled release of drug in response to external stimuli like pH and ultrasound triggers. To synthesize chitosan hydrogel, gamma irradiation and EGDE crosslinker were utilized due to its non-toxicity, thus these methods could apply in biomedical applications.

The first step is to optimize chitosan and PVA ratios to obtain the better physico-chemical properties of hybrid hydrogels:

1. At 10 kGy and 30 kGy, 75/25 CS/PVA could not form a gel meanwhile at 25 kGy approximately 20% gel fraction was attained. The gel fraction of the 50/50 CS/PVA hydrogel exhibited significant change greater than 4 times as compared to those of the 75/25 CS/PVA hydrogel at 25 kGy.
2. At 10, 25, and 30 kGy, the equilibrium swelling degrees of the 50/50 CS/PVA hydrogel were 8.4-, 4.7-, and 5.2-fold compared to the dried state after 24 h, respectively because the higher crosslinking of polymer chains at 25 kGy formed a stronger network with higher resistance to expansion. At pH 7, 10, and 13, the 50/50 CS/PVA hydrogel prepared at 25 kGy had a lower SR than those at pH 1 and 4. The swelling degree of the hydrogel at pH 1 increased by two-fold to approximately 7 (g/g) compared to that at pH 13.

3. The decomposition temperatures (T_d) of CS and blended hydrogels were 223 and 240–266 °C, respectively emphasizing the improvement in thermal stability of crosslinked hydrogel. The T_d of the 50/50 CS/PVA hydrogel slightly increased, revealing higher crosslink densities at higher radiation doses.
4. The highly interconnected porous structures of the blended hydrogels may be used for the loading and release of medicines owing to their better swelling characteristics as compared to neat PVA.
5. The release of amoxicillin from 50/50 CS/PVA hydrogel in the physiological environment of PBS is greater compared to in DI water with 85%, 50% at pH 2.1 and 7.4 in PBS media; 34% at pH 5.5 in DI water. The higher percentage of released drugs from CS/PVA hydrogel might be due to amoxicillin solubility which is impacted by pH and ionic strength. Following KP model, the drug release is controlled by diffusion and polymer network relaxation.

From these results, it is proposed that the created gamma-irradiated CS/PVA hydrogels be employed as medication carriers.

As for the second step, the release of Amox from the CS/EGDE/Amox hydrogel matrix in response to US was studied under various US powers (0-35 W) at 43 kHz.

1. As CS concentrations rose from 1 % to 3 % of the CS/EGDE solution, the values of G' and G'' tended to increase with increasing time. G' started to increase at about 200 s, 30 s, 11 s and 10 s for 1.5, 2, 2.5, and 3 %, respectively. The decrease trend in the gelation time was seen from 254 s, 70

s, and 40 s for 1.5 %, 2 % and 3 % CS concentrations, respectively meaning that gelation occurred faster at higher CS concentrations. Furthermore, the resultant gels became harder when CS content increased causing G' value at 0.1 % strain increased 2.2×10^3 Pa at 1.5 % CS/EGDE and 7.3×10^3 Pa at 3 % CS/EGDE.

2. The soft 1.5 % CS/EGDE hydrogel showed less densities than the hard 3 % CS/EGDE hydrogel in the Amox-free CS/EGDE before the drug was entrapped. Conversely, the water content was 2929 ± 24 % for the former, indicating more water retention than the latter 3 % CS/EGDE having 1814 ± 21 %. After post-ultrasonic irradiation values showed a slight increase in water retention with US irradiation. for the flexible 1.5 % and 2 % CS/EGDE/Amox, but not for the rigid hydrogel 3% CS/EGDE/Amox; on the contrary, the moisture content decreased.
3. A sponge network of CS forming a dense structure as the CS concentration increased from 1.5% to 3%, was exhibited in SEM images. The Amox-derived Sulfur on EDS pattern was found to be widely distributed within the inner sponge structure of the gel after immersion of each hydrogel in Amox solution. Furthermore, the morphology of 2 % CS/EGDE/Amox was somewhat shrunk and roughed by US irradiation because the hydrogel pores influenced by external US power causing the collapse of the porous structure after releasing Amox under US exposure.
4. Increasing US power from 10 W to 35 W, the Amox release amounts became high when increased the exposure time increased. Among those Amox entrapped hydrogels, the highest sustained release of Amox was observed with

2 % CS/EGDE/Amox. The quantity reached roughly 19 $\mu\text{g/ml}$ at 35 W for 120 min, 10 $\mu\text{g/ml}$ at 20 W, and 5 $\mu\text{g/ml}$ at 10 W.

5. The drug release data of the hydrogels were fitted with Higuchi model and Korsmeyer-Peppas model. Amox release followed a non-Fickian distribution with n values ranging from 0.45 to 0.70 for the CS/EGDE/Amox hydrogels at different CS concentrations, when US was operated at 35 W/43 kHz, and the r^2 value for all conditions was greater than 0.95, meaning well fitting. In the case of changing US powers from 10 W to 35 W of 2 % CS/EGDE/Amox sample, the results of n values were 0.54, 0.55, and 0.61, respectively. Thus, drug release occurs as a consequence of both diffusion and relaxation of the porous hydrogel matrix. However, the Amox released from 2 % CS/EGDE in absence of US was by diffusion only with n -value = 0.38.

In conclusion, this study demonstrated the use of covalently bonded CS/EGDE hydrogels as a carrier for antibiotics. The utilization of US stimulation resulted in a significant increase in the release rate of Amox, indicating a controlled release mechanism facilitated by the softening of the hydrogel and enhanced drug diffusion.

REFERENCES

1. Ahmed, E.M., Hydrogel: Preparation, characterization, and applications: A review. *J Adv Res*, 2015. **6**(2): p. 105-21.
2. Wang, M., et al., Preparation and characterization of novel poly (vinyl alcohol)/collagen double-network hydrogels. *Int J Biol Macromol*, 2018. **118**(Pt A): p. 41-48.
3. Abd Alla, S.G., M. Sen, and A.W. El-Naggar, Swelling and mechanical properties of superabsorbent hydrogels based on Tara gum/acrylic acid synthesized by gamma radiation. *Carbohydr Polym*, 2012. **89**(2): p. 478-85.
4. Wang, W., R. Narain, and H. Zeng, Hydrogels, in *Polymer Science and Nanotechnology*. 2020. p. 203-244.
5. Li, J. and D.J. Mooney, Designing hydrogels for controlled drug delivery. *Nature Reviews Materials*, 2016. **1**(12): p. 16071.
6. Bordbar-Khiabani, A. and M. Gasik Smart Hydrogels for Advanced Drug Delivery Systems. *International Journal of Molecular Sciences*, 2022. **23**, DOI: 10.3390/ijms23073665.
7. Billiet, T., et al., A review of trends and limitations in hydrogel-rapid prototyping for tissue engineering. *Biomaterials*, 2012. **33**(26): p. 6020-41.
8. Tabata, Y., Biomaterial technology for tissue engineering applications. *J R Soc Interface*, 2009. **6 Suppl 3**(Suppl 3): p. S311-24.
9. Ullah, F., et al., Classification, processing and application of hydrogels: A review. *Mater Sci Eng C Mater Biol Appl*, 2015. **57**: p. 414-33.
10. Catoira, M.C., et al., Overview of natural hydrogels for regenerative medicine applications. *Journal of Materials Science: Materials in Medicine*, 2019. **30**(10): p. 115.
11. Gyles, D.A., et al., A review of the designs and prominent biomedical advances of natural and synthetic hydrogel formulations. *European Polymer Journal*, 2017. **88**: p. 373-392.
12. Ahmed, E.M., Hydrogel: Preparation, characterization, and applications: A review. *Journal of Advanced Research*, 2015. **6**(2): p. 105-121.
13. Ranjan, N., et al., Chapter 5 - Hydrogels for additive manufacturing in

- scaffolding applications: A review, in *Innovative Processes and Materials in Additive Manufacturing*, S. Singh, C. Prakash, and S. Ramakrishna, Editors. 2023, Woodhead Publishing. p. 103-129.
14. Dutta, S., et al., Interpenetrating polymer networks for desalination and water remediation: a comprehensive review of research trends and prospects. *RSC Advances*, 2023. **13**(9): p. 6087-6107.
 15. Prestwich, G.D. and S. Atzet, Chapter I.2.7 - Engineered Natural Materials, in *Biomaterials Science (Third Edition)*, B.D. Ratner, et al., Editors. 2013, Academic Press. p. 195-209.
 16. Revete, A., et al., Advancements in the Use of Hydrogels for Regenerative Medicine: Properties and Biomedical Applications. *International Journal of Biomaterials*, 2022. **2022**: p. 3606765.
 17. Spinks, G.M., et al., Swelling Behavior of Chitosan Hydrogels in Ionic Liquid–Water Binary Systems. *Langmuir*, 2006. **22**(22): p. 9375-9379.
 18. Park, H., K. Park, and D. Kim, Preparation and swelling behavior of chitosan-based superporous hydrogels for gastric retention application. *Journal of Biomedical Materials Research Part A*, 2006. **76A**(1): p. 144-150.
 19. Qu, X., A. Wirsén, and A.C. Albertsson, Novel pH-sensitive chitosan hydrogels: swelling behavior and states of water. *Polymer*, 2000. **41**(12): p. 4589-4598.
 20. Lee, D., H. Zhang, and S. Ryu, Elastic Modulus Measurement of Hydrogels, in *Cellulose-Based Superabsorbent Hydrogels*, M.I.H. Mondal, Editor. 2018, Springer International Publishing: Cham. p. 1-21.
 21. Duan, J., et al., High Strength Chitosan Hydrogels with Biocompatibility via New Avenue Based on Constructing Nanofibrous Architecture. *Macromolecules*, 2015. **48**(8): p. 2706-2714.
 22. Schoenmakers, D.C., A.E. Rowan, and P.H.J. Kouwer, Crosslinking of fibrous hydrogels. *Nature Communications*, 2018. **9**(1): p. 2172.
 23. Wu, J., et al., An intrinsically stretchable humidity sensor based on anti-drying, self-healing and transparent organohydrogels. *Materials Horizons*, 2019. **6**(3): p. 595-603.
 24. Roy, N., et al., Importance of Viscoelastic Property Measurement of a New

- Hydrogel for Health Care. AIP Conference Proceedings, 2009. **1152**(1): p. 210-216.
25. Kocen, R., et al., Viscoelastic behaviour of hydrogel-based composites for tissue engineering under mechanical load. *Biomedical Materials*, 2017. **12**(2): p. 025004.
 26. Feksa, L.R., et al., Hydrogels for biomedical applications, in *Nanostructures for the Engineering of Cells, Tissues and Organs*. 2018. p. 403-438.
 27. <Novel crosslinking methods to design hydrogels.pdf>.
 28. Martínez-Ruvalcaba, A., E. Chornet, and D. Rodrigue, Viscoelastic properties of dispersed chitosan/xanthan hydrogels. *Carbohydrate Polymers*, 2007. **67**(4): p. 586-595.
 29. Bourges, X., et al., General properties of silylated hydroxyethylcellulose for potential biomedical applications. *Biopolymers*, 2002. **63**(4): p. 232-8.
 30. <Preparation method, Properties and Crosslinking of hydrogel a review.pdf>.
 31. Yang, C., et al., Electrodeposition induced covalent cross-linking of chitosan for electrofabrication of hydrogel contact lenses. *Carbohydrate Polymers*, 2022. **292**: p. 119678.
 32. Lin, X., et al., Poly(2-hydroxyethyl methacrylate-co-quaternary ammonium salt chitosan) hydrogel: A potential contact lens material with tear protein deposition resistance and antimicrobial activity. *Biomaterials Advances*, 2022. **136**: p. 212787.
 33. Jiao, Z., et al., Drug-free contact lens based on quaternized chitosan and tannic acid for bacterial keratitis therapy and corneal repair. *Carbohydrate Polymers*, 2022. **286**: p. 119314.
 34. Hyon, S.-H., et al., Poly(vinyl alcohol) hydrogels as soft contact lens material. *Journal of Biomaterials Science, Polymer Edition*, 1994. **5**(5): p. 397-406.
 35. Tang, G., et al., Recent Advances of Chitosan-Based Injectable Hydrogels for Bone and Dental Tissue Regeneration. *Frontiers in Bioengineering and Biotechnology*, 2020. **8**.
 36. Adekogbe, I. and A. Ghanem, Fabrication and characterization of DTBP-crosslinked chitosan scaffolds for skin tissue engineering. *Biomaterials*, 2005.

- 26(35)**: p. 7241-7250.
37. Rogina, A., et al., Cellular hydrogels based on pH-responsive chitosan-hydroxyapatite system. *Carbohydrate Polymers*, 2017. **166**: p. 173-182.
 38. Li, B., et al., Hydrosoluble, UV-crosslinkable and injectable chitosan for patterned cell-laden microgel and rapid transdermal curing hydrogel in vivo. *Acta Biomaterialia*, 2015. **22**: p. 59-69.
 39. Zheng, C., et al., Effective wound dressing based on Poly (vinyl alcohol)/Dextran-aldehyde composite hydrogel. *Int J Biol Macromol*, 2019. **132**: p. 1098-1105.
 40. Ren, G., et al., Electrospun poly(vinyl alcohol)/glucose oxidase biocomposite membranes for biosensor applications. *Reactive and Functional Polymers*, 2006. **66(12)**: p. 1559-1564.
 41. Wu, S., et al. Chitosan-Based Hydrogels for Bioelectronic Sensing: Recent Advances and Applications in Biomedicine and Food Safety. *Biosensors*, 2023. **13**, DOI: 10.3390/bios13010093.
 42. Quan, L., et al., Mussel-inspired chitosan-based hydrogel sensor with pH-responsive and adjustable adhesion, toughness and self-healing capability. *Polymers for Advanced Technologies*, 2022. **33(6)**: p. 1867-1880.
 43. Aycan, D. and N. Alemdar, Development of pH-responsive chitosan-based hydrogel modified with bone ash for controlled release of amoxicillin. *Carbohydr Polym*, 2018. **184**: p. 401-407.
 44. Nisar, S., et al., gamma-Radiation induced L-glutamic acid grafted highly porous, pH-responsive chitosan hydrogel beads: A smart and biocompatible vehicle for controlled anti-cancer drug delivery. *Int J Biol Macromol*, 2021. **182**: p. 37-50.
 45. Raza, M.A., et al., Synthesis and characterization of hydrogels based on carboxymethyl chitosan and poly(vinylpyrrolidone) blends prepared by electron beam irradiation having anticancer efficacy, and applications as drug carrier for controlled release of drug. *Carbohydr Polym*, 2021. **258**: p. 117718.
 46. Yang, X.L., et al., Core-Shell Chitosan Microcapsules for Programmed Sequential Drug Release. *ACS Appl Mater Interfaces*, 2016. **8(16)**: p. 10524-34.

47. Iqbal, D.N., et al., Enhanced antibacterial activity of chitosan, guar gum and polyvinyl alcohol blend matrix loaded with amoxicillin and doxycycline hyclate drugs. *Arabian Journal of Chemistry*, 2021. **14**(6).
48. Daraghmeh, N.H., et al., Chitin. *Profiles Drug Subst Excip Relat Methodol*, 2011. **36**: p. 35-102.
49. Peers, S., A. Montembault, and C. Ladaviere, Chitosan hydrogels for sustained drug delivery. *J Control Release*, 2020. **326**: p. 150-163.
50. Garg, U., et al., Current Advances in Chitosan Nanoparticles Based Drug Delivery and Targeting. *Adv Pharm Bull*, 2019. **9**(2): p. 195-204.
51. Herdiana, Y., et al., Drug release study of the chitosan-based nanoparticles. *Heliyon*, 2022. **8**(1): p. e08674.
52. Hamed, H., et al., Chitosan based hydrogels and their applications for drug delivery in wound dressings: A review. *Carbohydrate Polymers*, 2018. **199**: p. 445-460.
53. Selvakumaran, S., I. Muhamad, and N.A. Md Lazim, Designing Polymeric Nanoparticles for Targeted Drug Delivery System. 2014. p. 287-313.
54. Ding, B., et al., Tough and Cell-Compatible Chitosan Physical Hydrogels for Mouse Bone Mesenchymal Stem Cells in Vitro. *ACS Applied Materials & Interfaces*, 2016. **8**(30): p. 19739-19746.
55. Rivera-Hernández, G., et al., Polyvinyl alcohol based-drug delivery systems for cancer treatment. *International Journal of Pharmaceutics*, 2021. **600**: p. 120478.
56. Flores-Arriaga, J.C., et al., Synthesis of a PVA drug delivery system for controlled release of a Tramadol–Dexketoprofen combination. *Journal of Materials Science: Materials in Medicine*, 2021. **32**(5): p. 56.
57. Villanueva-Flores, F., et al., Poly(vinyl alcohol co-vinyl acetate) as a novel scaffold for mammalian cell culture and controlled drug release. *Journal of Materials Science*, 2019. **54**(10): p. 7867-7882.
58. Kamoun, E.A., et al., Crosslinked poly(vinyl alcohol) hydrogels for wound dressing applications: A review of remarkably blended polymers. *Arabian Journal of Chemistry*, 2015. **8**(1): p. 1-14.
59. Teodorescu, M. and S. Morariu, Drug delivery system based on PVA and clay

- for potential treatment of COVID-19. *Journal of Polymer Research*, 2022. **29**(2): p. 67.
60. Teixeira, M.A., M.T.P. Amorim, and H.P. Felgueiras, Poly(Vinyl Alcohol)-Based Nanofibrous Electrospun Scaffolds for Tissue Engineering Applications. *Polymers (Basel)*, 2019. **12**(1).
 61. Pella, M.C.G., et al., Chitosan-based hydrogels: From preparation to biomedical applications. *Carbohydr Polym*, 2018. **196**: p. 233-245.
 62. Mittal, H., et al., Recent progress in the structural modification of chitosan for applications in diversified biomedical fields. *European Polymer Journal*, 2018. **109**: p. 402-434.
 63. Fu, J., F. Yang, and Z. Guo, The chitosan hydrogels: from structure to function. *New Journal of Chemistry*, 2018. **42**(21): p. 17162-17180.
 64. Cui, Z., et al., Ionic interactions between sulfuric acid and chitosan membranes. *Carbohydrate Polymers*, 2008. **73**(1): p. 111-116.
 65. <Novel pH-sensitive citrate cross-linked chitosan film.pdf>.
 66. <The influence of multivalent phosphate structure on the properties.pdf>.
 67. Huang, S.-C., et al., Programmable Electrostatic Interactions Expand the Landscape of Dynamic Functional Hydrogels. *Chemistry of Materials*, 2020. **32**(5): p. 1937-1945.
 68. Bi, S., et al., The toughness chitosan-PVA double network hydrogel based on alkali solution system and hydrogen bonding for tissue engineering applications. *Int J Biol Macromol*, 2020. **146**: p. 99-109.
 69. Szalewicz, K., Hydrogen Bond, in *Encyclopedia of Physical Science and Technology (Third Edition)*, R.A. Meyers, Editor. 2003, Academic Press: New York. p. 505-538.
 70. Zhang, Z.-X., et al., Autonomous Chitosan-Based Self-Healing Hydrogel Formed through Noncovalent Interactions. *ACS Applied Polymer Materials*, 2019. **1**(7): p. 1769-1777.
 71. Collins, E.D. and C.L. Ottinger, Isotopes, Separation and Application, in *Encyclopedia of Physical Science and Technology (Third Edition)*, R.A. Meyers, Editor. 2003, Academic Press: New York. p. 109-126.

72. Clarke, R.H. and J. Valentin, The History of ICRP and the Evolution of its Policies: Invited by the Commission in October 2008. *Annals of the ICRP*, 2009. **39**(1): p. 75-110.
73. Eden, R.J., *Nuclear Physics*, 1956. **1**(8): p. 311.
74. L'Annunziata, M.F., 3 - Gamma- and X-Radiation — Photons, in *Radioactivity*, M.F. L'Annunziata, Editor. 2007, Elsevier Science B.V.: Amsterdam. p. 187-215.
75. Ioan, M.R., et al. COMPUTATIONAL METHOD FOR THE DETERMINATION OF INTENSE GAMMA-RAYS SOURCES ACTIVITY BY USING GEANT4. 2017.
76. Boujelbane, F., et al., Decomposition mechanism of hydroxychloroquine in aqueous solution by gamma irradiation. *Chem Zvesti*, 2022. **76**(3): p. 1777-1787.
77. Ferry, M., et al., Ionizing Radiation Effects in Polymers, in *Reference Module in Materials Science and Materials Engineering*. 2016, Elsevier.
78. Lousada, C.M., et al., Gamma radiation induces hydrogen absorption by copper in water. *Scientific Reports*, 2016. **6**(1): p. 24234.
79. Jiménez-Becerril, J., A. Moreno-López, and M. Jiménez-Reyes, Radiocatalytic degradation of dissolved organic compounds in wastewater. *Nukleonika*, 2016. **61**(4): p. 473-476.
80. Naikwadi, A.T., et al., Gamma Radiation Processed Polymeric Materials for High Performance Applications: A Review. *Frontiers in Chemistry*, 2022. **10**.
81. Parsons, B.J., 8 - Sterilisation of healthcare products by ionising radiation: sterilisation of drug-device products and tissue allografts, in *Sterilisation of Biomaterials and Medical Devices*, S. Lerouge and A. Simmons, Editors. 2012, Woodhead Publishing. p. 212-239.
82. Beerlage, C., et al., Change in Radiation Sterilization Process from Gamma Ray to X-ray. *Biomedical Instrumentation & Technology*, 2021. **55**(s3): p. 78-84.
83. B.G. Porto, K.M., C.M. Napolitano, and S.I. Borrely, Gamma radiation effects in packaging for sterilization of health products and their constituents paper and

- plastic film. *Radiation Physics and Chemistry*, 2018. **142**: p. 23-28.
84. Gomes, A.D., et al., Gamma sterilization of collagen/hydroxyapatite composites: Validation and radiation effects. *Applied Radiation and Isotopes*, 2021. **174**: p. 109758.
85. Sokary, R., et al., A potential antibiofilm, antimicrobial and anticancer activities of chitosan capped gold nanoparticles prepared by γ -irradiation. *Materials Technology*, 2021. **37**(7): p. 493-502.
86. Leyva-Gomez, G., et al., A novel hydrogel of poloxamer 407 and chitosan obtained by gamma irradiation exhibits physicochemical properties for wound management. *Mater Sci Eng C Mater Biol Appl*, 2017. **74**: p. 36-46.
87. Fan, L., et al., Preparation and characterization of chitosan/gelatin/PVA hydrogel for wound dressings. *Carbohydr Polym*, 2016. **146**: p. 427-34.
88. Guo, W., et al., Chitosan/polyvinyl alcohol/tannic acid multiple network composite hydrogel: preparation and characterization. *Iranian Polymer Journal*, 2021. **30**(11): p. 1159-1168.
89. Islam, A., T. Yasin, and I.u. Rehman, Synthesis of hybrid polymer networks of irradiated chitosan/poly(vinyl alcohol) for biomedical applications. *Radiation Physics and Chemistry*, 2014. **96**: p. 115-119.
90. Gad, Y.H., Preparation and characterization of poly(2-acrylamido-2-methylpropane-sulfonic acid)/Chitosan hydrogel using gamma irradiation and its application in wastewater treatment. *Radiation Physics and Chemistry*, 2008. **77**(9): p. 1101-1107.
91. Jawad, A.H., et al., Biofilm of cross-linked Chitosan-Ethylene Glycol Diglycidyl Ether for removal of Reactive Red 120 and Methyl Orange: Adsorption and mechanism studies. *Journal of Environmental Chemical Engineering*, 2019. **7**(2).
92. Rafat, M., et al., PEG-stabilized carbodiimide crosslinked collagen-chitosan hydrogels for corneal tissue engineering. *Biomaterials*, 2008. **29**(29): p. 3960-72.
93. Lou, C., et al., Dialdehyde-beta-cyclodextrin-crosslinked carboxymethyl chitosan hydrogel for drug release. *Carbohydr Polym*, 2020. **231**: p. 115678.
94. Gao, L., et al., Effects of genipin cross-linking of chitosan hydrogels on cellular adhesion and viability. *Colloids Surf B Biointerfaces*, 2014. **117**: p. 398-405.

95. Bratskaya, S., et al., Chitosan Gels and Cryogels Cross-Linked with Diglycidyl Ethers of Ethylene Glycol and Polyethylene Glycol in Acidic Media. *Biomacromolecules*, 2019. **20**(4): p. 1635-1643.
96. Abdulhameed, A.S., A.H. Jawad, and A.T. Mohammad, Synthesis of chitosan-ethylene glycol diglycidyl ether/TiO(2) nanoparticles for adsorption of reactive orange 16 dye using a response surface methodology approach. *Bioresour Technol*, 2019. **293**: p. 122071.
97. Liu, C., et al., Surface grafted chitosan gels. Part II. Gel formation and characterization. *Langmuir*, 2014. **30**(29): p. 8878-88.
98. He, M. and C.-C. Chu, Dual stimuli responsive glycidyl methacrylate chitosan-quaternary ammonium hybrid hydrogel and its bovine serum albumin release. *Journal of Applied Polymer Science*, 2013. **130**(5): p. 3736-3745.
99. Yin, M., et al., Functional chitosan/glycidyl methacrylate-based cryogels for efficient removal of cationic and anionic dyes and antibacterial applications. *Carbohydr Polym*, 2021. **266**: p. 118129.
100. Jabeen, S., et al., Influence of chitosan and epoxy cross-linking on physical properties of binary blends. *International Journal of Polymer Analysis and Characterization*, 2015. **21**(2): p. 163-174.
101. Garnica-Palafox, I.M., et al., Mechanical and structural response of a hybrid hydrogel based on chitosan and poly(vinyl alcohol) cross-linked with epichlorohydrin for potential use in tissue engineering. *J Biomater Sci Polym Ed*, 2014. **25**(1): p. 32-50.
102. Tripodo, G., et al., Hydrogels for biomedical applications from glycol chitosan and PEG diglycidyl ether exhibit pro-angiogenic and antibacterial activity. *Carbohydr Polym*, 2018. **198**: p. 124-130.
103. Zalipsky*, S., Functionalized Poly(ethylene glycol) for Preparation of Biologically Relevant Conjugates. *Bioconjugate Chem*, 1995. **6**(2): p. 150-165.
104. He, Q., et al., In Vitro Synthesis of Branchless Linear (1 → 6)- α -d-Glucan by Glucosyltransferase K: Mechanical and Swelling Properties of Its Hydrogels Crosslinked with Diglycidyl Ethers. *ACS Omega*, 2020. **5**(48): p. 31272-31280.
105. He, Q., et al., Highly swellable hydrogel of regioselectively aminated (1→3)- α -

- d-glucan crosslinked with ethylene glycol diglycidyl ether. *Carbohydrate Polymers*, 2020. **237**: p. 116189.
106. Tavsanlı, B. and O. Okay, Preparation and fracture process of high strength hyaluronic acid hydrogels cross-linked by ethylene glycol diglycidyl ether. *Reactive and Functional Polymers*, 2016. **109**: p. 42-51.
 107. Lawal, O.S., et al., Microporous hydrogels of cellulose ether cross-linked with di- or polyfunctional glycidyl ether made for the delivery of bioactive substances. *Colloid and Polymer Science*, 2011. **289**(11): p. 1261-1272.
 108. Kalidason, A., et al., Biodegradable Crosslinked Chitosan Gel Microbeads with Controlled Size, Prepared by Membrane Emulsification-External Gelation and Their Application as Reusable Adsorption Materials. *JOURNAL OF CHEMICAL ENGINEERING OF JAPAN*, 2022. **55**(1): p. 61-70.
 109. 6 - Drug delivery systems, in *Strategies to Modify the Drug Release from Pharmaceutical Systems*, M.L. Bruschi, Editor. 2015, Woodhead Publishing. p. 87-194.
 110. Park, H., A. Otte, and K. Park, Evolution of drug delivery systems: From 1950 to 2020 and beyond. *Journal of Controlled Release*, 2022. **342**: p. 53-65.
 111. Reza Rezaie, H., et al., The History of Drug Delivery Systems, in *A Review of Biomaterials and Their Applications in Drug Delivery*, H. Reza Rezaie, et al., Editors. 2018, Springer Singapore: Singapore. p. 1-8.
 112. Kundu, P., S. Das, and N. Chattopadhyay, Switching from endogenous to exogenous delivery of a model drug to DNA through micellar engineering. *Journal of Photochemistry and Photobiology B: Biology*, 2020. **203**: p. 111765.
 113. Raza, A., et al. Endogenous and Exogenous Stimuli-Responsive Drug Delivery Systems for Programmed Site-Specific Release. *Molecules*, 2019. **24**, DOI: 10.3390/molecules24061117.
 114. Gaohua, L., X. Miao, and L. Dou, Crosstalk of physiological pH and chemical pKa under the umbrella of physiologically based pharmacokinetic modeling of drug absorption, distribution, metabolism, excretion, and toxicity. *Expert Opinion on Drug Metabolism & Toxicology*, 2021. **17**(9): p. 1103-1124.
 115. Rizwan, M., et al. pH Sensitive Hydrogels in Drug Delivery: Brief History,

- Properties, Swelling, and Release Mechanism, Material Selection and Applications. *Polymers*, 2017. **9**, DOI: 10.3390/polym9040137.
116. Chatterjee, S., et al., Influence of pH-responsive compounds synthesized from chitosan and hyaluronic acid on dual-responsive (pH/temperature) hydrogel drug delivery systems of Cortex Moutan. *International Journal of Biological Macromolecules*, 2021. **168**: p. 163-174.
117. Nasef, S.M., E.E. Khozemy, and G.A. Mahmoud, pH-responsive chitosan/acrylamide/gold/nanocomposite supported with silver nanoparticles for controlled release of anticancer drug. *Scientific Reports*, 2023. **13**(1): p. 7818.
118. Popat, A., et al., A pH-responsive drug delivery system based on chitosan coated mesoporous silica nanoparticles. *Journal of Materials Chemistry*, 2012. **22**(22): p. 11173-11178.
119. Feril, L.B. and K. Tachibana, Use of ultrasound in drug delivery systems: emphasis on experimental methodology and mechanisms. *International Journal of Hyperthermia*, 2012. **28**(4): p. 282-289.
120. Cai, X., et al., Ultrasound-Responsive Materials for Drug/Gene Delivery. *Frontiers in Pharmacology*, 2020. **10**.
121. Huang, W.-C., et al., Ultrasound-Mediated Self-Healing Hydrogels Based on Tunable Metal–Organic Bonding. *Biomacromolecules*, 2017. **18**(4): p. 1162-1171.
122. Meng, Z., et al., Ultrasound-Mediated Remotely Controlled Nanovaccine Delivery for Tumor Vaccination and Individualized Cancer Immunotherapy. *Nano Letters*, 2021. **21**(3): p. 1228-1237.
123. Min, H.S., et al., Chemical gas-generating nanoparticles for tumor-targeted ultrasound imaging and ultrasound-triggered drug delivery. *Biomaterials*, 2016. **108**: p. 57-70.
124. Sanchez-Rexach, E., et al., Antimicrobial poly(ϵ -caprolactone)/thymol blends: Phase behavior, interactions and drug release kinetics. *European Polymer Journal*, 2016. **83**: p. 288-299.
125. Fasiku, V.O., et al., Chapter 3 - Antibiotic Polymer for Biomedical Applications, in *Antibiotic Materials in Healthcare*, V. Kokkarachedu, V. Kanikireddy, and R.

- Sadiku, Editors. 2020, Academic Press. p. 33-49.
126. Paarakh, M.P., et al., RELEASE KINETICS – CONCEPTS AND APPLICATIONS. *International Journal of Pharmacy Research & Technology (IJPR)*, 2023. **8**(1): p. 12-20.
 127. Li, H., Multi-Effect-Coupling pH-Stimulus (MECpH) Model for pH-Sensitive Hydrogel, in *Smart Hydrogel Modelling*, H. Li, Editor. 2009, Springer Berlin Heidelberg: Berlin, Heidelberg. p. 57-114.
 128. Almási, M., et al., Cytotoxicity study and influence of SBA-15 surface polarity and pH on adsorption and release properties of anticancer agent pemetrexed. *Materials Science and Engineering: C*, 2020. **109**: p. 110552.
 129. Abureesh, M.A., A.A. Oladipo, and M. Gazi, Facile synthesis of glucose-sensitive chitosan–poly(vinyl alcohol) hydrogel: Drug release optimization and swelling properties. *International Journal of Biological Macromolecules*, 2016. **90**: p. 75-80.
 130. Kong, J. and S. Yu, Fourier Transform Infrared Spectroscopic Analysis of Protein Secondary Structures. *Acta Biochimica et Biophysica Sinica*, 2007. **39**(8): p. 549-559.
 131. Bisen, D.S., et al., Reverse indentation size effects in gamma irradiated blood compatible blend films of chitosan-poly (vinyl alcohol) for possible medical applications. *Materials Science and Engineering: C*, 2017. **71**: p. 982-993.
 132. Casimiro, M.H., et al. Chitosan/PVA Based Membranes Processed by Gamma Radiation as Scaffolding Materials for Skin Regeneration. *Membranes*, 2021. **11**, DOI: 10.3390/membranes11080561.
 133. Duarte, R.M.B.O., et al., Exploring water-soluble organic aerosols structures in urban atmosphere using advanced solid-state ¹³C NMR spectroscopy. *Atmospheric Environment*, 2020. **230**: p. 117503.
 134. Jayasekara, R., et al., Preparation, surface modification and characterisation of solution cast starch PVA blended films. *Polymer Testing*, 2004. **23**(1): p. 17-27.
 135. Padavan, D.T., et al., Synthesis, characterization and in vitro cell compatibility study of a poly(amic acid) graft/cross-linked poly(vinyl alcohol) hydrogel. *Acta Biomaterialia*, 2011. **7**(1): p. 258-267.

136. Yang, J., et al., Effect of crosslinking processing on the chemical structure and biocompatibility of a chitosan-based hydrogel. *Food Chemistry*, 2021. **354**: p. 129476.
137. Lai, S., et al., Solid-State ¹³C NMR Study of Poly(vinyl alcohol) Gels. *Solid State Nuclear Magnetic Resonance*, 2002. **21**(3): p. 187-196.
138. Katoh, E. and I. Ando, High Resolution Solid State NMR, ¹³C, in *Encyclopedia of Spectroscopy and Spectrometry (Third Edition)*, J.C. Lindon, G.E. Tranter, and D.W. Koppenaal, Editors. 2017, Academic Press: Oxford. p. 75-85.
139. Enhancement of Radiation Crosslinking, in *Radiation Processing of Polymer Materials and its Industrial Applications*. 2012. p. 71-102.
140. Martel-Estrada, S.A., et al., The effect of radiation on the thermal properties of chitosan/mimosa tenuiflora and chitosan/mimosa tenuiflora/multiwalled carbon nanotubes (MWCNT) composites for bone tissue engineering. *AIP Conference Proceedings*, 2014. **1607**(1): p. 55-64.
141. Sunaryono, et al., Analysis of Distribution of Polyvinyl Alcohol Hydrogel Nanocrystalline by using SAXS Synchrotron. *IOP Conference Series: Materials Science and Engineering*, 2017. **202**(1): p. 012041.
142. Vo, N.T.N., et al., Poly(ethylene glycol)-interpenetrated genipin-crosslinked chitosan hydrogels: Structure, pH responsiveness, gelation kinetics, and rheology. *Journal of Applied Polymer Science*, 2020. **137**(41): p. 49259.
143. Ilgin, P., H. Ozay, and O. Ozay, A new dual stimuli responsive hydrogel: Modeling approaches for the prediction of drug loading and release profile. *European Polymer Journal*, 2019. **113**: p. 244-253.
144. Aycan, D. and N. Alemdar, Development of pH-responsive chitosan-based hydrogel modified with bone ash for controlled release of amoxicillin. *Carbohydrate Polymers*, 2018. **184**: p. 401-407.
145. Vigata, M., et al. Hydrogels as Drug Delivery Systems: A Review of Current Characterization and Evaluation Techniques. *Pharmaceutics*, 2020. **12**, DOI: 10.3390/pharmaceutics12121188.
146. Rungrod, A., et al., Synthesis of Poly(ϵ -caprolactone) Diacrylate for Micelle-Cross-Linked Sodium AMPS Hydrogel for Use as Controlled Drug Delivery

- Wound Dressing. *Biomacromolecules*, 2021. **22**(9): p. 3839-3859.
147. Kumari, P. and A. Meena, Application of enzyme-mediated cellulose nanofibers from lemongrass waste for the controlled release of anticancer drugs. *Environmental Science and Pollution Research*, 2021. **28**(34): p. 46343-46355.
148. Iresha, H. and T. Kobayashi, Ultrasound-triggered nicotine release from nicotine-loaded cellulose hydrogel. *Ultrason Sonochem*, 2021. **78**: p. 105710.
149. Jiang, H. and T. Kobayashi, Ultrasound stimulated release of gallic acid from chitin hydrogel matrix. *Mater Sci Eng C Mater Biol Appl*, 2017. **75**: p. 478-486.
150. Peppas, N.A. and B. Narasimhan, Mathematical models in drug delivery: How modeling has shaped the way we design new drug delivery systems. *Journal of Controlled Release*, 2014. **190**: p. 75-81.
151. Franzén, H.M., et al. Characterization and Properties of Hydrogels Made from Neutral Soluble Chitosans. *Polymers*, 2015. **7**, 373-389 DOI: 10.3390/polym7030373.
152. Jiang, H., K. Tovar-Carrillo, and T. Kobayashi, Ultrasound stimulated release of mimosa medicine from cellulose hydrogel matrix. *Ultrason Sonochem*, 2016. **32**: p. 398-406.
153. Noguchi, S. and K. Takaomi, Ultrasound response of viscoelastic changes of cellulose hydrogels triggered with Sono-devised rheometer. *Ultrason Sonochem*, 2020. **67**: p. 105143.



จุฬาลงกรณ์มหาวิทยาลัย
CHULALONGKORN UNIVERSITY

VITA

NAME Tran Vo Minh Tu

DATE OF BIRTH 4 September 1994

PLACE OF BIRTH Viet Nam

INSTITUTIONS ATTENDED Ho Chi Minh City University of Technology (HCMUT), Bachelor of Engineering, Chemical Engineering

HOME ADDRESS 37/9 Le Thi Hong Gam, ward 6, My Tho city, Tien Giang province, Viet Nam



จุฬาลงกรณ์มหาวิทยาลัย
CHULALONGKORN UNIVERSITY